ANALYTICAL AND KINETIC INVESTIGATIONS OF THE FERROUS-FERRIC REDOX SYSTEM IN AQUEOUS SULPHURIC ACID WITH PLATINUM ELECTRODES

HUANYU MAO

ANALYTICAL AND KINETIC INVESTIGATIONS OF THE FERROUS-FERRIC REDOX SYSTEM IN AQUEOUS SULPHURIC ACID WITH PLATINUM ELECTRODES

by

Huanyu Mao, B.Sc.

Submitted in partial fulfillment of the requirements for the degree of

Master of Science.

Memorial University of Newfoundland

St. John's, Newfoundland, Canada

July, 1987

ISBN 0-315-43350-7

This thesis is dedicated with

best wishes to my mother.

Acknowledgements

I wish to express my deep sense of gratitude to my supervisor, Professor Frank R. Smith for his great help, stimulating advice, continued encouragement and patient guidance throughout the past two and one-half years.

I am indebted to the glass blowers, Mr. Doug Seymour, Mr. Tom Perks, and Mr. Martin Hatswell for the construction and repair of glass apparatus. I would like to thank the staff of Memorial University's Technical Services department for the help in reconstruction of the potentiostat and rotating disc electrode, especially Mr. George Pardy of the electronics section and machinist Mr. Randy Thorne.

I would like also to thank Miss Teresa Barker for patiently typing this thesis, and also to Mr. John Kane for graphical drafting.

The financial support in the forms of the Memorial University of Newfoundland Graduate Fellowship and Teaching Assistantship offered by the Department of Chemistry are gratefully acknowledged.

Abstract

This thesis is composed of two parts, both based on electrochemical kinetic theory and experimental observations concerning the ferrous-ferric iron system.

In Part I, stirring effects on redox potentiometric titrations involving Fe^{2+} and Ce^{4+} are investigated in some detail. The mixture potential was considered to describe the experimental data. It has been observed that the measured potentials while the solution is stirred and while it is stationary are different. ΔE represents the difference between the two sorts of potential. The ΔE's were negative with a magnitude ca. 30 to 40 mV before equivalence; and they were positive with about the same magnitude after equivalence. The sign changed at equivalence. Some other redox systems also showed the same phenomenon. A set of experiments revealed that O_2 in the air caused the ΔE before the end-point, whereas ΔE's after the end-point did not need the presence of air. The sign of ΔE changed at equivalence regardless of the presence of air in the test system.

A theoretical interpretation applying electrochemical kinetics has been made to explain the existence of ΔE, the sign of ΔE and the sign change at equivalence. The theoretical treatment is supported by experiments using a rotating disc electrode.

In Part II, the rotating disc electrode is used to investigate the kinetics of the ferrous-ferric redox reaction on platinum in aqueous sulphuric acid. Very precise speed control with digital display and printing system was used. The reference and counter electrodes were constructed from the same metal to avoid possible contamination.

A low overpotential measurement was preferred. The mass transport effects were eliminated by making an extrapolation to infinite rotation speed of a plot of $(\frac{\partial \eta}{\partial i})_\omega$ against $\omega^{-\frac{1}{2}}$. The theory of this method is discussed in detail and a satisfactory equation for the method evaluated. Some of the advantages of this method are

exhibited by comparing it with conventional methods in which high overpotentials have to be applied to the electrode.

The heterogenous rate constant at 298.2 K was measured to be $3.9 \pm 0.4 \times 10^{-3}$ $cm \cdot s^{-1}$ on platinum with the roughness factor taken into account. The anodic transfer coefficient was 0.56 ± 0.03 for $FeSO_4$ and $Fe_2(SO_4)_3$ in 0.5 $mol \cdot L^{-1}$ H_2SO_4.

A deactivation upon "activation" has been found after applying a triangular sweep to a extremely clean system. The more thoroughly clean the system, the greater the negative effect on the activity. This work supports the idea that activation by triangular sweep is not necessary if the apparatus has been sufficiently cleaned. The formed oxide film during the activation sweep which decreased the electrode activity could be removed by chemical reduction, soaking the electrode in 0.1 $mol \cdot L^{-1}$ $FeSO_4$ solution, whereupon the rate constant recovered to the original value before "activation".

Table of Contents

Introduction

The purpose of the work at first was to measure the best rate constant for $Fe^{2+} \rightleftharpoons Fe^{3+} + e^-$ on a platinum rotating disc electrode. In the case of this work, the need for analysis of iron salts in solution was apparent. Therefore the investigation of the $Fe^{2+} + Ce^{4+}$ titration reaction began and developed into Part I of the thesis which is about the stirring effects in potentiometric redox titrations. Since the effects are related to electrochemical kinetics and have not been previously reported to our knowledge, a detailed investigation both experimentally and theoretically was carried out in Part I.

Part II describes the various experiences in attempting to activate the platinum electrode for use in the kinetic investigation. Although many previous workers had studied the $Fe^{2+} \rightleftharpoons Fe^{3+} + e^-$ reaction at platinum, we believe that none until now has taken such great care to use clean electrodes and apparatus and such highly pure chemicals. Also, a novel method of low overpotential measurement which has not been found in the published literature was used to make determination close to equilibrium. In this manner, many of the troubles that may be caused by applying high overpotentials such as oxide film on platinum and trace metal impurity deposition are largely avoided. For these reasons, as will appear in Part II, we believe that we have determined k° for the ferrous-ferric reaction in sulphuric acid medium as exactly as it is possible. We have also corrected the results to refer to the true surface area. We have not, however, attempted to make double-layer corrections.

There are individual introductory chapters for Part I and Part II as will be seen in the respective parts of the thesis.

PART ONE

Chapter 1. Conventional Views of Potentiometric Redox Titrations

Potentiometric titrations have been commonly used in analytical chemistry. Usually, a titration reaction is produced by the addition of known quantities of a reagent and the reaction is monitored by measurement of the cell e.m.f. Often potentiometric titrations are directed towards observing a sharp change of e.m.f. when the reaction between the titrant and the solution being titrated is complete. In many cases, the concentration of an unknown solution can be determined very accurately.

A typical cell schematic is as follows.

reference electrode ‖ titrand solution | indicator electrode

The e.m.f.'s observed during the titration can be predicted from a knowledge of the stoichiometry of the reaction and calculated by means of the Nernst equation.

In our case, a titrand solution initially containing iron(II) and a titrant solution of cerium(IV) as an oxidant were reacted in 1 mol L^{-1} H_2SO_4. The formal potentials[1] are as below:

$$Fe^{3+} + e^- \rightleftharpoons Fe^{2+} \qquad E^{o'} = +0.68\ V$$

$$Ce^{4+} + e^- \rightleftharpoons Ce^{3+} \qquad E^{o'} = +1.44\ V$$

The reference electrode is a silver-silver chloride electrode in saturated aqueous potassium chloride for which the potential[2] is +0.199 V at 25 °C. The cell can be represented as:

$$Ag, AgCl \mid KCl(satd) \parallel Fe^{2+}, Fe^{3+}, Ce^{3+}(1\text{-mol}\cdot L^{-1}\ H_2SO_4) \mid Pt$$

at any point before the equivalence point. The redox electrode potential is calculated by the Nernst equation,

$$E_{Fe} = E_{Fe^{3+},Fe^{2+}} = E^{o'}_{Fe^{3+},Fe^{2+}} + \frac{RT}{F} \ln \frac{[Fe^{3+}]}{[Fe^{2+}]} \qquad (1.1)$$

and the cell e.m.f. would be:

$$E_{cell} = E_{Fe} - E_{ref} = E^{o'}_{Fe^{2+},Fe^{3+}} + \frac{RT}{F} \ln \frac{[Fe^{3+}]}{[Fe^{2+}]} - E_{ref} \quad (1.2)$$

where $E^{o'}_{Fe^{2+},Fe^{3+}} = +0.68$ V, $E_{ref} = 0.199$ V. Define x as the fraction of the stoichiometric amount of oxidant added. Before the equivalence point, $(0 < x < 1)$, a considerable quantity of Fe^{2+} and Fe^{3+} are present, so the platinum indicator electrode rapidly attains a stable potential given at 25 ° C by

$$E_{cell} = 0.48 - 0.059 \log_{10} \left(\frac{1-x}{x}\right) \quad V \quad (1.3)$$

The potential versus added volume curve in this region rises little. When x changes from 0.1 to 0.9, the e.m.f. E_{cell} changes by only about 0.10 V.

Once past the equivalence point, the solution contains appreciable amounts of Ce^{3+} and Ce^{4+} but no Fe^{2+} and the redox potential is determined by the ratio of the concentrations of cerium(IV) to cerium(III). The equilibrium potential at any point after equivalence is given by:

$$E_{Ce} = E_{Ce^{3+},Ce^{4+}} = E^{o'}_{Ce^{3+},Ce^{4+}} + \frac{RT}{F} \ln \frac{[Ce^{4+}]}{[Ce^{3+}]} \quad (1.4)$$

and the cell e.m.f. would be

$$E_{cell} = E_{Ce} - E_{ref} = E^{o'}_{Ce^{3+},Ce^{4+}} + \frac{RT}{F} \ln \frac{[Ce^{4+}]}{[Ce^{3+}]} - 0.199 \quad V \quad (1.5)$$

The cerium(III) concentration is approximately equal to the concentration of iron(II) originally present, taking dilution into account, and the cell e.m.f. after the equivalence point $(x > 1)$ is given at 25 ° C by

$$E_{cell} = 1.24 - 0.059 \log_{10} \left(\frac{1}{x-1}\right) \quad V \quad (1.6)$$

This part of the curve is also rather flat because the ratio $\frac{1}{x-1}$ changes little. While x changes from 1.1 to 2.0, the cell e.m.f. only increases 0.05 V.

As the titration approaches the immediate vicinity of the equivalence point, the concentrations of Fe^{2+} and of Ce^{4+} become very small. At the equivalence point, the only substances present in appreciable amounts are Fe^{3+} and Ce^{3+}. The cell e.m.f. at this point can be deduced by adding together equations (1.3) and (1.6) to give:

$$2E_{cell} = 0.68 + 1.44 - (2 \times 0.199) - 0.059 \log_{10} \left(\frac{1-x}{x} \frac{1}{x-1}\right) \qquad (1.7)$$

which rearranges to

$$E_{cell} = \frac{1.72}{2} - 0.059 \log_{10} \left(\frac{1-x}{x-1}\right) + 0.059 \log_{10} x \qquad (1.8)$$

At the equivalence point $x = 1$ exactly, therefore the last two terms in (1.8) will be zero and the e.m.f. at the end-point should be

$$E_{cell} = \frac{E^{o'}_{Fe^{3+},Fe^{2+}} + E^{o'}_{Ce^{3+},Ce^{4+}}}{2} = \frac{1.72}{2} = 0.86 \text{ V} \qquad (1.9)$$

The calculated e.m.f.'s for the titration are presented in Table 1.1 and the titration is plotted as a curve of potential vs. added volume of titrant in Fig. 1.1. This has a typical sigmoid shape. The most prominent feature of this curve is the sharp change of potential observed in the vicinity of the stoichiometric equivalence point. The equivalence point can be located by the sharp point of potential change.

Figure 1.1 on next page

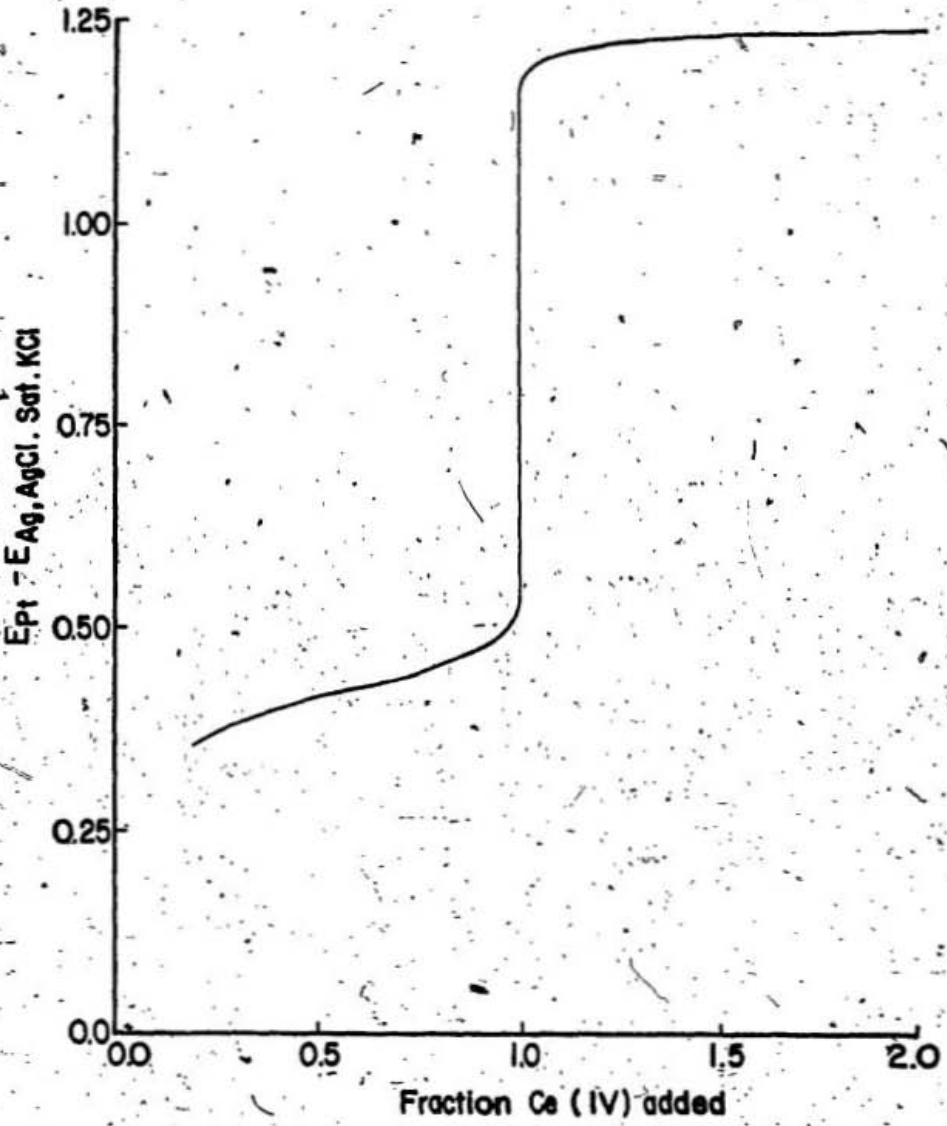

Fig. 1.1 The shape of a typical titration curve calculated by means of Nernst equation for the titration of Iron(II) with Cerium (IV).

Table 1.1. Calculated Cell E.M.F.'s for Fe^{2+} + Ce^{4+} Redox Titration.
(Potential Pt vs. Ag, AgCl, saturated KCl)

Fraction x	E_{cell}/V before equivalence	E_{cell}/V at equivalence	E_{cell}/V after equivalence
0.1	0.43	-	-
0.2	0.45	-	-
0.3	0.46	-	-
0.4	0.47	-	-
0.5	0.48	-	-
0.6	0.49	-	-
0.7	0.50	-	-
0.8	0.52	-	-
0.9	0.54	-	-
1.0	-	0.86	-
1.1	-	-	1.18
1.2	-	-	1.20
1.3	-	-	1.21
1.4	-	-	1.22
1.5	-	-	1.22
1.6	-	-	1.23
1.7	-	-	1.23
1.8	-	-	1.24
1.9	-	-	1.24
2.0	-	-	1.24

Many methods have been developed to locate the equivalence point since the first potentiometric titrations were reported in 1893[3]. Most of these methods centre on the best way of deducing the equivalence volume from the titration curve. This interest seems to have intensified over the last 20 years. Three methods of general interest are used to accurately obtain the equivalence volume. They are:

1. Graphical methods mentioned in most textbooks of analytical chemistry.
2. Methods based on the linearization of titration data[4].
3. Curve-fitting with computers[5].

However, all of these methods emphasize the mathematical treatment while the experimental procedures remain identical.

According to our work, there is some flaw in the conventional view. It is necessary to consider kinetic effects as well as thermodynamic relationships. It has been found in our work that the potential near equivalence is determined by some other mechanism than that envisaged in the conventional view detailed above. In particular, the effect of stirring does not agree with the conventional view. In most textbooks[6], even in some treatises[7], the purpose of stirring while the potentiometric titration is being carried out is to well mix the titrand and titrant solutions and to bring the system to equilibrium such that the Nernst equation can be applied. In our experiments, stirring played an important part in affecting the measured e.m.f.'s greatly throughout the titration.

A second objective of our work was to investigate a novel method to locate the end-point through experiments with and without stirring the solution. The equipment used in the experiment is the same as in the conventional potentiometric titration. The only difference is the manner in which the titration data are collected. The experimental methods and theoretical treatment will be given in the following chapters.

Chapter 2 The Effects of Stirring on Potentiometric Redox Titrations

In order to mix the titrated solutions well and hasten the achievement of equilibrium, adequate stirring is recommended.[6] Usually a magnetic stirrer and bar magnet are used in potentiometric titrations. It has been found in our work that the measured potentials are different, depending on whether the solution is being stirred or is stationary, in both cases after sufficient stirring to mix the solution. Table 2.1 shows some observations from a typical Ce^{4+} vs. Fe^{2+} potentiometric titration.

Table 2.1 Potential Difference Between Pt Electrode vs. Ag, AgCl, Saturated KCl Reference Electrode in $FeSO_4$ + $Ce(SO_4)_2$ + Aqueous H_2SO_4 System.

	Potential measured while stirring/mV	Potential measured while solution still/mV	Ce^{4+} solution added/mL
Just before end-point	589	630	21.00
Just after end-point	1090	1067	21.90

Some conclusions can be drawn from these data:

1. The measured potentials while the solution is stirred or is still are different for the same volume of added titrant.
2. Before the end-point the measured potential of the platinum while the solution is stirred is less positive than the measured potential in a still solution.
3. The situation is reversed after the end-point. The potential of platinum while the solution is stirred is more positive than the potential measured in a still solution.
4. There must be a point of crossover at which the measured potentials with stirring and in still solutions are equal.

2.1 Titrations of Iron(II) with Cerium(IV) and Other Oxidants in Air.

The typical experiment to show the phenomenon was carried out with a redox titration. The reaction is:

$$Ce^{4+}(aq) + Fe^{2+}(aq) \rightleftharpoons Ce^{3+}(aq) + Fe^{3+}(aq)$$

with Ce^{4+} solution as the titrant. A primary standard $Ce(NH_4)_2(NO_3)_6$ from G.F. Smith was used. About 3.4 g of $Ce(NH_4)_2(NO_3)_6$ was accurately weighed and 14 mL concentrated sulphuric acid (ACS grade) was added to the cerium(IV) salt and the solution well stirred for 2 minutes. Then 25 mL distilled water was cautiously added down the side of the beaker over a period of 5 minutes. The exothermic reaction aids conversion of $Ce(NO_3)_4$ to $Ce(SO_4)_2$. A second portion of 25 mL distilled water was added and solution was stirred for two more minutes. When all the solid had dissolved and the solution had cooled, it was transferred to a 250.0 mL volumetric flask and made up to mark with distilled water. The solution was about 0.011 $mol \cdot L^{-1}$ Ce^{4+} and 0.5 $mol \cdot L^{-1}$ H_2SO_4. The solution of Fe^{2+} to be determined was made up by dissolving about 2.78 g of Baker Analyzed $FeSO_4 7H_2O$ in 1 L of 0.5 $mol \cdot L^{-1}$ H_2SO_4 solution. The concentration of Fe^{2+} was about 0.01 $mol \cdot L^{-1}$.

A 25.00 mL Fe(II) solution and 20.00 mL Ce(IV) solution were pipetted into a beaker and mixed well by using magnetic stirring. Then a 5.000 mL microburette was used for precise titration. The reference electrode was a Ag, AgCl, saturated KCl electrode. Its potential was found to be 207 mV measured against a standard hydrogen electrode. The redox indicator electrode was a platinum foil electrode. For most experiments the potentials were measured during the titration with an Orion Research Model 601 pH/mV meter.

The experiment was carried out in the following steps:

(a) The desired amount of titrant was added, usually 0.10 mL each time, and stirring started. The potentials with stirring were read at the end of a two minute

period. If the titration is before the end-point, the potentials measured while stirring were very stable. The readings from the millivoltmeter were taken in less than two minutes by which time the solution is well mixed. After the end-point, the period of time had to be set to a fixed length as the potential changed continuously with time. These potentials were reported as $E_{stirring}$.

(b) The stirrer was switched off and the solution allowed to remain unstirred for 2 minutes. It is certain that the solution was well mixed in the previous step of stirring. In other words, the solution was completely homogeneous since it had been stirred for 2 minutes in the previous step. The potentials in the still condition were read at the end of the 2 minute unstirred period. These potentials were reported as E_{still}.

The stirring rate was set at a certain position of the magnetic stirrer control knob throughout the experiment to keep the stirring rate essentially constant. Table 2.2 shows a complete set of data. It is easily seen that there are differences between E_{still} and $E_{stirring}$ before the end-point and immediately after the end-point. The most prominent feature of the data is that ΔE changes its sign at the end-point, estimated from the large potential jump of the data, either $E_{stirring}$ or E_{still}.

This phenomenon has been repeated many times with different solutions and conditions. Tables 2.3 and 2.4 give other titration results comparing also with the second derivative data treatment. The solutions were again approximately 0.01 mol$\cdot$L^{-1} Fe^{2+} and 0.011 mol$\cdot$L^{-1} Ce^{4+}.

Table 2.2 E.M.F. Data of a Complete Titration of 0.01 mol·L^{-1} $FeSO_4$ in 0.5 mol·L^{-1} H_2SO_4 with 0.011 mol·L^{-1} $Ce(SO_4)_2$ in 0.5 mol·L^{-1} H_2SO_4.

Added Ce^{4+} solution volume/mL	$E_{stirring}$/mV	E_{still}/mV	$\Delta E = E_{stirring} - E_{still}$
20.00	568	614	-46
20.783	584	630	-46
20.900	587	632	-45
20.990	589	630	-41
21.090	593	630	-37
21.190	597	633	-36
21.290	602	636	-34
21.389	608	641	-33
21.490	617	649	-32
21.594	630	661	-31
21.694	657	690	-33
21.794	911	875 *	+36
21.891	1090	1067	+23
21.992	1121	1114	+7
22.090	1132	1128	+4
22.194	1140	1137	+3
22.290	1145	1143	+2
22.392	1150	1149	+1
22.490	1154	1152	+2
22.606	1157	1156	+1
22.793	1163	1162	+1
23.190	1170	1170	0
23.990	1182	1182	0

* End-point according to conventional methods.

Table 2.3 Titration Results with Approximately 0.01 mol·L^{-1} Fe^{2+} and 0.011 mol·L^{-1} Ce^{4+} Compared with Second Derivative Treatment for End-Point Location.

Added volume of Ce^{4+}/mL	$E_{stirring}$/mV	E_{still}/mV	ΔE/mV	d^2E/dv^2 ($E_{stirring}$)
21.762	592	619	-27	0.411
21.776	609	640	-31	20.25
21.974	647	676	-29	24.67
22.070	914	874	+40	-13.79
22.170	1057	1044	+13	-8.56
22.262	1113	1104	+9	-4.69

* End-point location.

Table 2.4 Results of Another Titration of Approximately 0.01 mol·L^{-1} Fe^{2+} and 0.011 mol·L^{-1} Ce^{4+} Compared with the Second Derivative.

Added volume Ce^{4+}/mL	$E_{stirring}$/mV	E_{still}/mV	ΔE/mV	d^2E/dv^2 ($E_{stirring}$)
20.00	548	582	-34	
20.182	616	670	-54	0.195
21.992	639	690	-51	29.00
22.092	952	901	+51	-16.30
22.192	1102	1093	+9	-13.29
22.290	1120	1116	+4	-0.42

* End-point location.

According to the comparison, the point of sign change of ΔE coincides closely with the end-point calculated by the second derivative method. Also there is a large change in the difference of potential from negative to positive at the end-point. This phenomenon was also found in redox titrations other than those using Ce^{4+} as oxidant. Experiments showed that titrations of MnO_4^- versus Fe^{2+} and $Cr_2O_7^{2-}$ versus Fe^{2+} in highly acidic solutions behaved similarly. Table 2.5 gives data for titrations in which the oxidant was approximately 0.002 mol·L^{-1} $KMnO_4$. It was titrated against about 0.01 mol·L^{-1} Fe^{2+} in aqueous H_2SO_4. There is also a large potential jump and a sign change at the end-point. The sign change coincided with the second derivative result.

Table 2.5 Data from a Titration Using 0.002 mol·L^{-1} $KMnO_4$ as Oxidant and 0.01 mol·L^{-1} $FeSO_4$ as Reductant in *ca.* 1 mol·L^{-1} H_2SO_4.

Added volume of $KMnO_4$/mL	$E_{stirring}$/mV	E_{still}/mV	ΔE/mV	d^2E/dv^2 ($E_{stirring}$)
21.386	590	634	-44	0.38
21.478	602	646	-44	0.91
21.590	627	675	-48	26.84
21.698	970	934	+36	-13.53
21.800	1149	1146	+3	-11.93

* End-point location.

With $K_2Cr_2O_7$, the results in Table 2.6 show the same phenomenon. The concentration of $K_2Cr_2O_7$ was 0.001943 mol·L^{-1} and again 0.01 mol·L^{-1} Fe^{2+} was used, acidified by adding 5 mL of 6 mol·L^{-1} H_2SO_4 and 10 mL of 6 mol·L^{-1} H_3PO_4 to increase the potential jump at the end-point.

Table 2.6 Data from a Titration with 0.0019 mol·L^{-1} $K_2Cr_2O_7$ as Oxidant and 0.01 mol·L^{-1} $FeSO_4$ as Reductant in *ca.* 1 mol·L^{-1} H_2SO_4 and 2 mol·L^{-1} H_3PO_4.

Added volume of $K_2Cr_2O_7$/mL	$E_{stirring}$/mV	E_{still}/mV	ΔE/mV	d^2E/dv^2 ($E_{stirring}$)
22.000	546.6	618.0	-71.4	0.203
22.108	565.0	628.6	-63.0	1.216
22.210	595.4	647.8	-51.6	7.730
22.302	691.8	684.0	+7.8	-6.086
22.408	730.0	730.0	+9.0	-1.623
22.502	765.6	760.8	+4.8	-0.380
22.602	782.2	781.0	+1.2	

* End-point location.

A big jump of ΔE and a sign change can be observed in the experimental results and the region of sign change also coincided with the end-point from the second derivative method. These observations suggest a novel method of estimating the end-point in titrations involving iron with oxidants such as cerium, permanganate and dichromate. This method may not be readily applicable to routine analysis but is still of interest.

This phenomenon in potentiometric redox titrations has not been previously reported in the literature. Many different experiments were done to try to find the cause of the phenomenon. The most significant experiment appeared to be keeping the titration reaction system away from air. Other experiments will be mentioned later.

2.2 Titrations of Iron(II) with Argon Protection

The consideration was that oxygen in the air might affect the titration through oxidation of ferrous ions thereby changing their concentration. In order to minimize air interference, a special cell shown in Fig. 2.1 was used for the rest of the experiments.

Figure 2.1 on next page

A is a platinum foil electrode with a water-sealed argon outlet, B is a silver, silver chloride saturated KCl reference electrode, C is a microburette, D is the argon inlet. D can be adjusted for bubbling gas through the solution to degas it before the start of the experiment, or passing it over the solution while the solution has to be kept still by opening valve E. 25.00 mL Fe^{2+} solution and 20.00 mL Ce^{4+} solution were added before observing the cell e.m.f. This is still about 2 mL of Ce^{4+} before equivalence. The rest of the Ce^{4+} solution was added from the microburette. The mixed solution was saturated with argon and stirred for 5 minutes to remove dissolved oxygen. Potential readings were begun at the end of this bubbling. During the still period, the valve was adjusted open. The readings for the still period were again taken at the end of 2 minutes without stirring. The following tables show titration results using the above cell.

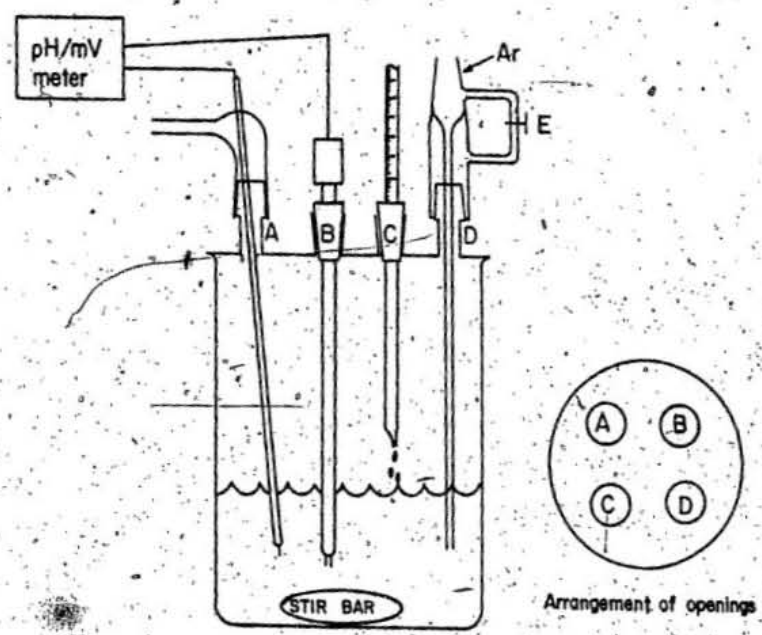

Fig. 2.1 The cell used to prevent air contact with solution.

Table 2.7 Data Taken from a Titration of 0.01 $mol \cdot L^{-1}$ Fe^{2+} versus 0.011 $mol \cdot L^{-1}$ Ce^{4+} in H_2SO_4 Carried Out Under Argon.

Added Ce^{4+} volume/mL	$E_{stirring}$/mV	E_{still}/mV	ΔE/mV
20.00	556.0	557.5	-1.5
20.698	590.0	591.6	-1.6
20.798	602.5	604.1	-1.6
20.900	627.4	628.8	-1.4
20.996	920.3	861.5	+58.6
21.098	1087.7	1077.4	+10.3
21.198	1116.3	1114.4	+1.9

Table 2.8 Data Taken from Another Titration of 0.01 $mol \cdot L^{-1}$ Fe^{2+} versus 0.011 $mol \cdot L^{-1}$ Ce^{4+} in H_2SO_4 Carried Out Under Argon.

Added Ce^{4+} volume/mL	$E_{stirring}$/mV	E_{still}/mV	ΔE/mV
20.00	547.7	548.9	-1.2
20.900	595.7	597.9	-2.2
20.994	616.7	618.8	-2.1
21.092	854.4	790.5	+63.9
21.190	1057.1	1043.6	+13.5
21.294	1112.6	1107.1	+5.5
22.292	1163.3	1162.2	+1.1

Comparing these results with the results of titrations in open air, the ΔE's are obvi-

ously different. The following table shows comparable data.

Table 2.9 A Comparison of ΔE Before, At and After the End-Point in Air and in Argon for Two Titrations of 0.01 mol·L^{-1} Fe^{2+} versus 0.011 mol·L^{-1} Ce^{4+} in H_2SO_4.

	OPEN TO AIR		UNDER ARGON	
	Added volume Ce^{4+}/mL	ΔE/mV	Added volume Ce^{4+}/mL	ΔE/mV
	20.00	-43	20.00	-1.5
Before	20.670	-34	20.698	-1.6
End-Point	20.770	-29	20.798	-1.6
	20.878	-28		
End-Point	21.974	-29	20.900	-1.4
Region	22.070	+40	20.996	+58.8
After	22.262	+9	21.098	+10.3
End-Point	22.660	+2	21.198	+1.9

Some conclusions can be drawn from this comparison.

1. Before the end-point, ΔE's in open air are much more negative than they are under argon atmosphere.
2. There is a potential jump at the end-point when the sign of ΔE changes, *both* in air and under argon.
3. After the end-point, the ΔE's tend to zero but a larger volume of Ce^{4+} solution must be added in the open air situation to bring ΔE nearly to zero.
4. Another observation is that, in general, the redox electrode potentials differ

absolutely, being more positive when air is present than when it is absent. Table 2.10 illustrates this point for a solution containing 0.01 mol·L^{-1} Fe^{2+} reacted with $KMnO_4$ well before equivalence.

Table 2.10 A Comparison of Cell EMF's Before End-Point From Several Experiments Carried Out in Open Air and Under Argon.
Electrolyte: 0.01 mol·L^{-1} Fe^{2+} and 0.002 mol·L^{-1} MnO_4^- in 2 mol·L^{-1} H_2SO_4

	OPEN TO AIR		UNDER ARGON	
	$E_{stirring}$/mV	E_{still}/mV	$E_{stirring}$/mV	E_{still}/mV
	557	589	541	544
	559	591	541	543
	558	592	541	542
	557	589	541	543
Average:	558	590	541	543

Fig. 2.2 illustrates schematically how ΔE varies in different stages of the titration.

Figure 2.2 on next page

This problem may be solved by starting with the potential difference between operating in open air and under argon, because this difference gives ample evidence of the involvement of oxygen. The measured potential of the noble metal redox electrode is not that of only one couple as in the conventional view: it must be a mixed potential. Our theoretical explanation for this phenomenon will begin with a detailed analysis of mixed potentials in the following chapter. First, however, some other experimental evidence will be presented.

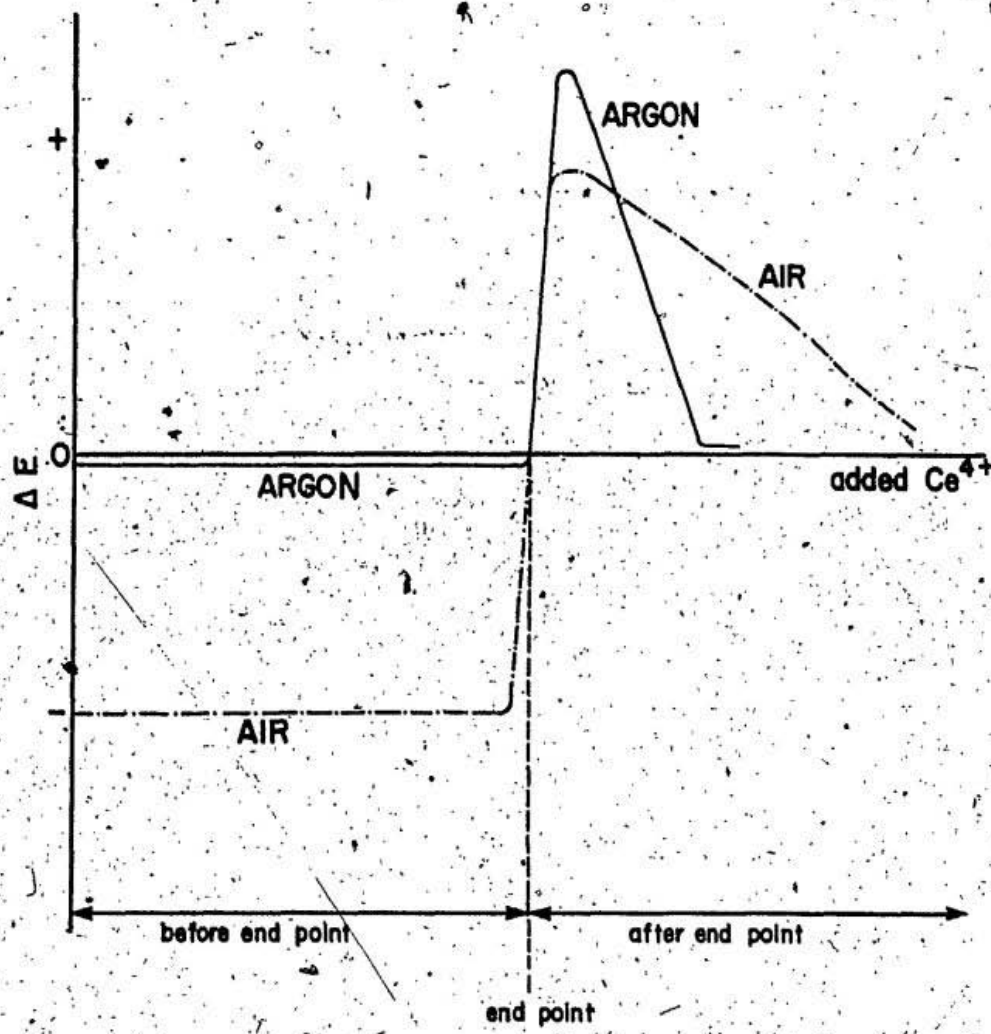

Fig. 2.2 Schematic ΔE versus added Ce^{4+} curve.

2.3 Iron(II) - Cerium(IV) Titrations at Other Concentrations.

A few experiments were done with iron(II) and cerium(IV) solutions of approximately 0.001 and 0.1 mol·L^{-1}. The general behaviour observed with 0.01 mol·L^{-1} solutions was confirmed but details were different, e.g. with 0.001 mol·L^{-1} solutions the differences of potential between stirred and unstirred cases were larger farther from the point of sign change of ΔE, while with 0.1 mol·L^{-1} solutions ΔE's were small except close to that point. The point of sign change appeared not to coincide well with the end-point determined by first or second derivative methods. Tables 2.11 and 2.12 illustrate these observations.

Table 2.11 Titration Results with Approximately 0.00085 mol·L^{-1} Fe^{2+} and 0.001 mol·L^{-1} Ce^{4+} in 0.5 mol·L^{-1} H_2SO_4 Compared with First and Second Derivative Treatment.

Added Ce^{4+} volume/mL	$E_{stirring}$/mV	E_{still}/mV	ΔE/mV	$\frac{dE}{dv}$ ($E_{stirring}$)	$\frac{d^2E}{dv^2}$ ($E_{stirring}$)
20.00	651	722	-71		
				0.100	
20.470	698	733	-35		+0.94
				0.406	
20.571	739	743	-4		-0.139
				0.327	
20.672	772	758	+14		+1.783
				0.537	
20.780	830	788	+42		+3.490
				0.000 *	
20.880	920	844	+76		-0.700
				0.830	
20.980	1003	914	+89		-1.478
				0.684	
21.078	1070	994	+76		-2.800
				0.415	
21.172	1109	1065	+44		-2.533
				0.226	
21.274	1126	1103	+23		
				0.060	
21.475	1138	1125	+13		

* End-point location.

Table 2.12 Titration Results with Approximately 0.085 $mol \cdot L^{-1}$ Fe^{2+} and 0.10 $mol \cdot L^{-1}$ Ce^{4+} in 0.5 $mol \cdot L^{-1}$ H_2SO_4 Compared with Second Derivative Treatment.

Added Ce^{4+} volume/mL	$E_{stirring}$/mV	E_{still}/mV	ΔE/mV	d^2E/dv^2 ($E_{stirring}$)
20.00	571	578	-7	
20.492	610	619	-9	0.371
20.590	629	634	-5	16.708
20.804	853	707	+146	8.652
20.888	1090	1088	+2	-26.859
20.990	1123	1122	+1	-2.011
21.088	1135	1134	+1	-0.387

* End-point location.

2.4 Other Experiments

In order to ensure that observations were not dependent on a particular instrument a Radiometer, Copenhagen PHM84 research pH meter was used for some of the e.m.f. measurements, without significant difference. Larger platinum indicator electrodes gave larger potential differences between $E_{stirring}$ and E_{still}, while changing the silver, silver chloride reference electrode was without effect.

In some experiments two platinum electrodes were added to the cell and a constant current of about 1.5 μA passed through them using a 15 V D.C. power and 10 MΩ resistance, the potential difference between them being monitored throughout the Fe^{2+} – Ce^{4+} titration using a Keithley 172 multimeter. The potential difference during stirring was always less than the p.d. measured in still solution as might have

been expected *i.e.* $\Delta V = V_{stirring} - V_{still}$ was always negative, unlike the potential difference $\Delta E = E_{stirring} - E_{still}$ already defined, which changed sign near the equivalence point. These experiments were performed because at first it was thought possible that the ΔE observations were caused by small currents flowing through the measuring instruments. This explanation was clearly ruled out by the potentiometric experiments with polarized indicator electrodes described above.

Finally, some potentiometric experiments were done with acid-base titrations using a glass electrode and a silver, silver chloride reference electrode and then with an α/β palladium hydride electrode as the H_3O^+ ion indicator. The glass electrode, as anticipated, proved totally insensitive to stirred or unstirred conditions. However, the palladium hydride electrode showed sensitivity to mass transport conditions. ΔE's, as defined earlier, were positive when the titration was carried out in air but became negative under argon protection. No sign change occurred during the titration. Time did not permit further investigation of these interesting effects of air on acid-base potentiometric titrations with α/β PdH indicator electrodes. We presume that mixed potentials are again involved.

Chapter 3 Theory of Stirring and Air Effects in Potentiometric Redox Titrations.

To give a theoretical explanation for the phenomena detailed in Chapter 2, we start with a discussion of mixed potentials. The kinetic factors are then considered by deriving a relationship between the measured potentials and the stirring rate under the experimental circumstances from some basic equations of electrode kinetics. The kinetic treatment should be able to answer the following questions:

1. Why is there a difference between $E_{stirring}$ and E_{still} before the end-point in open air and why does it disappear in an argon atmosphere?
2. Why is there a difference between $E_{stirring}$ and E_{still} after the end-point and why is it independent of the presence or absence of air?
3. Why does the difference of potential change sign from before the end-point to after the end-point?

3.1 The Mixed Potential in a Redox System.

A single redox reaction in electrochemistry is really a redox couple. In general a reaction

$$Ox_1 + ne^- \rightleftharpoons Red_1 \qquad (3.1.1)$$

is usually named as a redox couple Ox_1/Red_1. Most physical chemistry textbooks deal only with the behavior of this single redox couple. However in practice one often encounters two or more couples simultaneously present in a system. Such a system has a potential which reflects the contributions of all couples present.[8]

If two or more couples are in equilibrium, the equilibrium potential can be obtained by considering any one couple. Let a multi-couple system have the form:

$$Ox_1 + n_1e^- \rightleftharpoons Red_1 \qquad (3.1.1)$$

$$Ox_2 + n_2e^- \rightleftharpoons Red_2 \qquad (3.1.2)$$

$$Ox_i + n_ie^- \rightleftharpoons Red_i \qquad (3.1.3)$$

Consider the situation where two couples are simultaneously present at equilibrium with each other. More important, if all or any one of the reactions are reversible, the rate of reaction is fairly rapid, the whole system comes to equilibrium and all of the concentrations remain constant. The potential is then given by Nernst equations as:

$$E_{eq} = E_1^{o'} + \frac{RT}{n_1F} \ln \frac{[Ox_1]}{[Red_1]} \qquad (3.1.4)$$

$$E_{eq} = E_2^{o'} + \frac{RT}{n_2F} \ln \frac{[Ox_2]}{[Red_2]} \qquad (3.1.5)$$

$$E_{eq} = E_i^{o'} + \frac{RT}{n_iF} \ln \frac{[Ox_i]}{[Red_i]} \qquad (3.1.6)$$

where E_{eq} is the potential at equilibrium; $E_i^{o'}$ is the formal potential for an individual couple.

The potential is then calculated by using any one of these couples for which its equilibrium concentrations are conveniently available. The measured potential in equilibrium will be independent of any kinetic factors such as k^o and α. In particular, the measured potential should not change with stirring, once equilibrium has been reached.

However, relatively few mixed systems come to equilibrium with each other and with the electrode very rapidly. The measured potential drifts from the calculated Nernst potential. This is partly because homogeneous redox reactions are rarely fast, and partly because only a minority of redox couples are electrochemically reversible[8]. Since the reaction rate must be involved, kinetic aspects have to be considered in

order to solve problems arising in a system in which two or more couples are not in equilibrium.

The potential shift from equilibrium can be defined by the overpotential:

$$\eta = E - E_{eq} \qquad (3.1.7)$$

where E is the measured potential. We shall use the following conventions: if η is positive, the electrode reaction is anodic and the corresponding current is defined as positive or anodic current; a negative overpotential causes negative or cathodic current to flow. The overpotential η is a kinetically related parameter as in the Butler-Volmer equation[9]:

$$j_i = j_{ai} - j_{ci} = j_{oi}\left[\exp\left(\frac{\alpha_i n_i F \eta}{RT}\right) - \exp\left(\frac{-(1-\alpha_i) n_i F \eta}{RT}\right)\right] \qquad (3.1.8)$$

where the subscript i represents an individual electrochemical reaction couple and j_{oi} is the exchange current density for reaction i. α_i is the transfer coefficient appropriate to the i'th electrochemical reaction; and n_i is the number of electrons transferred. One can draw a current-potential curve according to equation (3.1.8) in Fig. 3.1.

An electrode system in which two or more couples are present together in solution but not in equilibrium with each other is called a "polyelectrode"[10]. Its treatment is greatly simplified by an additivity principle. The principle is based on the assumption that the couples present act independently of each other. Thus at any given potential the net observed current is their algebraic sum. There will be one potential at which the net observed current is zero, the point at which the anodic current due to one couple exactly balances the cathodic current of the other couple, for a system restricted to just two couples. Fig. 3.2 shows this principle diagrammatically.

Figures 3.1 and 3.2 on next page.

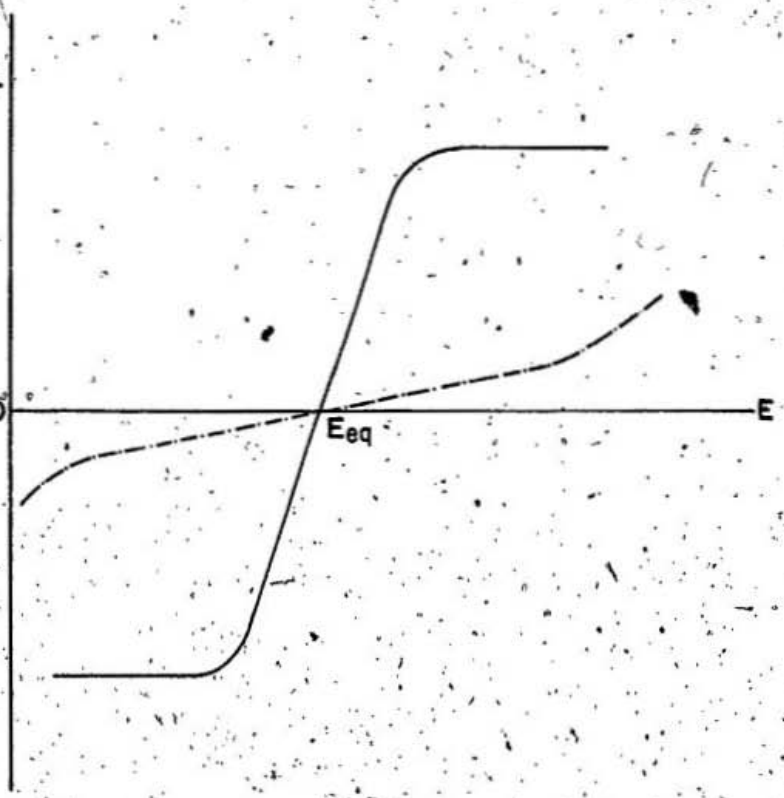

Fig. 3.1 Current-overpotential curves for the system $Ox + ne^- \rightleftharpoons Red$
Solid line represents a fast electrode reaction; dashed-line represents a slow electrode reaction.

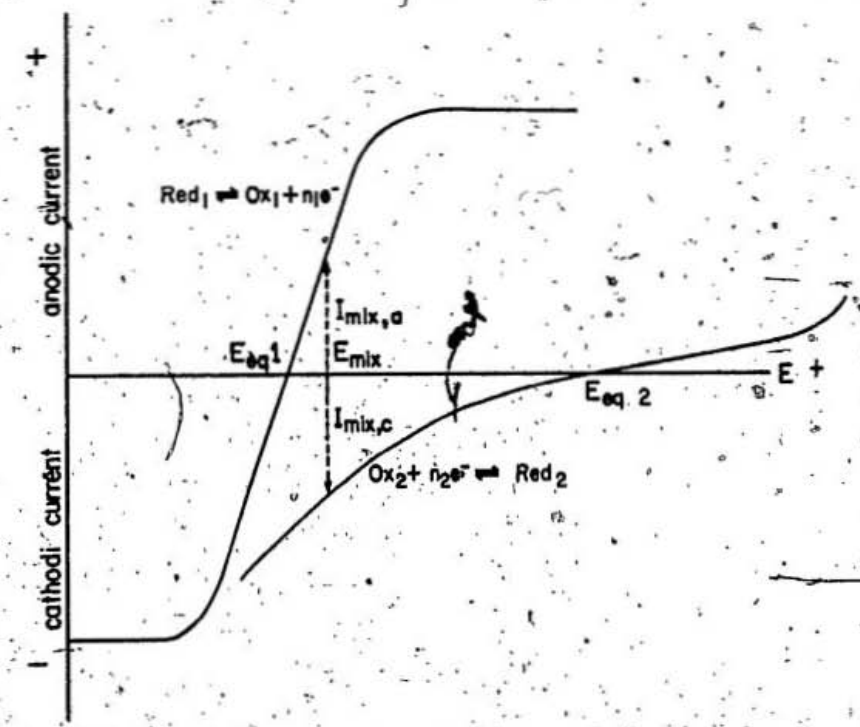

Fig. 3.2 Schematic current-potential curves for two redox couples present together but not in equilibrium with each other.

The point of zero net current is normally called the mixed or mixture potential, E_{mix}[11]. It is the potential measured with a voltmeter when a mixture of couples is present together at an electrode. The two currents balanced out at E_{mix} are equal in magnitude but of opposite signs. These two mixed currents $i_{mix,a}$ and $i_{mix,c}$ represent not only the rates of the two half-reactions $Red_1 \rightarrow Ox_1 + n_1e^-$ and $Ox_2 + n_2e^- \rightarrow Red_2$ but also the rate of the overall redox reaction that takes place between the couples at E_{mix}. More important, E_{mix} is affected by many kinetic effects which will be discussed in later sections of this chapter. The mathematical treatment for the particular pairs of couples Fe^{2+}/Fe^{3+}, O_2/H_2O and Ce^{3+}/Ce^{4+} will be given there.

3.2 The Mixed Potential in Potentiometric Titrations.

Charlot et al. mentioned mixed potentials caused by oxygen in potentiometric titrations of iron[12], but only when the concentration of Fe^{3+} is very small. Then dissolved oxygen becomes electroactive in place of Fe^{3+}, and a Fe^{2+}/O_2 mixed potential is produced. However, according to the present work, the O_2/H_2O couple influences the potential throughout the titration. Charlot et al.[12] also refer to experimental evidence that potentiometric titrations of ferrous iron with permanganate ion and with dichromate ion do not show the expected potential at equivalence because of irreversibility associated with the MnO_4^-/Mn^{2+} redox couple which, unlike the Ce^{4+}/Ce^{3+} couple, is a many-electron transfer and probably occurs through a number of steps. The potential after equivalence in the case of permanganate, it was argued, is a mixed potential involving O_2 generation from water, as we later maintain must also be the case for the cerium system as well. Reference is made[12] to work of Willard and Fenwick[13] in 1932 in which pairs of dissimilar metals, *e.g.* Pt and Pd were used to detect potentiometric end-points, instead of the conventional platinum indicator combined with a reference electrode.

Lewartowicz[14] has more recently combined a platinum and a gold electrode immersed in 0.5 mol·L^{-1} H_2SO_4 containing various concentrations of Fe^{2+} and Fe^{3+} ions as an electrometric sensing device for traces of oxygen. Such a cell with $[Fe^{2+}] = 3.1 \times 10^{-4}$ mol·L^{-1} and $[Fe^{3+}] = 0.9 \times 10^{-4}$ mol·L^{-1} had an e.m.f. of 4.9 mV in 1000 ppm O_2, electrolytically generated in Ar or N_2, the platinum becoming more positive the higher the O_2 content while the gold electrode remains constant. At constant $[Fe^{2+}] + [Fe^{3+}]$ the sensitivity to oxygen increased with increase of $[Fe^{2+}]$ and was largest of all at the lowest total $[Fe^{2+}] + [Fe^{3+}]$. The phenomena were correctly, we believe, identified as involving mixed potentials of Fe^{2+} oxidation and O_2 reduction. Nevertheless, neither Lewartowicz's[14] nor Willard and Fenwick's[13] observations include any of the type presently under consideration.

Recalling Table 2 in Chapter 2, the difference of potential between stirring and still (ΔE) was 32 mV when the solution was open to the air while it was only 2 mV on average when the solution was reasonably protected from air. The concentration of Fe^{3+} in our work was large, not small as in Charlot's case.[12] Furthermore, the air and stirring effects were found by observing the magnitude of ΔE which has been specially defined in our work. The higher the ΔE observed, the more stirring influenced the value of E. We have two reasons to make the assumption that a mixed potential is established:

1. Different potential shifts between unstirred and stirred solution were found in the presence and absence of air.
2. Both stirring and mixed potentials are kinetically related quantities.

For a redox titration, oxygen is the only likely reactive component in air and it has been shown to be important by carrying out an experiment with pure oxygen present. Therefore, a couple of O_2/H_2O probably exists in the titration system. The reaction is normally

$$O_2 + 4H^+ + 4e^- \rightleftharpoons 2H_2O \qquad E^\circ = +1.229\ V \qquad (3.2.1)$$

The main reaction in the titration is

$$Ce^{4+} + Fe^{2+} \rightleftharpoons Ce^{3+} + Fe^{2+} \qquad (3.2.2)$$

Since this reaction is very fast, both couples Ce^{4+}/Ce^{3+} and Fe^{3+}/Fe^{2+} come to equilibrium rapidly. From the discussion to be given in the last section, the potential before equivalence in the absence of oxygen can be obtained from the Nernst equation. In most potentiometric titrations, the experiments are carried out in the open air. It is therefore important to study how oxygen affects the titration.

To analyse the potentials involving oxygen, kinetic factors have to be considered since the reaction (3.2.1) is very irreversible[15] and so has a very low exchange current density of about 10^{-10} A·cm^{-2}. Using equation (3.1.8) for the O_2/H_2O system, the current-potential curve can be drawn as the dot-dashed line in Fig. 3.1. The i-E curve is very flat. It could be horizontal for a highly irreversible couple. Some anodic data for the O_2/H_2O couple in 0.05 M H_2SO_4 provided by Bockris and Huq[16] can help to decide the shape of the curve, *i.e.* $j_o = 2 \times 10^{-10}$ A·cm^{-2} and $\alpha = 0.6$. Then overpotentials of 0.2, 0.5 and 1.0 V would give current densities j of approximately 10^{-8}, 10^{-5} and 1.0 A·cm^{-2}, respectively.[17] The current density in our experimental conditions (less purity of reagents and simple cleaning of the electrodes) would probably be less.

Comparing the i-E curves in Fig. 3.1 for a fast redox couple such as Fe^{2+}/Fe^{3+}, the curve can have a steep slope around the equilibrium point since this couple is fairly reversible with an exchange current density of about 5×10^{-3} A·cm^{-2}. The curve eventually rises to the limiting currents $i_{l,a}$ and $i_{l,c}$ on either side of the equilibrium point. The limiting currents $i_{l,a}$ and $i_{l,c}$ are defined by the following equations[18]

$$i_{l,a} = nFAm_R C_R^* \qquad (3.2.3)$$

$$i_{l,c} = nFAm_O C_O^* \qquad (3.2.4)$$

where A is the geometric electrode area; m_O and m_R are mass transfer coefficients. In approximate treatments of convective systems, m_O and m_R correspond to $\frac{D_O}{\delta_O}$ and $\frac{D_R}{\delta_R}$, respectively, where δ_O and δ_R are the thicknesses of the hypothetical stagnant layer at the electrode surface under cathodic and anodic conditions, respectively. They will be discussed in a later section. C_O^* and C_R^* are the bulk concentrations of oxidized and reduced species, respectively. It is necessary to mention that $i_{l,a}$ could be very much smaller than $i_{l,c}$ when the titration is before but close to equivalence. The i-E curve then has the shape of Fig. 3.3.

Figure 3.3 next page.

It has been shown that a single couple has an equilibrium point, E_{eq}, at which the measured potential is independent of stirring or other kinetic effects. A solution containing 0.001 mol·L^{-1} Fe^{2+} and 0.009 mol·L^{-1} Fe^{3+} in 0.5 mol·L^{-1} H_2SO_4 was tested. The solution was degassed with argon and then covered with argon to avoid O_2 establishing a mixed potential. Table 3.2.1 shows the results obtained:

Table 3.2.1 Measured Equilibrium Potentials for the Couple Fe^{2+}/Fe^{3+} in Ar Atmosphere*

$E_{stirring}$/mV vs. Ag,AgCl, sat'd KCl	E_{still}/mV vs. Ag,AgCl, sat'd KCl
534	534
534	534
535	535

* Solution was stirred 2 min, unstirred 2 min, stirred 2 min, etc.

Similar results reported in Table 3.2.2 were obtained with the couple Mn^{2+}/MnO_4^- in Ar atmosphere.

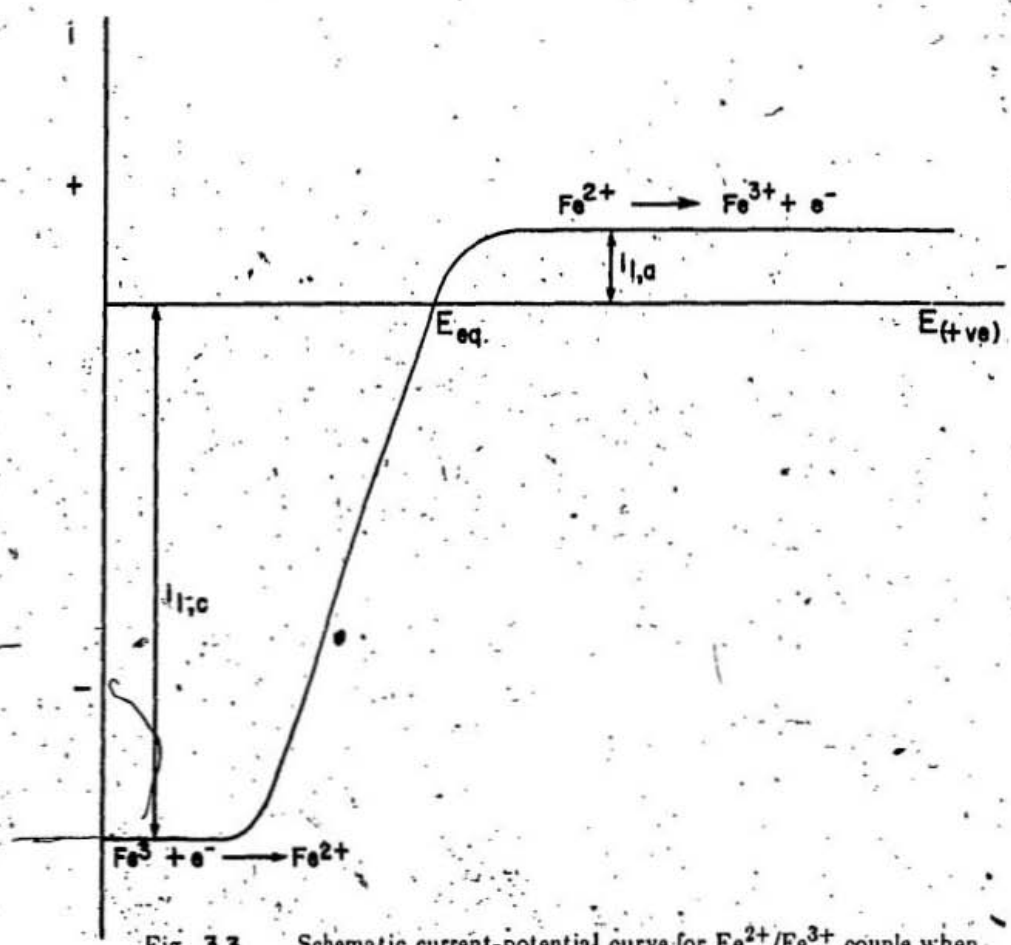

Fig. 3.3 Schematic current-potential curve for Fe^{2+}/Fe^{3+} couple when the titration is near but before equivalence.

Table 3.2.2 Measured Equilibrium Potentials for the Couple Mn^{2+}/MnO_4^- in Ar Atmosphere*

$E_{stirring}$/mV vs. Ag,AgCl, sat'd KCl	E_{still}/mV vs. Ag,AgCl, sat'd KCl
1229	1229
1228	1228
1228	1229

* Solution was stirred 2 min, unstirred 2 min, stirred 2 min, etc.

Both tables show that the equilibrium potentials do not change with stirring. The reason is that no current flows at the equilibrium potential. However the story will be different if we put the Fe^{2+}/Fe^{3+} and O_2/H_2O couples together. The mixed potential can be easily found in Fig. 3.4.

Figure 3.4 next page.

There is only one point, E_{mix}, at which no net current is flowing. The cathodic current is exactly balanced with the anodic current at the potential E_{mix}. This diagram illustrates two experimental observations;

1. The mixed potential E_{mix} is always larger than the single couple equilibrium potential measured under argon. Table 3.2.3 supports this idea in which the potentials are measured under otherwise identical conditions, i.e. concentration, temperature, stirring rate, etc.

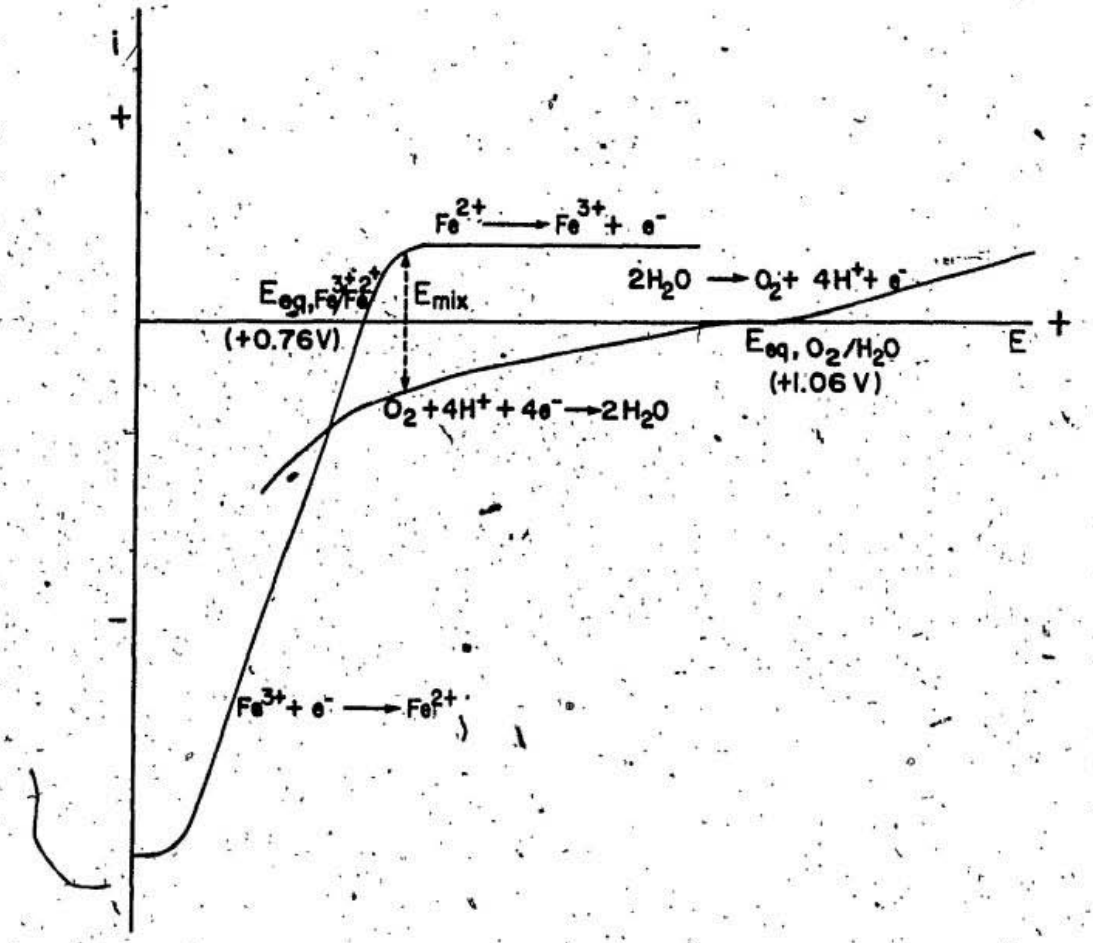

Fig. 3.4 Current-potential curve for two-couple system of Fe^{2+}/Fe^{3+} and O_2/H_2O under conditions before equivalence.

Table 3.2.3 Comparison of Potentials for the Couple Fe^{2+}/Fe^{3+} Measured in Open Air and Under Argon Atmosphere

In Open Air	In Argon
E/mV vs. Ag,AgCl, sat'd KCl	E/mV vs. Ag,AgCl, sat'd KCl
557, 559, 558, 557	541, 541, 541, 541
Average 558	Average 541

The equilibrium point for Fe^{2+}/Fe^{3+} will always be to the left of the mixed potential point according to Table 3.2.3 and Fig. 3.4.

2. When the solution is stirred the point E_{mix} will move further to the left. This can be illustrated using equation (3.2.5).

$$i_{l,a} = FAm_{Fe^{2+}} C^{\circ}_{Fe^{2+}} \qquad (3.2.5)$$

The relationship $m_R = K \frac{D_R}{\delta_R}$ exists under all conditions. It is easy to understand qualitatively that the greater the stirring of the solution the smaller the thickness δ_R so that as m_R increases the $i_{l,a}$ will increase also. This is the situation for the Fe^{2+},Fe^{3+} couple. Considering the O_2/H_2O couple, the $i_{mix,c}$ in Fig. 3.3 would change little with stirring because it is a very slow reaction, the determining step is not the diffusion but the charge transfer corresponding to its low exchange current density, about $j_o = 2.0 \times 10^{-10}$ A·cm^{-2}. The shift caused by stirring can be illustrated qualitatively in Fig. 3.5.

Figure 3.5 on next page.

The experimental data shows that in all the titrations $\Delta E = E_{stirring} - E_{still} < 0$

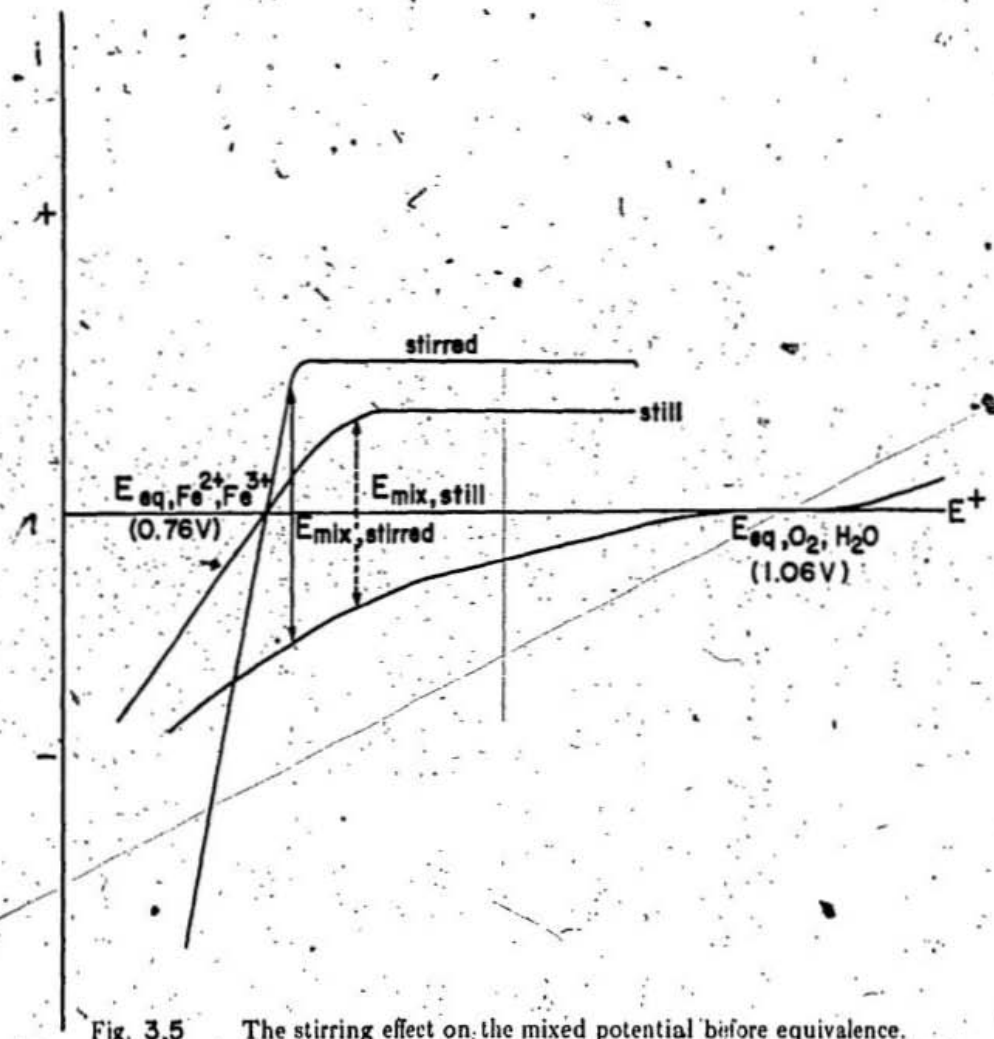

Fig. 3,5 The stirring effect on the mixed potential before equivalence.

before the end-point as expected from Fig. 3.5. A quantitative treatment for this shift will be presented in a later section.

3.3 The Situation Immediately after Equivalence

In this region of the titration two features are different from the region before equivalence. The first is that ΔE is always positive, whether or not the solution is open to the air or under an argon atmosphere, compared to the negative values observed before equivalence. The second is that the ΔE's eventually tend to zero far beyond equivalence.

The first feature may be explained by the generation of oxygen. Since the titration has passed equivalence, there is spare oxidant in the solution, for example, Ce^{4+}, MnO_4^-, or $Cr_2O_7^-$. They have such high oxidizing potentials that they could possibly react with water, *e.g.*, in the case of Ce^{4+}.

$$4Ce^{4+} + 4H_2O \rightleftharpoons O_2 + 4H^+ + 4Ce^{3+} \qquad (3.3.1)$$

Some oxygen is produced by the reaction, even though at a very low concentration, an equilibrium could be established in the absence of air and oxygen could be the component which together with another redox couple produces a mixed potential. Therefore, it may not matter if the solution is in air or in an inert atmosphere as long as there is water in the system.

The current-potential curve for the Ce^{3+}, Ce^{4+} couple would be as in Fig. 3.6. The different magnitudes of $i_{l,c}$ and $i_{l,a}$ are caused by the differing concentrations of Ce^{4+} and Ce^{3+}, recalling equations (3.2.3) and (3.2.4), the concentration of cerium(III) being greater than that of cerium(IV) near equivalence. The mixed potential established by the couples Ce^{3+}/Ce^{4+} and O_2/H_2O may be seen by putting their current-potential curves together as in Fig. 3.7.

Figures 3.6 and 3.7 on next pages.

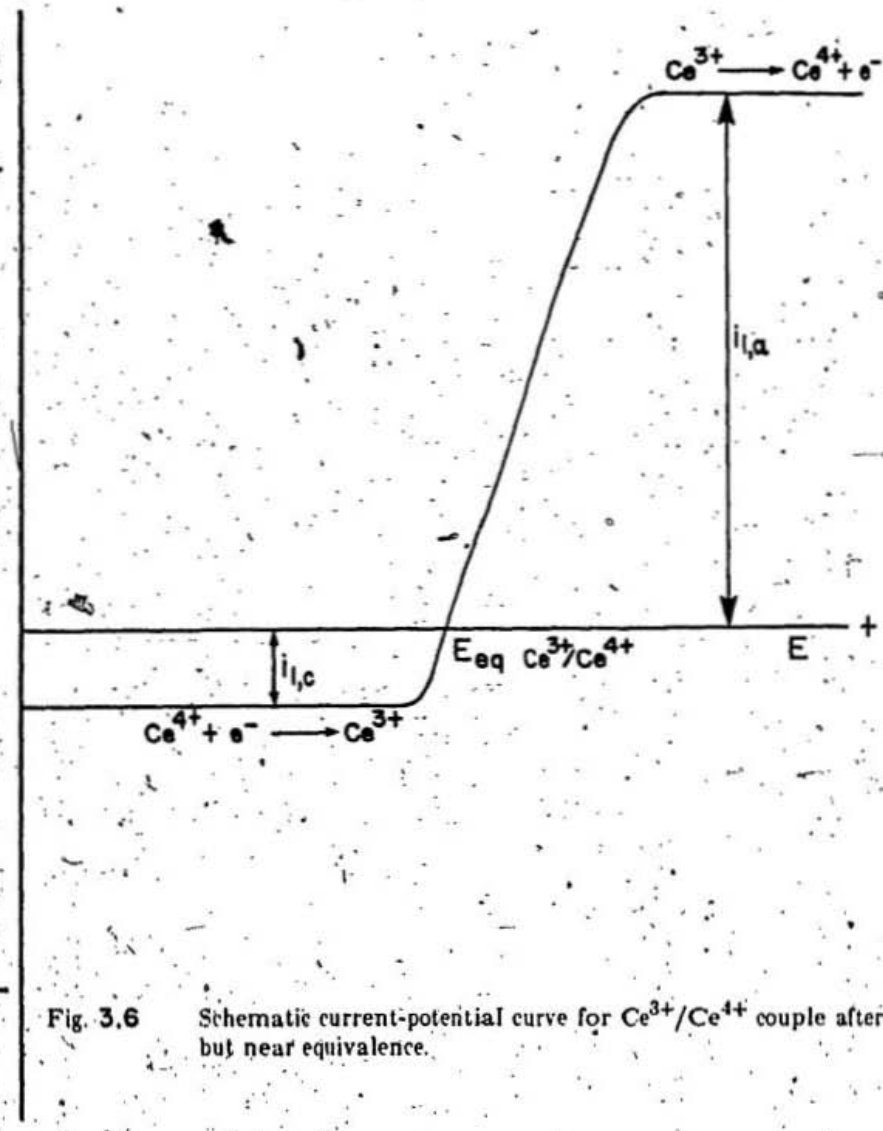

Fig. 3.6 Schematic current-potential curve for Ce^{3+}/Ce^{4+} couple after but near equivalence.

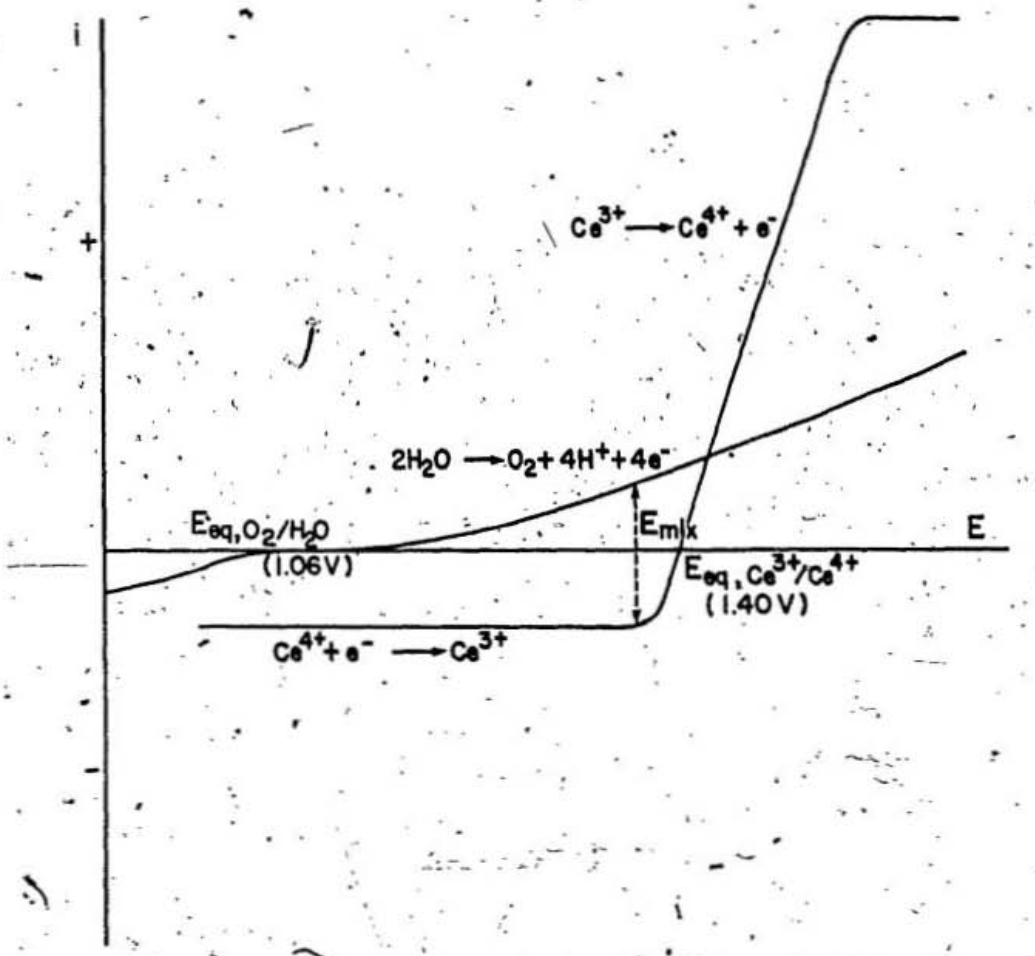

Fig. 3.7 Schematic diagram showing the mixed potential produced by Ce^{3+}/Ce^{4+} and O_2/H_2O couples.

The mixed potential is located between the equilibrium potentials of the O_2/H_2O couple and the Ce^{3+}/Ce^{4+} couple, in the range 1.00 V to 1.38 V vs. Ag,AgCl, sat'd KCl reference electrode.

In contrast to the case of Fe^{2+}/Fe^{3+} and H_2O/O_2 couples before equivalence, *when the solution is well stirred*, the mixed potential will shift to the right instead of to the left. Because stirring decreases the thickness of the diffusion layer δ_O and increases the surface concentration $C_{Ce^{4+}}$ (x=0), E_{mix} shifts to more positive values as observed. The E_{mix} shift is shown qualitatively in Fig. 3.8.

Figure 3.8 on next page.

Considering the mixed potentials in Fig. 3.7, E_{m2} is more positive than E_{m1} thus $\Delta E = E_{stirring} - E_{still} > 0$. They are positively signed. The data in Table 3.3.1 are taken from different measurements. They are about 0.2 ml added titrant beyond the end-point in each case.

Table 3.3.1 Data Showing the E_{mix} Shift to More Positive Values After the End-Point for the Couple Ce^{3+}/Ce^{4+} (from several sets of observations).

$E_{stirring}$/mV	E_{still}/mV	ΔE/mV
1072	1059	+13
1057	1045	+12
1072	1058	+14
1061	1025	+36
1071	1055	+16
1042	1019	+23
1057	1044	+13

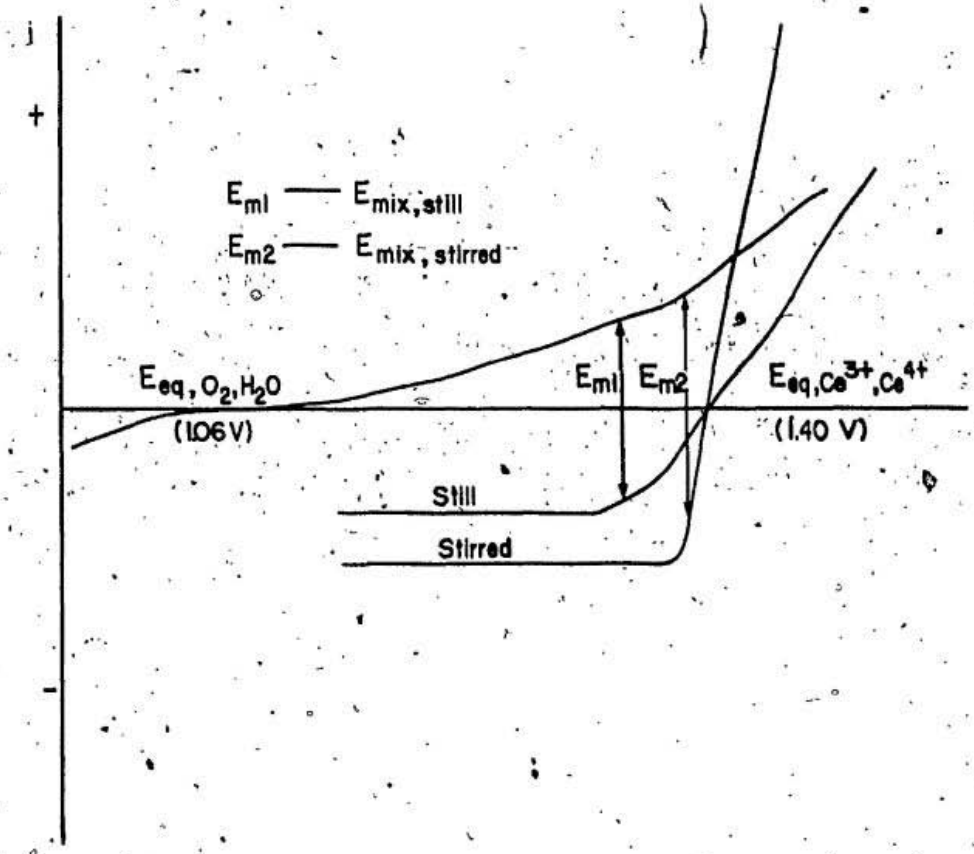

Fig. 3.8 The stirring effect on the mixed potential after equivalence.

The change of sign of ΔE can be explained schematically by comparing the mixed potentials before and after equivalence. Putting all the current-potential curves for Fe^{2+}/Fe^{3+}, Ce^{3+}/Ce^{4+} and O_2/H_2O couples together, we have the features shown in Fig. 3.9. Taken together with Fig. 3.5 and 3.8 the diagrams show that stirring can cause $E_{mix,b}$ to shift to less positive potentials so that $\Delta E = E_{stirring} - E_{still}$ becomes negative. They also show that stirring will shift $E_{mix,a}$ to more positive potentials so that $\Delta E = E_{stirring} - E_{still}$ becomes positive. When the potential is between the two mixed potential systems, the concentrations of both Fe^{2+} and Ce^{4+} are too small to establish a mixed potential. The situation will be that of Fig. 3.10 in which the limiting currents for Fe^{2+} oxidation and Ce^{4+} reduction are diminished to negligible values.

Figures 3.9 and 3.10 on next page.

From Fig. 3.10, the point E_{eq,O_2,H_2O} is the only zero current point. This is the situation of a single couple at equilibrium, with a potential independent of stirring. The O_2/H_2O couple might control the potential if its exchange current were large enough. Competition would, however, exist between this couple and the main redox couples Fe^{2+}/Fe^{3+} and Ce^{3+}/Ce^{4+}, controlling the potential in the classical Nernstian way ($E_{equivalence} = \frac{E^{o'}_{Fe^{2+},Fe^{3+}} + E^{o'}_{Ce^{3+},Ce^{4+}}}{2}$). Calculation of the equivalence concentrations of Fe^{2+} and Ce^{4+} is possible from the equilibrium constant of (3.2.2) and, since the rate constants of the two redox couples ($Fe^{2+} \rightarrow Fe^{3+} + e^-$ and $Ce(III) \rightarrow Ce(IV) + e^-$) are likely to be larger than that of the O_2/H_2O couple, the exchange currents for these reactions may exceed that of the latter by a large margin. It is concluded in a later section that the Nernst mechanism is the *actual mechanism of potential control at equivalence.*

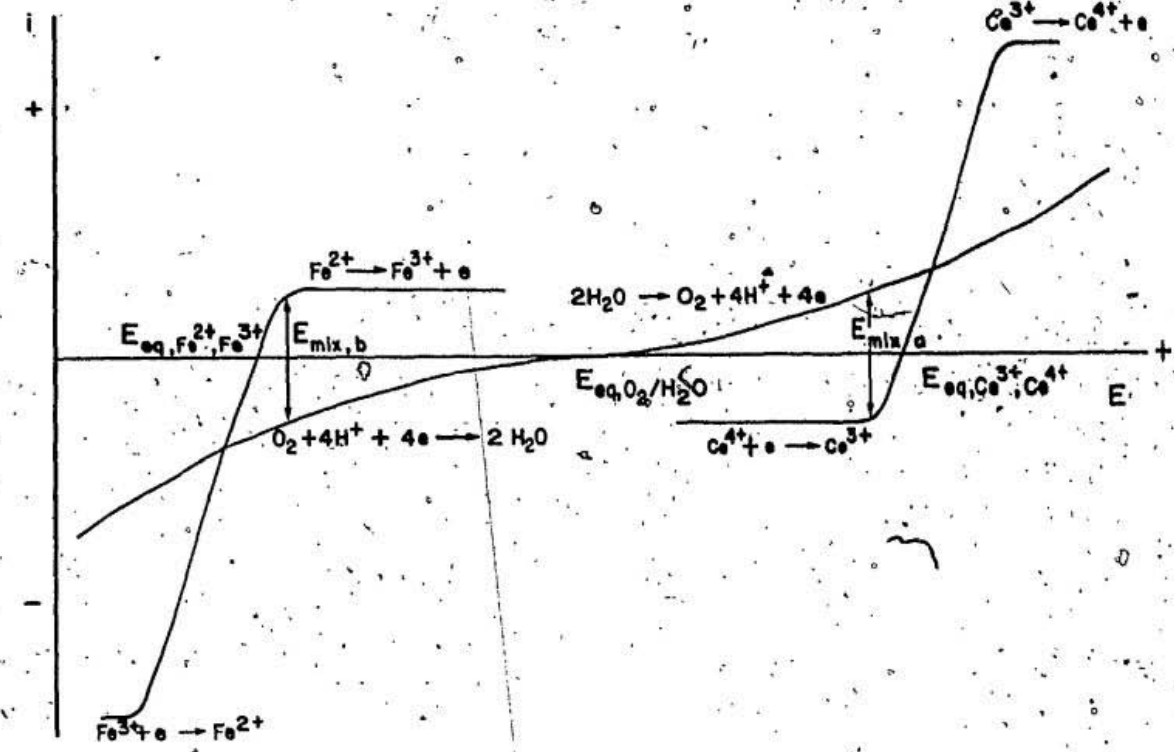

Fig. 3.9 The mixed potentials before and after equivalence.

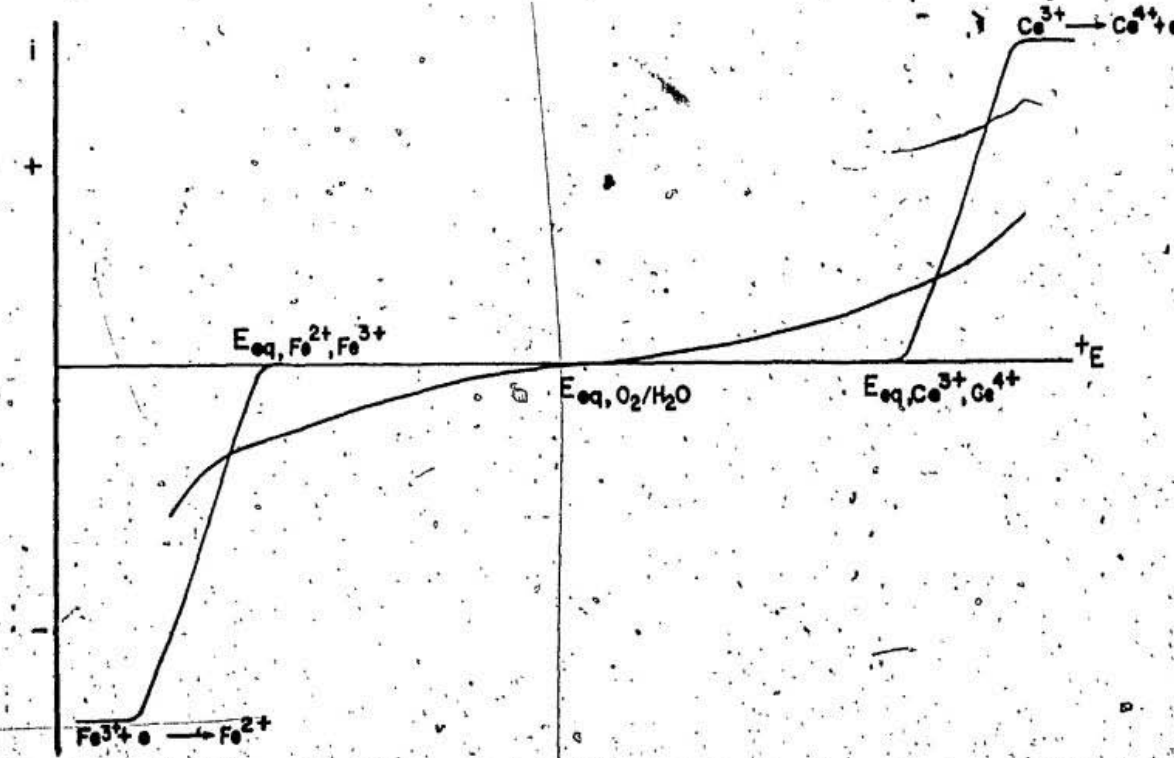

Fig. 3.10 Schematic diagram showing there is no mixed potential at equivalence.

3.4 Quantitative Treatment

(a) Before Equivalence:

The mixed potential discussed qualitatively above may also be treated quantitatively. Let us begin with the situation before equivalence in a potentiometric redox titration.

The treatment of the system having a mixed potential is based on the currents, $i_{mix,a}$ and $i_{mix,c}$ to be balanced at the mixed potential, E_{mix}, and the corresponding reactions are the anodic reaction

$$Fe^{2+} \rightleftharpoons Fe^{3+} + e^- \qquad (3.4.1)$$

and the cathodic reaction

$$O_2 + 4H^+ + 4e^- \rightleftharpoons 2H_2O \qquad (3.4.2)$$

The reaction (3.4.1) gives the current, $i_{mix,a}$, which is approximately proportional to the concentration difference $C^*_{Fe^{2+}} - C_{Fe}(x=0)$, where $C^*_{Fe^{2+}}$ is the bulk concentration and $C_{Fe^{2+}}(x=0)$ is the electrode surface concentration of Fe^{2+}, $m_{Fe^{2+}}$ is the mass transfer coefficient and A is the electrode surface area.

$$\frac{i_{mix,a}}{FA} = m_{Fe^{2+}} \left(C^*_{Fe^{2+}} - C_{Fe^{2+}}(x=0)\right) \qquad (3.4.3)$$

Combining equation (3.4.3) with (3.2.3) in the last section, we have with n=1 and appropriate substitutions

$$i_{mix,a} = i_{l,a}\left(\frac{C^*_{Fe^{2+}} - C_{Fe^{2+}}(x=0)}{C^*_{Fe^{2+}}}\right) \qquad (3.4.4)$$

The potential E_{mix} can be obtained from the Nernst equation by considering the concentrations of Fe^{2+} and Fe^{3+} at the surface of electrode.

$$E_{mix} = E^{o'}_{Fe^{2+},Fe^{3+}} - \frac{RT}{F} \ln\left[\frac{C_{Fe^{2+}}(x=0)}{C_{Fe^{3+}}(x=0)}\right] \qquad (3.4.5)$$

where $C_{Fe^{3+}}(x=0)$ is the concentration of Fe^{3+} near the electrode surface. There is another relationship between $C_{Fe^{2+}}(x=0)$ and $C_{Fe^{3+}}(x=0)$ which is useful in this case. The current $i_{mix,a}$ can also be expressed in terms of the concentration gradient of Fe^{3+} as:

$$\frac{i_{mix,a}}{FA} = - m_{Fe^{3+}} (C^{*}_{Fe^{3+}} - C_{Fe^{3+}}(x=0)) \qquad (3.4.6)$$

Combining it with (3.4.3),

$$m_{Fe^{2+}} (C^{*}_{Fe^{2+}} - C_{Fe^{2+}}(x=0)) = m_{Fe^{3+}} (C_{Fe^{3+}}(x=0) - C^{*}_{Fe^{3+}}) \qquad (3.4.7)$$

If we assume the mass transfer coefficients for Fe^{2+} and Fe^{3+} are identical we then get

$$C_{Fe^{2+}}(x=0) + C_{Fe^{3+}}(x=0) = C^{*}_{Fe^{2+}} + C^{*}_{Fe^{3+}} = C_T \qquad (3.4.8)$$

where C_T is the total bulk concentration of Fe^{2+} and Fe^{3+} in the solution. In the case of a titration approaching but before equivalence, the bulk concentrations would be $C^{*}_{Fe^{3+}} >> C^{*}_{Fe^{2+}}$ for a reaction $Fe^{2+} \rightarrow Fe^{3+} + e^{-}$. We have the comparisons: $C_{Fe^{3+}}(x=0) > C^{*}_{Fe^{3+}}$ and $C^{*}_{Fe^{2+}} > C_{Fe^{2+}}(x=0)$. The overall comparison series would be

$$C_{Fe^{3+}}(x=0) > C^{*}_{Fe^{2+}} >> C^{*}_{Fe^{2+}} > C_{Fe^{2+}}(x=0) \qquad (3.4.9)$$

Obviously the first concentration in (3.4.9) must be much greater than the last term, *i.e.*

$$C_{Fe^{3+}}(x=0) >> C_{Fe^{2+}}(x=0) \qquad (3.4.10)$$

As an approximation,

$$C_T = C_{Fe^{2+}}(x=0) + C_{Fe^{2+}}(x=0) \sim C_{Fe^{3+}}(x=0) \qquad (3.4.11)$$

Substitute equation (3.4.11) into (3.4.5)

$$E_{mix} = E^{o'}_{Fe^{2+},Fe^{3+}} - \frac{RT}{F} \ln \left[\frac{C_{Fe^{2+}}(x=0)}{C_T} \right] \qquad (3.4.12)$$

The surface concentration $C_{Fe^{2+}}$ (x=0) can be found from rearrangement:

$$C_{Fe^{2+}}(x=0) = C_T \exp\left[\frac{F}{RT}\left(E^{o'}_{Fe^{2+},Fe^{3+}} - E_{mix}\right)\right] \qquad (3.4.13)$$

In order to eliminate the surface concentration term, equations (3.4.13) and (3.4.4) are combined to give an equation

$$i_{mix,a} = i_{l,a}\left[1 - \frac{C_T}{C^*_{Fe^{2+}}} \exp\left\{\frac{F}{RT}\left(E^{o'}_{Fe^{2+},Fe^{3+}} - E_{mix}\right)\right\}\right] \qquad (3.4.14)$$

At the mixed potential, the two currents $i_{mix,a}$ and $i_{mix,c}$ have the same magnitude but flow in opposite directions, *i.e.*,

$$i_{mix,a} + i_{mix,c} = 0 \qquad (3.4.15)$$

The current $i_{mix,c}$ can be found in a different way. For the O_2/H_2O couple, the mixed potential is far away from its equilibrium value. The Tafel equation can be used as follows[17]:

$$i_{mix,c} = -j_o A \exp\left\{\frac{\alpha n F}{RT}\left(E^{o'}_{O_2} - E_{mix}\right)\right\} \qquad (3.4.16)$$

where j_o is the exchange current density for the O_2/H_2O couple, α is the anodic transfer coefficient and n is the number of electrons transferred, here being 4.

By substituting equations (3.4.16), (3.4.14) into (3.4.15)

$$i_{l,a}\left[1 - \frac{C_T}{C^*_{Fe^{2+}}} \exp\left\{\frac{F}{RT}\left(E^{o'}_{Fe^{2+},Fe^{3+}} - E_{mix}\right)\right\}\right] =$$

$$j_o A \exp\left[\frac{4\alpha F}{RT}\left(E^{o'}_{O_2} - E_{mix}\right)\right] \qquad (3.4.17)$$

Rearranging equation (3.4.17)

$$A\frac{j_o}{i_{l,a}} e^{4\alpha\frac{F}{RT}E^{o'}_{O_2}} \cdot e^{-4\alpha\frac{F}{RT}E_{mix}} = 1 - \frac{C_T}{C^*_{Fe^{2+}}} e^{\frac{F}{RT}E^{o'}_{Fe^{2+}}} \cdot e^{-\frac{F}{RT}E_{mix}} \qquad (3.4.18)$$

To simplify equation (3.4.18), let

$$A \frac{j_o}{i_{l,a}} e^{4\alpha \frac{F}{RT} E^o_{O_2}} = a \; ; \qquad (3.4.19)$$

and

$$\frac{C_T}{C^*_{Fe^{2+}}} e^{\frac{F}{RT} E^o_{Fe^{2+},Fe^{3+}}} = b \; ; \qquad \frac{F}{RT} = f$$

Substitute (3.4.19) into equation (3.4.18)

$$a\, e^{-4\alpha f E_{mix}} = 1 - b\, e^{-f E_{mix}} \qquad (3.4.20)$$

Divide (3.4.20) by $e^{-f E_{mix}}$ to give

$$a\, e^{(1-4\alpha) f E_{mix}} - e^{f E_{mix}} + b = 0 \qquad (3.4.21)$$

This is a transcendental equation. It can be solved either by numerical solution with a computer or under the special condition in which the constant α has a certain value. The cathodic transfer coefficient $1 - \alpha$ for the couple O_2/H_2O cannot be obtained from our measurements but Spiro and Ravno[17] give the Tafel slopes for 20 ° C.

$$b_c = 2.303\, \nu_s\, RT/nF(1-\alpha) = 0.11\ V \qquad (3.4.22)$$

$$b_a = 2.303\, \nu_s\, RT/nF\alpha = 0.09\ V \qquad (3.4.23)$$

where the stoichiometric number $\nu_s = (2.303\ RT/4F)(b_a^{-1} - b_c^{-1})$ and b_c is the Tafel slope for the cathodic branch and b_a is the Tafel slope for the anodic branch. The anodic transfer coefficient can then be obtained from (3.4.22) using $\nu_s = 3.68$ from Hoare[19]

$$\alpha = \frac{2.303 \bullet 3.68 \bullet 8.314 \bullet 293.2}{4 \bullet 96500 \bullet 0.09} = 0.59 \pm 0.06 \qquad (3.4.24)$$

If we assume $\alpha = 0.5$, equation (3.4.21) can be simplified as

$$a\, e^{-f E_{mix}} - e^{f E_{mix}} + b = 0 \qquad (3.4.25)$$

let $x = e^{f E_{mix}}$,

$$a\, x^{-1} - x + b = 0 \qquad (3.4.26)$$

rearrange (3.4.26) and multiply both sides by -x

$$x^2 - b\, x - a = 0 \qquad (3.4.27)$$

It can be easily solved since

$$x = \frac{b \pm \sqrt{b^2 + 4a}}{2} \qquad (3.4.28)$$

Returning to $e^{f E_{mix}} = x$

$$e^{f E_{mix}} = \frac{1}{2}\left[b \pm \sqrt{b^2 + 4a}\right] \qquad (3.4.29)$$

Take logarithms of both sides:

$$f E_{mix} = \ln \frac{1}{2} + \ln (b \pm \sqrt{b^2 + 4a}) \qquad (3.4.30)$$

To decide the sign before the square root, the value in the brackets in (3.4.30) must be positive to give a real solution for E_{mix}, that is

$$b \pm \sqrt{b^2 + 4a} \geq 0 \qquad (3.4.31)$$

Apparently, whether the inequality is tenable is decided by the value of a, recall (3.4.19)

$$a = \frac{j_o A}{i_{l,a}} e^{4\alpha \frac{F}{RT} E_{\delta_2}} \qquad (3.4.19)$$

Substituting:

$$i_{l,a} = F A m_{Fe^{2+}} C^{\circ}_{Fe^{2+}} \qquad (3.2.5)$$

into (3.4.19)

$$a = \frac{j_o}{Fm_{Fe^{2+}}C^*_{Fe^{2+}}} e^{4\alpha\frac{F}{RT}E^{\circ}_{\delta_2}} \qquad (3.4.32)$$

Since all the parameters in equation (3.4.32) have positive sign, we have $a > 0$ and $a \neq 0$. Therefore

$$\sqrt{b^2 + 4a} > b \qquad (3.4.33)$$

Hence the $b - \sqrt{b^2 + 4a}$ is an impossible solution for equation (3.4.27) the only possible solution being

$$x = \frac{b + \sqrt{b^2 + 4a}}{2} \qquad (3.4.34)$$

Rewrite (3.4.34)

$$E_{mix} = \frac{RT}{F} \ln \frac{1}{2} + \frac{RT}{F} \ln (b + \sqrt{b^2 + 4a}) \qquad (3.4.35)$$

substitute (3.4.19), (3.4.32) to (3.4.35)

$$E_{mix} = \frac{RT}{F}\ln\frac{1}{2} + \frac{RT}{F}\ln\left[\frac{C_T}{C^*_{Fe^{2+}}} e^{\frac{F}{RT}E^{\circ}_{Fe^{2+},Fe^{3+}}} + \left\{\left(\frac{C_T}{C^*_{Fe^{2+}}} e^{\frac{F}{RT}E^{\circ}_{Fe^{2+},Fe^{3+}}}\right)^2 + \frac{4j_o}{Fm_{Fe^{2+}}C^*_{Fe^{2+}}} e^{\frac{4\alpha F}{RT}E^{\circ}_{\delta_2}}\right\}^{\frac{1}{2}}\right] \qquad (3.4.36)$$

This equation looks very complicated, but the only parameters that should change with stirring are $m_{Fe^{2+}} = \frac{D_{Fe^{2+}}}{\delta_{Fe^{2+}}}$ and possibly j_o for the O_2/H_2O couple. It has been mentioned in the previous section that j_o for O_2/H_2O is very small, about 2×10^{-10} $A \cdot cm^{-2}$, *i.e.* it is a charge transfer controlled reaction, relatively independent of mass transfer, so that stirring effects on it can be ignored compared with the change of anodic current $\Delta i_{l,a} = FAC^*_{Fe^{2+}}\Delta(\frac{D_{Fe^{2+}}}{\delta_{Fe^{2+}}})$. Apparently, when the solution is stirred,

$m_{Fe^{2+}}$ must increase since the diffusion layer is thinner than the diffusion layer in still solution. Therefore the term $\frac{4j_o}{Fm_{Fe^{2+}}C^*_{Fe^{2+}}} e^{\frac{4\alpha F}{RT}E^{\ominus}_{O_2}}$ should decrease when the solution is stirred so that the overall effect of stirring is to decrease the mixed potential. This has been seen in the titration experiments detailed in the earlier chapter.

A numerical solution of equation (3.4.21) without assuming α to be 0.5 shows a similar relation between E_{mix} and $m_{Fe^{2+}}$ as in Fig. 3.11 for α ranging from 0.3 to 0.7.

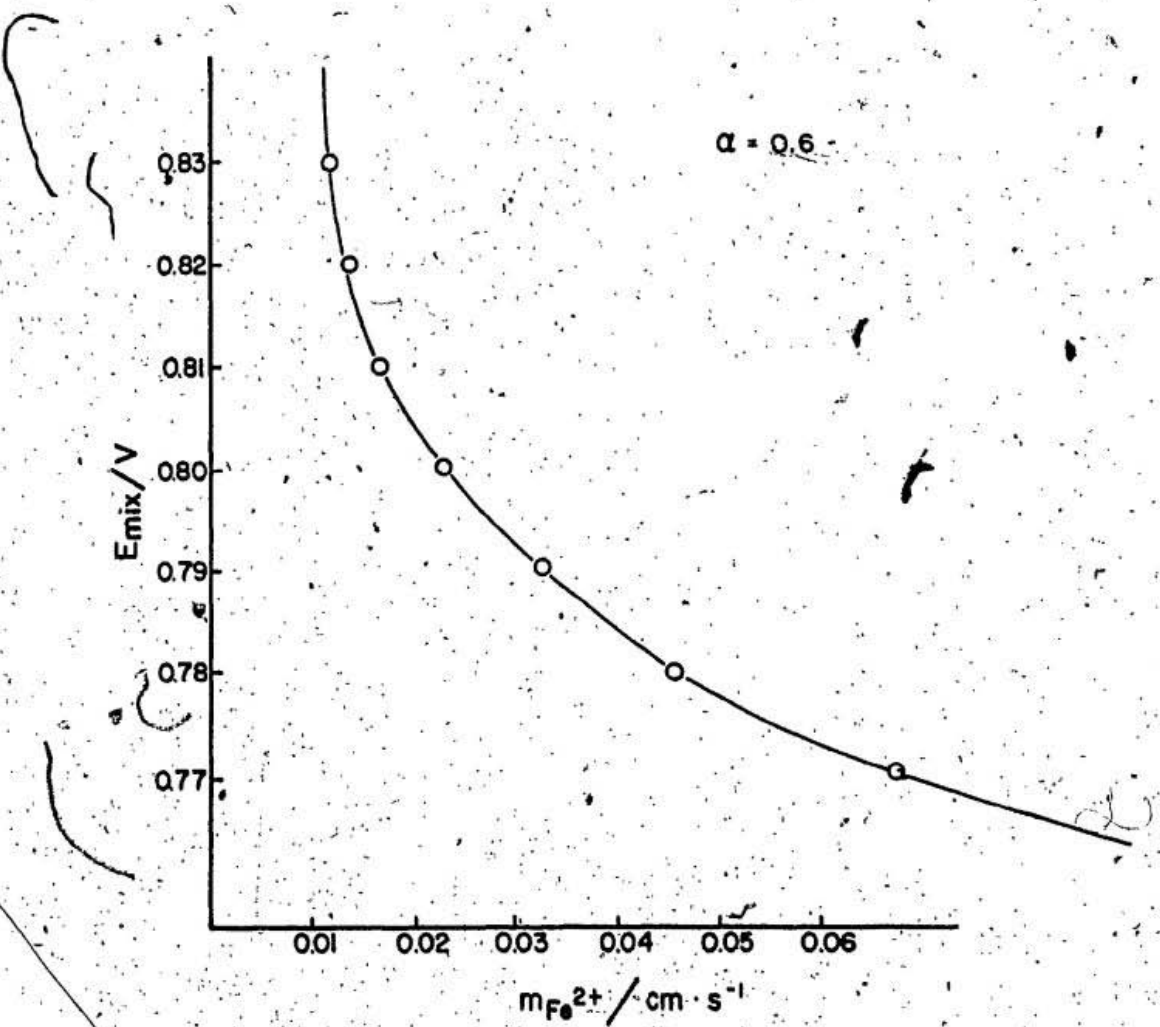

Fig. 3.11 The relation between E_{mix} and $m_{Fe^{2+}}$

A more precise experiment was carried out with a rotating disc electrode. The mixed potential change and the rotation speed were recorded simultaneously with a X-Y recorder and the rotation speed changed from zero to about 2500 rpm within 10 seconds.

With the rotating disc electrode, the Levich equation can be applied to equation (3.4.36). Equation (3.2.5) would become

$$i_{l,a} = FAD_{Fe^{2+}}^{\frac{2}{3}} \nu^{-\frac{1}{6}} C_{Fe^{2+}}^{*} \omega^{\frac{1}{2}} \qquad (3.4.37)$$

where $D_{Fe^{2+}}$ is the diffusion coefficient of Fe^{2+} ions, ν is the kinematic viscosity of water and ω is the rotation speed in radians per second. Equation (3.4.36) will become

$$E_{mix} = \frac{RT}{F}\ln\frac{1}{2} + \frac{RT}{F}\ln\left[\frac{C_T}{C_{Fe^{2+}}^{*}} e^{f E^{\circ}_{Fe^{2+},Fe^{3+}}} + \left\{\left(\frac{C_T}{C_{Fe^{2+}}^{*}} e^{f E^{\circ}_{Fe^{2+},Fe^{3+}}}\right)^2 + \frac{4 j_o e^{4\alpha f E^{\circ}_{\delta_2}}}{F D_{Fe^{2+}}^{\frac{2}{3}} \nu^{-\frac{1}{6}} C_{Fe^{2+}}^{*} \omega^{\frac{1}{2}}}\right\}^{\frac{1}{2}}\right] \qquad (3.4.38)$$

The measured potential E_{mix} decreased with increase of rotation speed. In order to find a simple relationship from equation (3.4.38) further approximation has to be made by comparing the values of the term in the square root and rearranging. Replace $\frac{C_T}{C_{Fe^{2+}}} e^{f E^{\circ}_{Fe^{2+},Fe^{3+}}}$ by b and substitute $i_{l,a}$ back and rearrange (3.4.38) to give

$$E_{mix} = \frac{RT}{F}\ln\frac{1}{2} + \frac{RT}{F}\ln\left\{b + \left(b^2 + \frac{4 j_o e^{4\alpha f E^{\circ}_{\delta_2}}}{i_{l,a}}\right)^{\frac{1}{2}}\right\} \qquad (3.4.39)$$

Taking b out of the second term on the right gives

$$E_{mix} = \frac{RT}{F} \ln \frac{b}{2} + \frac{RT}{F} \ln \left\{ 1 + \left[1 + \frac{4 j_o e^{4\alpha f E^{o'}_{O_2}}}{i_{l,a} \left[\frac{C_T}{C^*_{Fe^{2+}}} e^{f E^{o'}_{Fe^{2+},Fe^{3+}}} \right]^2} \right]^{\frac{1}{2}} \right\} \quad (3.4.40)$$

In our case $C_T = C^*_{Fe^{2+}} + C^*_{Fe^{3+}} \sim 0.01$ mol·L^{-1}, and if for example $C^*_{Fe^{2+}} = \frac{1}{10} C_T$, then $\frac{C_T}{C^*_{Fe^{2+}}} = 10$. Rewrite (3.4.40)

$$E_{mix} = \frac{RT}{F} \ln \frac{b}{2} + \frac{RT}{F} \ln \left\{ 1 + \left[1 + \frac{4 j_o e^{(4\alpha f E^{o'}_{O_2} - 2 f E^{o'}_{Fe^{2+},Fe^{3+}})}}{10^2 i_{l,a}} \right]^{\frac{1}{2}} \right\} \quad (3.4.41)$$

Assume $\alpha = 0.5$ again and substitute:

$$f = \frac{F}{RT} = \frac{96485}{8.314 \bullet 293.2} = 39.58 \text{ V}^{-1},$$

$E^{o'}_{O_2} = 1.06$ V and $E^{o'}_{Fe^{2+},Fe^{3+}} = 0.68$ V into (3.4.41) giving

$$E_{mix} = \frac{RT}{F} \ln \frac{b}{2} + \frac{RT}{F} \ln \left\{ 1 + \left[1 + \frac{4 j_o e^{30.08}}{10^2 i_{l,a}} \right]^{\frac{1}{2}} \right\} \quad (3.4.42)$$

With j_o of 2×10^{-10} A·cm^2 and $i_{l,a}$ approximately 250 μA under our experimental conditions, the value in the square brackets will be $\left[1 + (1 + 3.7 \times 10^5)^{\frac{1}{2}} \right]$. Since $3.7 \times 10^5 \gg 1$ and its square root 610 $\gg 1$ the most significant term in equation (3.4.38) is that containing j_o and $i_{l,a}$ so that it may be simplified without causing much error:

$$E^{'}_{mix} = \frac{RT}{F} \ln \left(\frac{C_T}{2 C^*_{Fe^{2+}}} e^{f E^{o'}_{Fe^{2+},Fe^{3+}}} \right) + \frac{RT}{2F} \ln \left(\frac{4 j_o e^{2f(2\alpha E^{o'}_{O_2} - E^{o'}_{Fe^{2+},Fe^{3+}})}}{F D^{\frac{2}{3}}_{Fe^{2+}} \nu^{-\frac{1}{6}} C^2_T (C^*_{Fe^{2+}})^{-1}} \right) - \frac{RT}{4F} \ln \omega \quad (3.4.43)$$

Therefore E_{mix} should decrease when the rotation speed ω increases with the use of a rotating disc electrode. Fig. 3.12 is a plot from the X - Y recorder. The mixed potential decreased with increase of rotating speed. Furthermore, plotting the curve of Fig. 3.12 as logarithm of rotation speed, a fairly good linear relation is found in Fig. 3.13, giving experimental support to the theoretical treatment above. Equation (3.4.43) predicts a negative slope of the E_{mix} vs ln ω plot of $\frac{RT}{4F}$ which at 20 ° C has the value -0.0063 V per unit increment of ln ω. The experimental slope from Fig. 3.13 is -0.008 V which is quite good agreement.

Figures 3.12 and 3.13 on next page.

(b) After Equivalence:

In order to treat the titration after equivalence, the formal potential for the couple: $O_2 + 4H^+ + 4e^- \rightleftharpoons 2H_2O$ needs to be discussed. The measurement of the standard potential of the O_2/H_2O couple has a long story[19]. The standard potential for this couple was calculated from thermodynamic data. It should be 1.229 V vs. SHE but nobody obtained this value in an electrochemical system until recent years because the solution used in the measurement had to be extremely pure. Instead, the formal equilibrium potential of O_2/H_2O couple is usually observed to be about 1.06 V, without special preparation. Under our experimental conditions, the reagents and water were not specially prepared so that the formal potential is taken to be 1.06 V. The equilibrium potential for the couple O_2/H_2O at 25 ° C is.

$$E_{eq,O_2/H_2O} = 1.06 + \frac{0.059}{4} \log_{10} P_{O_2} \quad V \qquad (3.4.44)$$

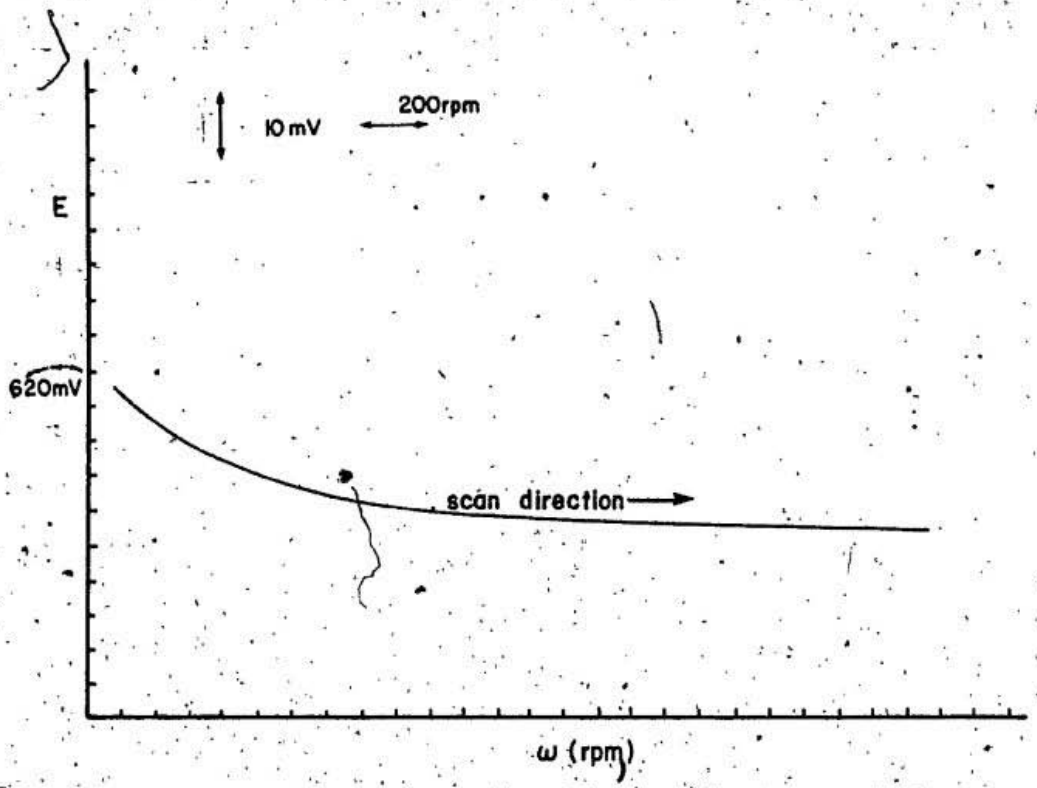

Fig. 3.12 The measured potential changes with rotating speed before the end-point.

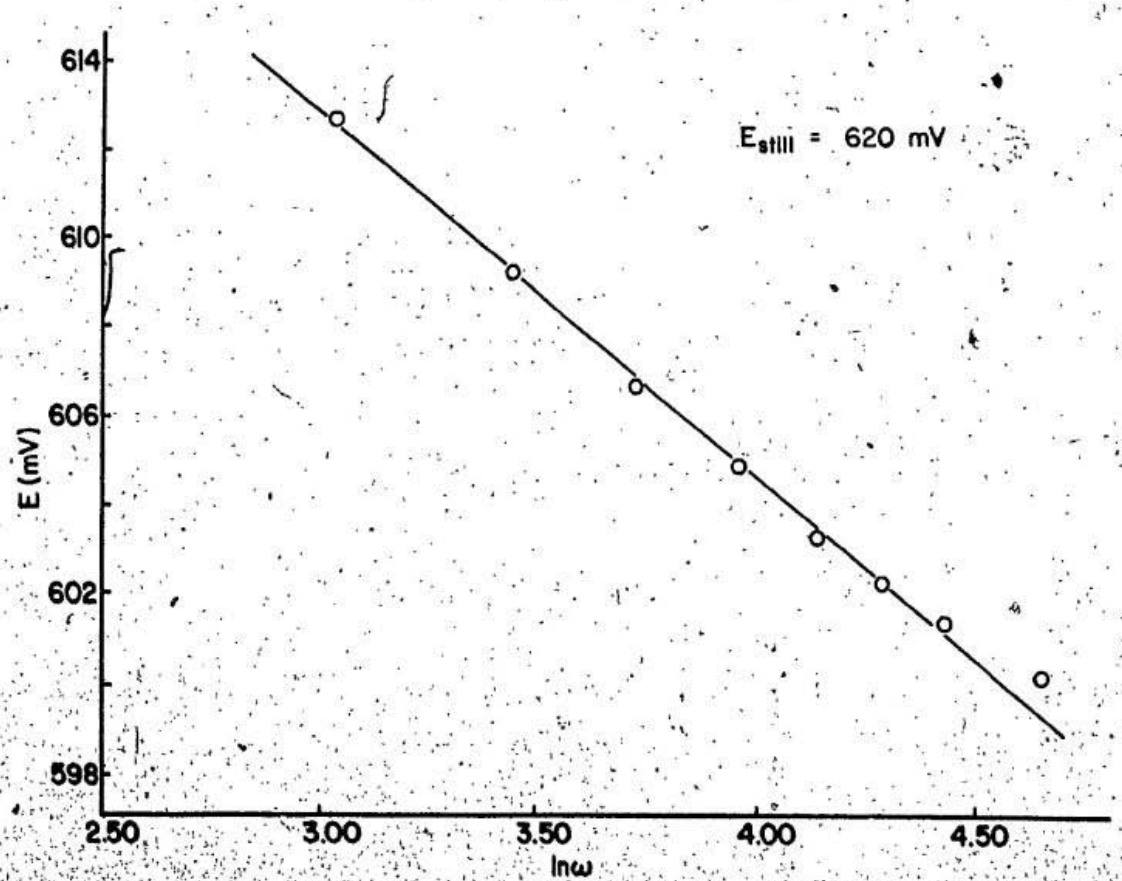

Fig. 3.13 A plot of E vs lnω BEFORE END-POINT

Thus the potential $E_{eq,O_2/H_2O}$ is close to 1.06 V since the last term on the right hand side contributes little even when the partial pressure of oxygen, P_{O_2}, is significantly different from standard pressure. According to the experimental data presented in the last chapter, the average potential found when $\Delta E > 0$ is about 1.0 V vs. Ag,AgCl, saturated KCl reference (or 1.0 V + 0.21 V = 1.21 V vs. SHE). This point is about 0.2 V above the formal potential of the O_2/H_2O couple, i.e. the overpotential $\eta \sim 0.2$ V. The reaction

$$H_2O \longrightarrow O_2 + 4H^+ + 4e^- \qquad (3.4.45)$$

gives the anodic current to balance the cathodic current of the reaction:

$$Ce^{4+} + e^- \longrightarrow Ce^{3+} \qquad (3.4.46)$$

The net anodic current of oxygen evolution can be obtained from equation (3.1.8).

$$i_a = j_o A(e^{+4\alpha f\eta} - e^{-(1-\alpha)4f\eta}) \qquad (3.4.47)$$

If we assume $\alpha = 0.5$, equation (3.4.47) could be simplified for an overpotential of 0.2 V:

$$i_a = j_o A(e^{+0.5 \times 4 \times 39.58 \times 0.2} - e^{-0.5) \times 4 \times 39.58 \times 0.2})$$

$$\sim 2 \times 10^{-10} A(e^{15.83} - e^{-15.83}) \sim 1.5 \times 10^{-3} \text{ amperes}$$

Since the first term in brackets is much larger than the second one, (3.4.47) can be simplified to

$$i_a = j_o A\, e^{4\alpha f\eta} \qquad (3.4.48)$$

This has the form of the Tafel equation. For the case of a 4-electron reaction, a very small overpotential can make one of the terms in the brackets quickly negligible. For instance for the first term $e^{\alpha nf\eta}$ to be 100 times greater than the second term $e^{-(1-\alpha)nf\eta}$, how much overpotential is necessary?

$$\frac{\text{last term}}{\text{first term}} = \frac{e^{0.5 \bullet 4 \bullet 39.58 \bullet \eta}}{e^{-0.5 \bullet 4 \bullet 39.58 \bullet \eta}} = 100$$

then

$$\eta = \frac{\ln 100}{2 \bullet 0.5 \bullet 4 \bullet 39.58} = 0.029 \text{ V} \qquad (3.4.49)$$

Equation (3.4.49) implies that the Tafel equation can be used for any 4-electron reaction with an overpotential of only 0.029 V. This is also the reason the Tafel equation could be used in the treatment of O_2 reduction in the titration before equivalence.

Substitute $E_{mix} - E_{eq,O_2,H_2O} = \eta$ into (3.4.48) and solve for E_{mix}

$$E_{mix} = E_{eq,O_2,H_2O} + \frac{RT}{4\alpha F} \ln (+i_a) - \frac{RT}{4\alpha F} \ln j_o A \qquad (3.4.50)$$

where i_a has a positive value according to our convention. To find the cathodic current, two factors have to be considered:

1. Immediately beyond equivalence, the concentration of Ce^{4+} is very low so that the cathodic current i_c could be very close to the limiting current $i_{l,c}$
2. The potential immediately beyond equivalence is about 0.15 V less positive than the equilibrium potential of the Ce^{3+}/Ce^{4+} couple. We first approximate that

$$i_c \sim i_{l,c} = FAm_{Ce^{4+}} C^*_{Ce^{4+}} \qquad (3.4.51)$$

At the mixed potential the two currents are balanced so that we have

$$i_a + i_c = 0 \qquad (3.4.52)$$

Substitute (3.4.51) into (3.4.50)

$$E_{mix} = E_{eq,O_2,H_2O} - \frac{RT}{4\alpha F} \ln j_o A + \frac{RT}{4\alpha F} \ln \frac{FAD_{Ce^{4+}} C^*_{Ce^{4+}}}{\delta} \qquad (3.4.53)$$

In this case, when the solution is stirred, the diffusion layer thickness δ decreases and the third term on the right increases; therefore the mixed potential E_{mix} should increase as observed in the experiment. This is opposite to the phenomenon in the titration before equivalence.

A more precise experiment was also carried out using a rotating disc electrode so that the Levich equation for the limiting current can be substituted in (3.4.50).

$$E_{mix} = E_{eq,O_2,H_2O} - \frac{RT}{4\alpha F} \ln j_o A + \frac{RT}{4\alpha F} \ln 0.62\, F A D_{Ce^{4+}}^{\frac{2}{3}} \nu^{-\frac{1}{6}} C_{Ce^{4+}}^{*} \omega^{\frac{1}{2}} \qquad (3.4.54)$$

Rearranging (3.4.54) we have

$$E_{mix} = E_{eq,O_2,H_2O} - \frac{RT}{4\alpha F} \ln j_o A + \frac{RT}{4\alpha F} \ln 0.62\, F A D_{Ce^{4+}}^{\frac{2}{3}} \nu^{-\frac{1}{6}} C_{Ce^{4+}}^{*} + \frac{RT}{8\alpha F} \ln \omega \qquad (3.4.55)$$

The mixed potential E_{mix} should increase linearly with $\ln \omega$ as is seen in the following diagrams. Plotting data as a function of the logarithm of rotation speed a linear relation between the mixed potential and $\ln \omega$ is found in Fig. 3.15, giving experimental support to the theoretical treatment. According to equation (3.4.55) a positive slope of the E_{mix} vs $\ln \omega$ plot of $\frac{RT}{8\alpha F}$ is predicted, which at 20 °C is $+(0.00315/\alpha)$ V. Experimentally, Fig. 3.15 yields a slope of +0.012 V suggesting α is about 0.25, a possible value.

Figures 3.14 and 3.15 on next page.

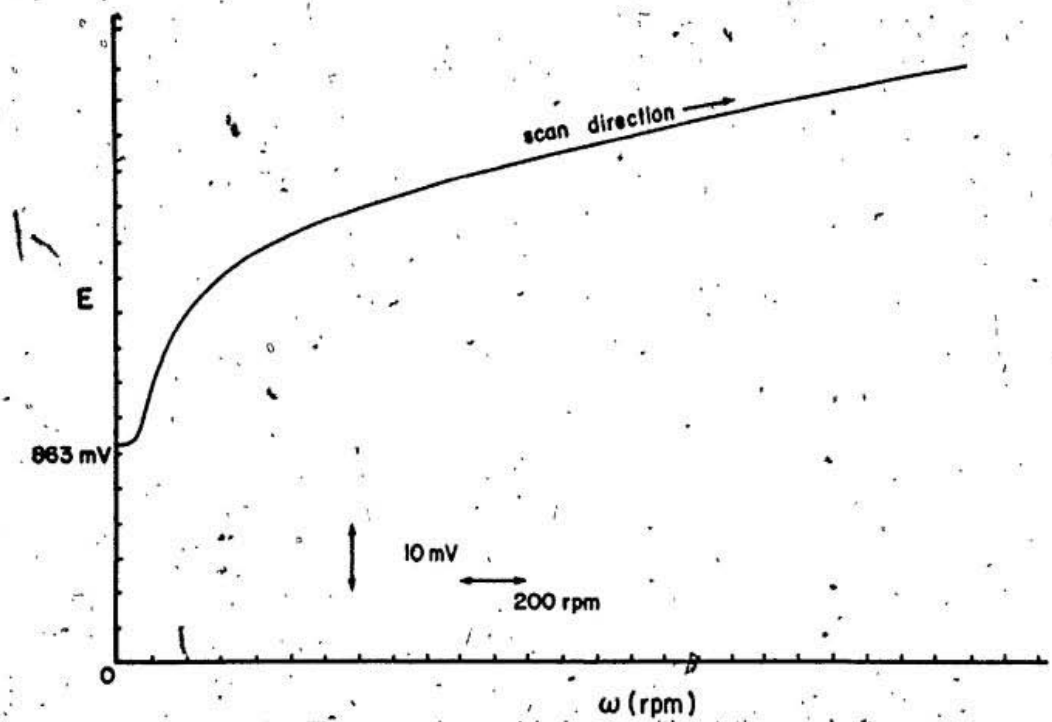

Fig. 3.14. The measured potential changes with rotating speed after end-point.

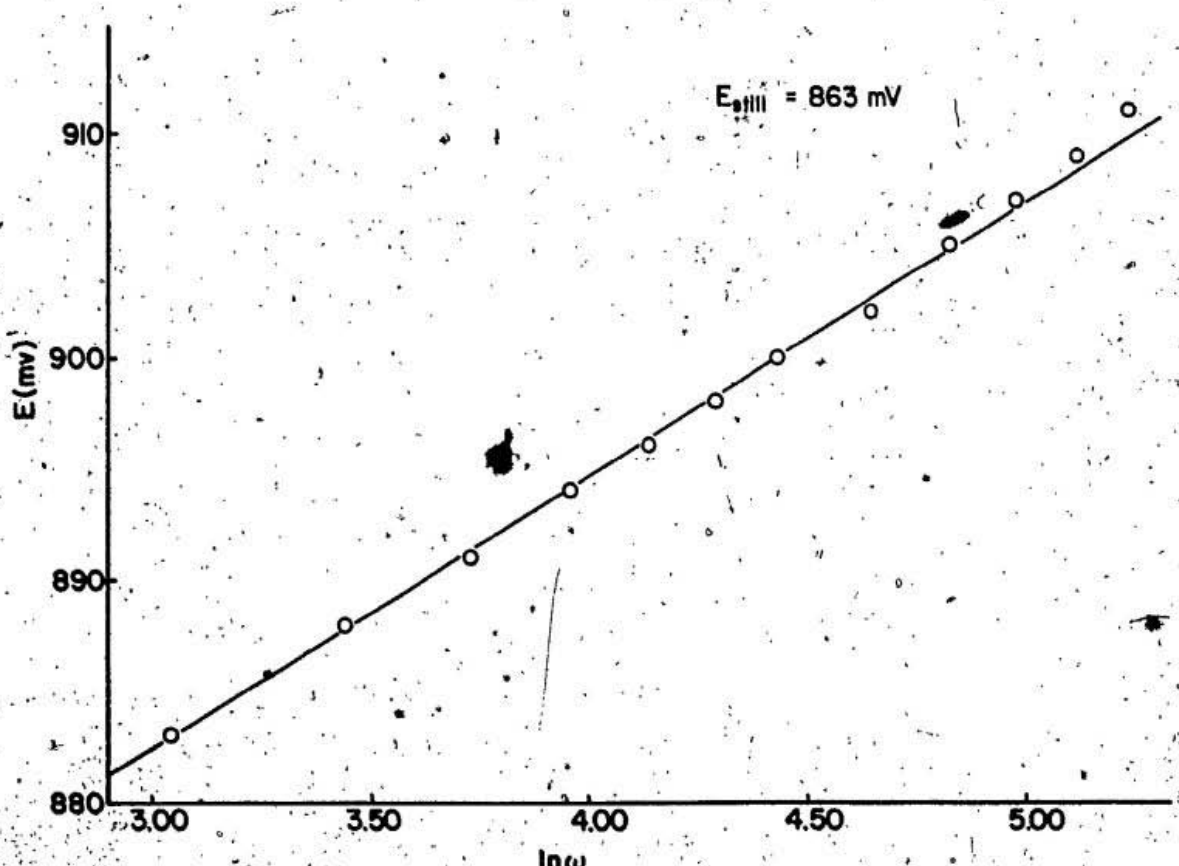

Fig. 3.15 Plot of E vs lnω AFTER END-POINT.

(c) Far Beyond Equivalence:

The ΔE's decrease with additional Ce^{4+} titrant. It can be found in Table 3.3.2 and Fig. 2.2.

Table 3.3.2 $E_{stirring} - E_{still}$ After Equivalence for *ca.* 0.01 mol·L^{-1} Fe^{2+} + Ce^{4+} Titration in H_2SO_4

Added Ce^{4+} /mL	$E_{stirring}$/mV	E_{still}/mV	ΔE
22.014	647	676	-29
22.114	914	874	+40
22.210	1057	1044	+13
22.302	1113	1104	+9
22.410	1128	1123	+5
22.510	1135	1132	+3
22.608	1141	1139	+2
22.700	1146	1140	+6
22.810	1150	1149	+1
22.912	1153	1153	0
23.303	1157	1156	+1
23.212	1162	1161	+1
25.000	1186	1186	0

The reason for this phenomenon is that the concentration of Ce^{4+} increases so that the $i_{l,c}$ is enhanced. However the current i_a for O_2/H_2O remains small. The mixed potential E_{mix} has to move to more positive values closer and closer to the equilibrium potential of the Ce^{3+}/Ce^{4+} couple. Obviously the cathodic overpotential caused by the mixed potential is becoming smaller and smaller. Eventually the overpotential will not be able to bring the cathodic reaction into the diffusion controlled

range so that its current $i_c << i_{l,c}$ and equation (3.4.51) cannot be used. But the reaction can be treated by using the linear current-potential equation if the overpotential for the Ce^{3+}/Ce^{4+} couple is sufficiently small. Under this situation of small overpotential the Butler-Volmer equation can be simplified as

$$i_c = i_o(-nf\eta) \tag{3.4.56}$$

For the reaction $Ce^{4+} + e^- \rightarrow Ce^{3+}$, the cathodic current is then

$$i_c = -\frac{F}{RT} j_{o,Ce^{4+}} A(E_{mix} - E_{eq,Ce^{3+},Ce^{4+}}) \tag{3.4.57}$$

Since at the mixed potential the currents are balanced $i_a = -i_c$, equation (3.4.57) can be substituted into (3.4.50)

$$E_{mix} = E_{eq,O_2H_2O} + \frac{RT}{4\alpha F} \ln \left[\frac{F}{RT} j_{o,Ce^{4+}} A(E_{mix} - E_{eq,Ce^{3+},Ce^{4+}}) \right]$$

$$- \frac{RT}{4\alpha F} \ln j_{o,O_2,H_2O} A \tag{3.4.58}$$

Although potential E_{mix} has a complicated relation with other electrochemical parameters, E_{mix} no longer depends on stirring since no mass transport control term is present in equation (3.4.58). The measured potential does not change with stirring, as observed sufficiently beyond equivalence.

(d) At Equivalence

It was suggested in Section 3.3 that the absence of a mechanism for a mixed potential because of the very small concentrations of Fe^{2+} and Ce^{4+} at equivalence could result in a classical Nernst potential being set up. The criterion is that potential control is assumed by a reaction (or reactions) with the largest exchange current(s). First we consider the equilibrium concentrations of ionic species at equivalence.

From the formal potentials for the two redox couples given in Chapter 1, the equilibrium constant K is 1.2×10^{13}. Taking account of dilution, the concentrations of Fe^{3+} and Ce^{3+} at equivalence are about 5×10^{-6} mol·cm^{-3} each. Hence those of Fe^{2+} and Ce^{4+} are about 1.5×10^{-12} mol·cm^{-3}. These concentrations may be used to estimate the exchange current density for $Fe^{2+} \rightleftharpoons Fe^{3+} + e^-$ as

$$j_o = F(C^*_{Fe^{2+}})^{\frac{1}{2}} (C^*_{Fe^{3+}})^{\frac{1}{2}} \bullet k^o -$$

$$= 96{,}485 \bullet (1.5 \times 10^{-12} \bullet 5 \times 10^{-6})^{\frac{1}{2}} \bullet 5 \times 10^{-3}$$

$$= 1.3 \times 10^{-6} \text{ A·cm}^{-2}.$$

An exchange current density of 1.3 μA·cm^{-2} is significantly greater than that for the O_2/H_2O couple in air-saturated solution, which may be estimated at 1×10^{-10} A·cm^{-2}, taking the solubility as one fifth of that of oxygen[20] which is 1.33×10^{-3} mol·L^{-1}:

$$j_o = 4F(C^*_{O_2})^{(1-\alpha)} (C^*_{H_2O})^{\alpha} \bullet k^o$$

$$= 4 \bullet 96{,}485 \bullet (2.7 \times 10^{-7})^{0.4} (5.5 \times 10^{-2})^{0.6} \bullet 6 \times 10^{-13}$$

$$= 1 \times 10^{-10} \text{ A·cm}^{-2}.$$

The exchange current density for the Ce^{4+}/Ce^{3+} couple is more difficult to ascertain because k^o for it is not well established, but is likely to be greater than that for O_2/H_2O. We conclude that the potential is most likely to be established by the two main redox couples and we reject as improbable Charlot's[11] suggestion of a mixed potential involving Fe^{3+} reduction and Ce^{3+} oxidation since these would not establish a single potential.

References

1. J.H. Kennedy, "Analytical Chemistry: Principles", Harcourt Brace Jovanovich, New York, 1984, pp 725, 7.
2. G.J. Hills, D.J.G. Ives and G.J. Janz in "Reference Electrodes", ed. D.J.G. Ives and G.J. Janz, Academic Press, New York, 1961, Chapters 3 and 4.
3. R. Behrend, *Z. Physik Chem.*, 1893, **11**, 466.
4. G. Gran, *Analyst (London)*, 1952, **77**, 661.
5. N. Ingri, W. Kakolowicz, L.G. Sillén and B. Warnqvist, *Talanta*, 1967, **14**, 1261.
6. D.A. Skoog and D.M. West, "Principles of Instrumental Analysis", Holt, Rinehart and Winston, New York, 2nd Edn., 1984, p 560.
7. E.P. Serjeant, "Potentiometry and Potentiometric Titrations", Wiley, New York, 1984.
8. M. Spiro, *Chem. Soc. Rev.*, 1986, **15**, 141-165.
9. A.J. Bard and L.R. Faulkner, "Electrochemical Methods", Wiley, New York, 1980, Chapter 3.
10. P van Rysselberghe, *Electrochim. Acta*, 1964, **9**, 1343.
11. J.O'M. Bockris, Electrode Kinetics, in "Modern Aspects of Electrochemistry", ed. J. O'M. Bockris and B.E. Conway, Butterworths, London, 1954, Vol. 1, Chapter 4.
12. G. Charlot, J.B. Lambling, B. Tremillon, "Electrochemical Reactions", Elsevier, Amsterdam, 1962, Chapter 7.
13. H.H. Willard and F. Fenwick, *J. Amer. Chem. Soc.*, 1922, **44**, 2504.
14. E. Lewartowicz, *J. Electroanal. Chem.*, 1963, **6**, 11.
15. T.P. Hoar, *Proc. Roy. Soc. A*, 1933, **142**, 628.

16. J.O'M. Bockris and A.K.M.S. Huq, *Proc. Roy. Soc. A*, 1956, 237, 277.

17. M. Spiro and Ravnö, *J. Chem. Soc.*, 1965, 78.

18. A.J. Bard and L.R. Faulkner, "Electrochemical Methods", Wiley, New York, 1980, Chapter 1.

19. J.P. Hoare, "The Electrochemistry of Oxygen", Wiley-Interscience, New York, 1968, p 143.

20. I.M. Kolthoff and J.J. Lingane, "Polarography", Volume II, J. Wiley-Interscience, New York, 1965, p 554.

PART TWO

Chapter 1 Overview of Previous Work.

The heterogeneous kinetics of the ferrous-ferric electrode reaction

$$Fe^{2+}(aq) \rightleftharpoons Fe^{3+}(aq) + e^- \qquad (1.1)$$

is relatively simple and it has been shown to be a first order reaction in both directions by Gerischer's determination[1] of the concentration dependence of the exchange current density (from 2 to 15 $mA \cdot cm^{-2}$) in 10^{-2} $mol \cdot L^{-1}$ Fe(II) and in 8.6×10^{-3} $mol \cdot L^{-1}$ Fe(III), both in 1 $mol \cdot L^{-1}$ H_2SO_4. Further study of this system can help the investigation of heterogeneous electrode processes and identify the catalytic properties, the effects of the solution on the rate constant, the dependencies on different electrode materials and the effects of surface condition on the reaction rate. Previous work on the ferrous-ferric electrode reaction in aqueous sulphuric acid or alkali sulphates will be reviewed.

The ferrous-ferric system has been studied by many methods and numerous workers but the agreement among the rate constants is not satisfactory, the discrepancies being only accepted as an inevitable result of the use of solid electrodes. A comparison table is provided in a later chapter. The electrode kinetic study of the Fe(II)-Fe(III) couple on solid electrodes cannot be considered to be complete.

Anson[2] measured the exchange current density, j_o, for the Fe(II)-Fe(III) couple at platinum in aqueous H_2SO_4 by using a galvanostatic method. A constant current in the form of a step function was passed between the platinum working and counter electrodes in a Fe^{2+}- and Fe^{3+}-containing solution. The potential applied to the working electrode was monitored by observing its time dependence with a cathode ray oscilloscope. The exchange current density corresponding to each prevailing current density was evaluated. This method does not require knowledge of the diffusion coefficients for reactant and product for the measurement of j_o. A series of

exchange current densities were determined with different common concentrations of Fe(II) and Fe(III). A plot of the averaged values of j_o in each solution against the common concentration C is a straight line with a slope of k^oF, the line passing through the origin. The electrode was pretreated to achieve a good reproducibility before the experiments. The electrode was anodically oxidized in the test solution containing Fe^{2+} and Fe^{3+} ions, then it was immersed in a solution containing only Fe^{2+} to produce a layer of "finely divided" platinum by chemical reduction of the pre-formed oxide film. Anson proposed that finely divided platinum is formed when the electrode is immersed in the ferrous sulphate solution after a layer of oxide film has been formed so that the electrode reactivity is thereby increased. This idea has been tested; it was also found that the electrode reactivity was increased after immersion in aqueous ferrous sulphate.

Agarwal[3] measured the rate constant k^o of the Fe^{2+}, Fe^{3+} system and the charge transfer coefficient with equal concentrations of 0.002 mol·L^{-1} of Fe^{2+} and Fe^{3+} in 0.5 mol·L^{-1} H_2SO_4 by the method of faradaic rectification. The alternating voltages used in his experiment were 4 mV and 8 mV at frequencies from 50 to 5000 Hz. Three polished bright platinum foil electrodes of area 1.6 cm^2 each composed the cell. The redoxokinetic potential has been calculated at sufficiently high frequency to find α which equalled 0.42. The rate constant is obtained from the slope of the shift in mean potential with angular frequency over a range of low frequencies 0 to 200 Hz. The rate constants, determined at four different temperatures ranging from 25 °C to 40 °C, ranged from 0.033 cm·s^{-1} to 0.050 cm·s^{-1}. Comparing this result with Anson's work (k^o = 0.0053 cm·s^{-1} in 0.5 mol·L^{-1} H_2SO_4 at 25 °C) the agreement is poor. Agarwal's determination can be carried out very close to equilibrium and the reactant concentrations can be very low. Another advantage of this technique is the comparative freedom from double-layer charging current effects. However this work treats the oxidant and reductant as having equal diffusion

coefficients but for the Fe^{2+} and Fe^{3+} ions, their diffusion coefficients are not actually equal. Neither was pretreatment used to increase the electrode reactivity nor to clean the electrode surface. The solution was covered with liquid paraffin to protect it from the atmosphere which may result in adsorption of organic substances on the electrodes decreasing the reactivity of the platinum. (In fact the rate constant is larger than that of Anson.[2])

The ferrous-ferric reaction was studied potentiostatically by Barnartt.[4] His method is based on the theoretical relation for a quasi-reversible reaction at a planar electrode[5] to obtain the charge-transfer current for a given i-t curve. A "ratio method" of analysis was utilized to evaluate the charge transfer current. In this work the measured ratio of current at time t to that at 4t gives the value of $\lambda\sqrt{t}$ which corresponds to the selected time; λ is a constant, directly proportional to the exchange current density j_o and inversely proportional to the redox ion concentration. The rate constant from this work is 0.003 $cm{\cdot}s^{-1}$ on bright platinum with the concentrations $C_{Fe^{2+}} = C_{Fe^{3+}} = 0.097 mol{\cdot}L^{-1}$ at 25 °C. The kinetic parameters for this system were also measured on a bright gold electrode, the exchange current density unexpectedly being an order of magnitude larger on gold. Barnartt assumed that some specific anion adsorbed on the platinum electrode surface. In these experiments, the procedures may not have been satisfactory because the working platinum or gold electrode acts as a cathode and may have trace amounts of metal or hydrogen deposited on its surface. Neither is cleaning with $CrO_3 - H_2SO_4$ mixture usually considered to be satisfactory in electrochemical kinetics measurements.

A platinum rotating electrode (RDE) at one rotation speed (2300 rpm) was used by Samec and Weber[6] to study the kinetics of the ferrous-ferric reaction in sulphate media. Their measurements allow determination of the potential-dependent rate constants, k_f and k_b, from the current-potential curve and the limiting currents $i_{l,c}$ and $i_{l,a}$. At any point of the curve, the equation

$$-\log F k_f A C^{*}_{Fe^{3+}} = \log \left[\left(\frac{1}{i} - \frac{1}{i_{l,c}} \right) - \left(\frac{1}{i} + \frac{1}{i_{l,a}} \right) e^{\frac{F\eta}{RT}} \right] \qquad (1.2)$$

can be used. A similar expression can be written to evaluate k_b. Experimentally k_f and k_b are evaluated at various overpotentials, η, and plots of k_f and k_b vs η give two straight lines intersecting at $\eta = 0$ where k^o is evaluated. The RDE was activated in the same solution by periodic triangular voltages in a potential range 0.056 V to 1.556 V vs SHE. The formation of iron-sulphate complexes is discussed in detail and a conclusion was drawn that the main contributors to the reaction rate are $FeSO_4^+$ and $FeSO_4$ complexes in the sulphuric acid solution. The standard rate constants, k^o, were 0.0032 $cm \cdot s^{-1}$ in 0.5 $mol \cdot L^{-1}$ H_2SO_4 and 0.008 $cm \cdot s^{-1}$ in 0.5 $mol \cdot L^{-1}$ Na_2SO_4, before double layer corrections, but taking into account the roughness factor of 2.7 evaluated from H adsorption. This method of treatment of the experimental data to find the rate constants for charge transfer can be evaluated only if the recorded current-potential curve shows sufficient deviation from reversible behavior.

Using a similar method Galus and Adams[7] determined the rate constant in 1 $mol \cdot L^{-1}$ H_2SO_4 with equal Fe(II) and Fe(III) concentrations at 10^{-3} $mol \cdot L^{-1}$; k^o was found as 0.0043 $cm \cdot s^{-1}$. The rotating disc electrode technique was claimed to yield accurate rate constants in this range. The transfer coefficient was also given as $\alpha = 0.46$. Like Weber and Samec[6] only one (higher) rotating speed of 6000 rpm was used. The platinum electrode was pretreated according to Anson's method[2] using electrochemical oxidation at 1.5 V vs SCE followed by chemical reduction in 10^{-3} $mol \cdot L^{-1}$ ferrous sulphate.

The rotating disc electrode technique was also preferred by Angell and Dickinson.[8] The rate constant for the ferrous-ferric reaction was evaluated from current-potential curves according to Randles'[9] method using equations

$$\frac{\alpha n F \eta}{RT} = \ln i_o + \ln Y \qquad (1.3)$$

where

$$Y = \frac{1 - e^{\frac{nF}{RT}\eta}}{i} + \frac{e^{\frac{nF}{RT}\eta}}{i_{l,a}} - \frac{1}{i_{l,c}} \qquad (1.4)$$

From the slope of the linear ln Y vs η plot αn may be calculated, yielding $\alpha = 0.5$, and the intercept at zero overpotential gives the exchange current i_o. The RDE was set up at various fixed rotation speeds. The authors concluded, in contrast to other workers, that the rate constant for the ferrous-ferric reaction was almost independent of electrode material and only slightly dependent on the nature of the background electrolyte. In their work the rate constant in 0.5 mol·L^{-1} H_2SO_4 is approximately the same on platinum and gold electrodes.

Earlier work from this laboratory is to be found in the publication[10] and thesis of Su[11] and the thesis of Wadden[12], reviewed briefly[13]. Su used a crude rotating disc electrode of platinum, palladium or gold in a wide range of concentrations of sulphuric or hydrochloric acids. Both ferrous and ferric ions were present at equal but wide ranging concentrations. As in the present work, measurements were close to equilibrium and were extrapolated to infinite rotation speed[11].

Wadden's study[12] involved the same RDE set-up as the present one, with the three noble metals used by Su[11]. Temperature was varied in order to determine activation parameters for the ferrous-ferric redox reaction, which was confined to perchlorate medium, steps being taken to minimise chloride impurity which is known to catalyse the process. Wadden treated his data similarly to the present work, with the exception that analog plots of $\frac{1}{i}$ versus $\omega^{\frac{1}{2}}$ were drawn, rather than printing out digitally. Results of previous workers are summarized in tabular form in Chapter 5.

Chapter 2 Theory of Electrode Kinetics

2.1 Charge Transfer

We briefly review certain aspects of homogeneous kinetics since the heterogeneous and homogeneous reactions have a common theoretical starting ground, the well known Arrhenius Equation:

$$k = A\, e^{-E_A/RT} \tag{2.1.1}$$

where k is the rate constant, the coefficient A is known generally as the frequency factor, E_A is the activation energy, R and T are the gas constant and absolute temperature, respectively. Reaction paths can be expressed in terms of potential energy along a reaction coordinate. As the reaction takes place, the coordinate changes from those of the reactant(s) to those of the product(s). The reactant has to rise and pass over a maximum to fall into the product region. The height of the maximum above the two valleys is identical to the activation energy. In another notation the enthalpy of activation given by $\Delta H^{\neq} = \Delta E^{\neq} + \Delta(PV)^{\neq}$ is employed. In condensed phases, as in the present case, $\Delta(PV)^{\neq}$ is often negligible. Equation (2.1.1) may then be written as

$$k = A\, e^{-\Delta H^{\neq}/RT} \tag{2.1.2}$$

Since the normalized standard entropy of activation $\Delta S^{\neq}/R$ appears in an exponential term as a dimensionless constant, the frequency factor can be written as $A' e^{T\Delta S^{\neq}/RT}$ or $A' e^{\Delta S^{\neq}/R}$ and substituting in (2.1.2):

$$k = A' e^{-(\Delta H^{\neq} - T\Delta S^{\neq})/RT} = A' e^{-\Delta G^{\neq}/RT} \tag{2.1.3}$$

where $\Delta G^{\neq}$ is the Gibbs free energy of activation.

The absolute rate theory is often adopted to predict the values of A' and $\Delta G^{\neq}$ for electrode kinetics. The rate constant can be put in the form of equation (2.1.4) by using statistical mechanics for a system in dynamic equilibrium

$$k = \kappa \frac{k_B T}{h} e^{-\Delta G^{\neq}/RT} \qquad (2.1.4)$$

where κ is the transmission coefficient that could have a value from zero to unity, k_B and h are the Boltzmann and Planck constants, respectively. Apparently the rate constant of equation (2.1.4) is dependent on temperature but independent of reactant concentration.

Many kinetic models have been developed. One of them which will be introduced is based on the electrochemical potential developed by Parsons[14]. This approach defines the electrochemical potential ($\bar{\mu}_i$) as the work which must be done to bring a particle i from a point where the potential is zero to a point in a phase where the potential is ϕ. This potential is in principle a measurable quantity. The phase can be divided into a homogeneous volume deprived of charge and double layer and a shell with charge and double layer. The electrochemical potential can be divided according to this model into work w_1, required for the transfer of i to a point in the homogeneous volume and the work w_2, required for transfer to the point through a double layer. The electrochemical potential is composed of the chemical part μ_i and the electrical part so it may be written as $\bar{\mu}_i = \mu_i + w_2$. Since $w_2 = z_i F \phi_i$

$$\bar{\mu}_i = \mu_i + z_i F \phi_i \qquad (2.1.5)$$

where z_i is the charge on the ion and ϕ is the inner potential of the double layer. Generally $\Delta\bar{G} = \Delta G + (\Delta G)_e$, the electrochemical free energy change $\Delta\bar{G}$ is divided into a chemical free energy change ΔG and electrical free energy change $(\Delta G)_e$. In the same way, an electrochemical activation free energy $\Delta\bar{G}^{\neq}$ can also be divided into two components:

$$\Delta\bar{G}^{\neq} = \Delta G^{\neq} + (\Delta G^{\neq})_e \qquad (2.1.6)$$

where $\Delta G^{\neq}$ is the chemical activation free energy. It does not change with potential,

whereas $(\Delta G^{\neq})_e$ is the activation free energy of the electrical component(s) wholly responsible for the effects of potential. For the particular reaction:

$$Fe^{2+} \rightleftharpoons Fe^{3+} + e \qquad (2.1.7)$$

the forward reaction is the anodic oxidation of Fe^{2+} to Fe^{3+} plus an electron. The two electrochemical free energies of activation are written as:

$$\Delta\overline{G}_f^{\neq} = \Delta G_f^{\neq} + (\Delta G_f^{\neq})_e \qquad (2.1.8)$$

$$\Delta\overline{G}_b^{\neq} = \Delta G_b^{\neq} + (\Delta G_b^{\neq})_e \qquad (2.1.9)$$

where subscripts f and b represent the forward and backward reactions, respectively. The electrical part of the activation free energy for the forward reaction is assumed to be a fixed fraction α of the overall electrical free energy change. For the forward reaction:

$$(\Delta G_f^{\neq})_e = \alpha\,(\Delta G^{\circ})_e \qquad (2.1.10)$$

and

$$(\Delta G_b^{\neq})_e = -(1-\alpha)(\Delta G^{\circ})_e \qquad (2.1.11)$$

where $(\Delta G^{\circ})_e$ is the overall electrical free energy change, and α is defined as an anodic transfer coefficient. The standard electrochemical free energy for Fe^{2+}, the reactant, is

$$\overline{G}^{\circ}_{Fe^{2+}} = \overline{\mu}^{\circ}_{Fe^{2+}} = \mu^{\circ}_{Fe^{2+}} + 2\,F\phi^S \qquad (2.1.12)$$

where ϕ^S is the electrostatic potential of the solution phase. The standard electrochemical free energy for the products Fe^{3+} and e^- in the metal is

$$\overline{G}^{\circ}_{Fe^{3+}+e^-} = \overline{\mu}_{Fe^{3+}} + \overline{\mu}_{e^-} = \mu^{\circ}_{Fe^{3+}} + 3\,F\phi^S + \mu_e^{\circ M} - F\phi^M \qquad (2.1.13)$$

where ϕ^M is the electrostatic potential of the metal phase. The overall electrical free energy is the difference between $(\overline{G}^{\circ}_{Fe^{3+}+e^-})_e$ and $(\overline{G}^{\circ}_{Fe^{2+}})_e$ which simplifies to

$$(\Delta G^{\circ})_e = F(\phi^S - \phi^M) = -F(\phi^M - \phi^S) \qquad (2.1.14)$$

A measurable potential E of any scale can be related to the interfacial potential difference $(\phi^M - \phi^S)$ by a constant: $E = (\phi^M - \phi^S) + K$. The overall electrical free energy change can be written

$$(\Delta G^{\circ})_e = -F(\phi^M - \phi^S) = FK - FE \qquad (2.1.15)$$

Using equations (2.1.4) and (2.1.8) for the forward reaction

$$k_f = \kappa \frac{k_B T}{h} e^{-\Delta G^{\neq}/RT} = \kappa \frac{k_B T}{h} e^{-[\Delta G_f^{\neq}/RT + (\Delta G_f^{\neq})_e/RT]} \qquad (2.1.16)$$

The forward electrical free energy is

$$(\Delta G_f^{\neq})_e = \alpha KF - \alpha FE \qquad (2.1.17)$$

Substitute (2.1.17) to (2.1.16)

$$k_f = \kappa \frac{k_B T}{h} e^{[-\Delta G_f^{\neq}/RT - \frac{\alpha KF}{RT} + \frac{\alpha FE}{RT}]} \qquad (2.1.18)$$

Combine the constants which are potential-independent in equation (2.1.18) as k_f°:

$$k_f = k_f^{\circ} e^{\frac{\alpha F}{RT}E} \qquad (2.1.19)$$

The same derivation for the backward reaction, with combination of constants as k_b°, gives

$$k_b = k_b^{\circ} e^{-(1-\alpha)\frac{F}{RT}E} \qquad (2.1.20)$$

According to the definition of the electrode forward reaction rate,

$$v_f = k_f C_{Fe^{3+}}(0,t) = \frac{i_a}{nFA} \qquad (2.1.21)$$

and for the backward reaction

$$v_b = k_b C_{Fe^{3+}}(0,t) = \frac{i_c}{nFA} \qquad (2.1.22)$$

the net reaction rate is

$$v_{net} = v_f - v_b = k_f C_{Fe^{2+}}(0,t) - k_b C_{Fe^{3+}}(0,t) = \frac{i}{nFA} \qquad (2.1.23)$$

The net current i would be

$$i = nFA\,[k_f\, C_{Fe^{2+}}(0,t) - k_b\, C_{Fe^{3+}}(0,t)] \qquad (2.1.24)$$

substituting equations (2.1.19) and (2.1.20) into (2.1.24)

$$i = nFA\,[k_f^{\circ}\, C_{Fe^{2+}}(0,t)\, e^{\frac{\alpha F}{RT}E} = k_b^{\circ}\, C_{Fe^{3+}}(0,t)\, e^{-\frac{(1-\alpha)F}{RT}E}] \qquad (2.1.25)$$

The equation (2.1.25) has another form by adding and subtracting $E^{\circ\prime}$ and rearrangement

$$i = nFA\,[C_{Fe^{2+}}(0,t)\, k_f^{\circ}\, e^{\frac{\alpha F}{RT}E^{\circ\prime}} \cdot e^{\frac{\alpha F}{RT}(E-E^{\circ\prime})} - C_{Fe^{3+}}(0,t)\, k_b^{\circ}\, e^{-\frac{(1-\alpha)F}{RT}E^{\circ\prime}} \cdot e^{-\frac{(1-\alpha)F}{RT}(E-E^{\circ\prime})}] \qquad (2.1.26)$$

A standard rate constant k° is defined[15]

$$k^{\circ} = k_f^{\circ}\, e^{\frac{\alpha F}{RT}E^{\circ\prime}} = k_b^{\circ}\, e^{-\frac{(1-\alpha)F}{RT}E^{\circ\prime}} \qquad (2.1.27)$$

substituting (2.1.27) into (2.1.26)

$$i = nFA\,k^{\circ}\,[C_{Fe^{2+}}(0,t)\, e^{\frac{\alpha F}{RT}(E-E^{\circ\prime})} - C_{Fe^{3+}}(0,t)\, e^{-\frac{(1-\alpha)F}{RT}(E-E^{\circ\prime})}] \qquad (2.1.28)$$

If the system is at equilibrium, the net current, i is zero and the surface concentration is identical to the bulk concentration $C^{*}_{Fe^{2+}}$ or $C^{*}_{Fe^{3+}}$. Then equation (2.1.28) would give for $i = 0$

$$nFA\,k^{\circ}\,C^{*}_{Fe^{2+}}\, e^{\frac{\alpha F}{RT}(E_{eq}-E^{\circ\prime})} = nFA\,k^{\circ}\,C^{*}_{Fe^{3+}}\, e^{-\frac{(1-\alpha)F}{RT}(E_{eq}-E^{\circ\prime})} \qquad (2.1.29)$$

where E_{eq} is the equilibrium potential of the electrode system. The exchange current is defined using either side of equation (2.1.29), *e.g.*

$$i_o = nFA\, k^o\, C^*_{Fe^{2+}}\, e^{\frac{\alpha F}{RT}(E_{eq}-E^o)} \qquad (2.1.30)$$

It can be simplified using the Nernst relation to

$$i_o = nFA\, k^o\, [C^*_{Fe^{2+}}]^{(1-\alpha)}\ \ [C^*_{Fe^{3+}}]^{\alpha} \qquad (2.1.31)$$

The test solution is usually made up with equal concentrations, $C^*_{Fe^{2+}}$ and $C^*_{Fe^{3+}}$. In this case (2.1.31) becomes

$$i_o = nFA\, k^o C \qquad (2.1.32)$$

where $C = C^*_{Fe^{2+}} = C^*_{Fe^{3+}}$ is the common concentration of both ions. Combining (2.1.28) and (2.1.31), one gets

$$\frac{i}{i_o} = \frac{C_{Fe^{2+}}(0,t)\, e^{\frac{\alpha F}{RT}(E-E^o)}}{C^*_{Fe^{2+}}} \left(\frac{C^*_{Fe^{3+}}}{C^*_{Fe^{2+}}}\right)^{\alpha} - \frac{C_{Fe^{3+}}(0,t)\, e^{-\frac{(1-\alpha)}{RT}(E-E^o)_n}}{C^*_{Fe^{3+}}} \left(\frac{C^*_{Fe^{3+}}}{C^*_{Fe^{2+}}}\right)^{1-\alpha} \qquad (2.1.33)$$

The ratio terms of $C^*_{Fe^{3+}}$ to $C^*_{Fe^{2+}}$ can be replaced by using the Nernst relation $\frac{C^*_{Fe^{3+}}}{C^*_{Fe^{2+}}} = e^{\frac{F}{RT}(E_{eq}-E^o)}$ then (2.1.33) has the form

$$\frac{i}{i_o} = \frac{C_{Fe^{2+}}(0,t)}{C^*_{Fe^{2+}}}\, e^{\frac{\alpha F}{RT}(E-E_{eq})} - \frac{C_{Fe^{3+}}(0,t)}{C^*_{Fe^{3+}}}\, e^{-\frac{(1-\alpha)F}{RT}(E-E_{eq})} \qquad (2.1.34)$$

or using the definition of overpotential $\eta = E - E_{eq}$

$$\frac{i}{i_o} = \frac{C_{Fe^{2+}}(0,t)}{C^*_{Fe^{2+}}}\, e^{\frac{\alpha F}{RT}\eta} - \frac{C_{Fe^{3+}}(0,t)}{C^*_{Fe^{3+}}}\, e^{\frac{-(1-\alpha)F\eta}{RT}} \qquad (2.1.35)$$

This equation can be simplified further to give the well-known Butler-Volmer equation[16] if the current is very low and the solution is well stirred so that the bulk concentration is very close to the surface concentraton.

$$i = i_o\,(e^{\frac{\alpha F}{RT}\eta} - e^{-\frac{(1-\alpha)F}{RT}\eta}) \qquad (2.1.36)$$

If the overpotential η is limited to a very small value, for instance, ± 0.005 V, the

terms $e^{\frac{\alpha F}{RT}\eta}$ and $e^{-\frac{(1-\alpha)F}{RT}\eta}$ can be approximated as $(1+\frac{\alpha F}{RT}\eta)$ and $(1-\frac{(1-\alpha)F}{RT}\eta)$ respectively, thus the equation (2.1.36) will have the form

$$i = i_o \frac{F}{RT}\eta \qquad (2.1.37)$$

The net current is linearly related to overpotential in this narrow potential range. It is necessary to mention that the i_o is the true charge transfer exchange current only under the condition that the net current i is independent of mass transfer.

If the applied overpotential is sufficiently high, either negative or positive, one of the bracketed terms in (2.1.36) becomes negligible, the equation can have the following forms (for n = 1 as in the present case):

$$\text{for large positive } \eta: \quad i = i_o e^{\frac{\alpha F}{RT}\eta} \qquad (2.1.38)$$

$$\text{for large negative } \eta: \quad i = -i_o e^{\frac{-(1-\alpha)}{RT}\eta} \qquad (2.1.39)$$

They can be used to evaluate the kinetic parameters α and i_o by plotting $\log_{10} i$ with η, as in Tafel plots.

Allen and Hickling[17] suggested an alternative method for plotting $i-\eta$ data, which allows the use of both low and high overpotentials of either sign, based on the equation (2.1.36) to give:

$$i = i_o e^{\frac{\alpha nF}{RT}\eta}(1 - e^{\frac{nF}{RT}\eta}) \qquad (2.1.40)$$

and hence

$$\ln\left[\frac{i}{1 \mp e^{\frac{nF}{RT}\eta}}\right] = \ln i_o + \frac{\alpha nF}{RT}\eta \qquad (2.1.41)$$

This equation was used in some of the present work.

2.2 Mass Transport to a Rotating Disc

The rotating disc electrode (RDE) allows determination of the chemical composition and kinetic parameters of an electrochemical system. Levich[18] solved the hydrodynamic equations combined with Fick's laws of diffusion. The reaction of interest is

$$Fe^{2+} \rightleftharpoons Fe^{3+} + e^- \qquad (2.2.1)$$

Both the mass transport and electron transfer rates affect the overall reaction rate. For a slow electrode reaction, the determining step is usually charge transfer. A sufficient quantity of reactants is brought to the surface by mass transport, the effect of which is negligible in the electrode kinetics for this type of reaction. If a fast electrode reaction occurs on the surface, the reaction rate is held back from the maximum by the slowness of disposing of the products and of bringing the reactants up to the surface. The rate may be limited by the slowness of mass transport. In this case, the intrinsic charge transfer rate can only be discovered by eliminating the mass transfer hindrance.

The mass transport is described by the Nernst-Planck equation[19] for one dimensional mass transfer along the x-axis of species j

$$J_j(x) = -D_j \frac{\partial_j C_j(x)}{\partial x} - \frac{z_j F}{RT} D_j C_j \frac{\partial \phi(x)}{\partial x} + C_j v(x) \qquad (2.2.2)$$

where $J_j(x)$ is the flux of species j at distance x from the surface. D_j is the diffusion coefficient; C_j is the concentration of species j; z_j is the charge of the species j and $\partial\phi(x)/\partial x$ is the potential gradient in the x-direction, v(x) is the velocity with which a volume element in solution moves along the x-axis. The equation shows that mass transport is composed of three parts; the first term represents the diffusion component and directs that the species j moves down the chemical potential gradient; the second term is the contribution of migration which is the movement of charged

species through a medium under the influence of an applied electric field. This effect in our experiment was suppressed by using an excess of unreactive supporting electrolyte, *i.e.* H_2SO_4. The third term is the contribution of convection to the flux. In the case of the RDE, a forced convection is generated by electrode rotation.

Fick's second law for the one-dimensional case in the absence of migration has the form

$$\frac{\partial C_j}{\partial t} = \frac{\partial^2 C_j}{\partial x^2} D_j - v_x \frac{\partial C_j}{\partial x} \qquad (2.2.3)$$

where x refers to the vertical distance below and perpendicular to the RDE surface. With the RDE, mass transfer is composed of two steps. The first is movement by forced convection bringing the bulk solution to the outer boundary of a diffusion layer which is a very thin lamina of solution adjacent to the electrode surface. The laminar flow layer can be held if the flow rate is below that characterized by a certain critical Reynolds number.[20] Secondly, there is transport of reactant across this quiescent layer, determined by diffusion. The diffusion rate increases as the diffusion layer δ decreases with increasing disc rotation speed. For instance, δ is 0.14 cm in water at 25 °C at a rotation speed of 1 rad.s^{-1}, decreasing to 0.043 cm at 10 rad.s^{-1}. More importantly, the diffusion layer thickness is essentially constant at a fixed rotating speed, a steady-state flow velocity v_x being established. Equation (2.2.3) is solved for $\frac{\partial C_j}{\partial t} = 0$ and simplifies to

$$D_j \frac{\partial^2 C_j}{\partial x^2} = v_x \frac{\partial C_j}{\partial x} \qquad (2.2.4)$$

The boundary conditions for the differential equation are

$$\text{at} \quad x \to \infty; \quad C_j = C_j^*$$

$$\text{and at} \quad x = 0; \quad C_j = C_j\,(x=0)$$

The equation is solved[21] to give the stationary concentration distribution as a function of x:

$$C_j(x) = \frac{C_j^* - C_j(x=0)}{1.61\, D_j^{\frac{1}{3}}\, \nu^{\frac{1}{6}}\, \omega^{-\frac{1}{2}}} \int_0^{\infty} \exp\left[\frac{1}{D_j}\int_0^x v_x dx\right] dx + C_j(x=0) \qquad (2.2.5)$$

The diffusion coefficient of reactant j is dependent on the size, charge and hydration number of the diffusing reactant. It is free from any electrocatalytic effects arising from the condition of the electrode's surface. ν is the kinematic viscosity of the solvent and ω is the rotation speed in $rad.s^{-1}$.

The diffusion current density can be found from equation (2.2.5), according to Fick's first law:

$$J_j = \frac{dn_j}{dt} = -D_j A \frac{dC_j}{dx} \qquad (2.2.6)$$

where dn_j is the change in the quantity of diffusing species j across an area A in a time period dt and $\frac{dC_j}{dx}$ is the concentration gradient. For the reaction $Fe^{2+} \rightleftharpoons Fe^{3+} + e^-$, when a potential difference favourable to the forward reaction is applied to the electrode, the surface concentration would decrease creating a concentration gradient $\left(\frac{dC_{Fe^{2+}}}{dx}\right)_{x=0}$. The steady state flux $J_{Fe^{2+}}$ equals the reaction rate v

$$v = J_{Fe^{2+}} = -D_{Fe^{2+}} A \left(\frac{dC_{Fe^{2+}}}{dx}\right)_{x=0} \qquad (2.2.7)$$

As a current

$$i = FA\, D_{Fe^{2+}} \left(\frac{dC_{Fe^{2+}}}{dx}\right)_{x=0} \qquad (2.2.8)$$

also for the back reaction

$$i = -FA\, D_{Fe^{2+}} \left(\frac{dC_{Fe^{2+}}}{dx}\right)_{x=0} \qquad (2.2.9)$$

The concentration gradients are obtained from equation (2.2.5) as *e.g.*

$$\left(\frac{dC_{Fe^{2+}}}{dx}\right)_{x=0} = 0.62\, D_{Fe^{2+}}^{\frac{1}{3}}\, \nu^{-\frac{1}{6}}\, \omega^{\frac{1}{2}}\, (C^{*}_{Fe^{2+}} - C_{Fe^{2+}(x=0)}) \qquad (2.2.10)$$

Substituting this into (2.2.7) the diffusion current is

$$i = 0.62\, FA\, D_{Fe^{2+}}^{\frac{2}{3}}\, \nu^{-\frac{1}{6}}\, \omega^{\frac{1}{2}}\, (C^{*}_{Fe^{2+}} - C_{Fe^{2+}(x=0)}) \qquad (2.2.11)$$

This is the well known Levich equation in which the diffusion layer thickness is

$$\delta = 1.61\, D^{\frac{1}{3}}\, \nu^{\frac{1}{6}}\, \omega^{-\frac{1}{2}} \qquad (2.2.12)$$

Levich approximated[18] by truncating the series of v_x in (2.2.5). More exact expressions have been developed by later workers. For the range of $\frac{D}{\nu} < 4 \times 10^{-3}$, Gregory and Riddiford[22] approximated the series expansion by numerical evaluation to obtain the limiting current

$$i_l = \frac{0.554}{0.8934 + 0.316(\frac{D}{\nu})^{0.36}} (FA\, D^{\frac{2}{3}}\, \nu^{-\frac{1}{6}}\, \omega^{\frac{1}{2}}\, C^{*}_{Fe^{2+}}) \qquad (2.2.13)$$

For the present work $D_{Fe^{2+}} = 5.8 \times 10^{-6}$ cm^2·s^{-1} [23] and $\nu = 0.01$ cm^2·s^{-1}, and $\frac{D_{Fe^{2+}}}{\nu} = 5.8 \times 10^{-4} < 4 \times 10^{-3}$. The approximation of Gregory and Riddiford[22] is more suitable for this work. For a larger range of $\frac{D}{\nu}$, Newman[24] expanded the series in v_x even further to obtain a more exact expression.

$$v_x = \sqrt{\omega\nu}\, [-0.51023\, \frac{\omega}{\nu} x^2 + \frac{1}{3} (\frac{\omega}{\nu})^{\frac{3}{2}} x^3 - 0.10265\, (\frac{\omega}{\nu})^2 x^2 + \cdots\ ] \qquad (2.2.14)$$

equation (2.2.14) is substituted into the current expression

$$i = FA\, D \left(\frac{dC_{Fe^{2+}}}{dx}\right)_{x=0} = \frac{FA\, D(C^{*}_{Fe^{2+}} - C_{Fe^{2+}(x=0)})}{\int_0^{\infty} \exp\left(\int_0^{x} \frac{v_x}{D}\, dx\right) dx} \qquad (2.2.15)$$

This equation applies when the reactant is an ion in a solution with excess unreactive electrolyte. The expression of current is

$$\frac{i}{FA(C^{*}_{Fe^{2+}} - C_{Fe^{2+}}(x=0))\sqrt{w\nu}} = \frac{0.62048\left(\frac{\nu}{D}\right)^{-\frac{2}{3}}}{1 + 0.2980\left(\frac{\nu}{D}\right)^{-\frac{1}{3}} + 0.14514\left(\frac{\nu}{D}\right)^{-\frac{2}{3}}} \quad (2.2.16)$$

In the region of $\frac{D}{\nu} < 0.01$, the maximum deviation is about 0.1% referring to a numerical evaluation of equation (2.2.15), and thus is still subject to error. For two cases, when $\frac{D}{\nu}$ is 0.01 and when $\frac{D}{\nu} = 5.7 \times 10^{-4}$ as in this work, the percentage deviations are compared for three approaches.

Table 2.1 Comparison of Series Expansions with a Numerical Solution of Equation (2.2.15): Percentage Errors

$\frac{D}{\nu}$	Levich[18]	Gregory and Riddiford[22]	Newman[24]
0.01	7.16	0.36	0.069
5.7×10^{-4}	2.79	0.14	0.005

2.3 Combined Mass Transport and Charge Transfer

(a) Measurement Close to Equilibrium

An important application of the Levich equation or the modified equations of Gregory and Riddiford, or of Newman is to extracting electron transfer rate constants. Many methods have been developed which are discussed in Part II, Chapter 1. However, high overpotentials are applied to the RDE system in most of these methods so that the surface condition is affected by the high overpotentials. F.R.

Smith developed an approach involving measurement of currents very close to equilibrium. This method had been tried by Su in 1972[11] and by Wadden in 1978[12]. Fairly good agreement was achieved comparing their results with other workers even though the mathematical treatment was incomplete. An attempt will be made to give a more exact treatment for this approach. It begins with the previous equation

$$\frac{i}{i_o} = \frac{C_{Fe^{2+}}(0,t)}{C^*_{Fe^{2+}}} e^{\frac{\alpha F}{RT}\eta} - \frac{C_{Fe^{3+}}(0,t)}{C^*_{Fe^{3+}}} e^{\frac{-(1-\alpha)F}{RT}\eta} \qquad (2.1.35)$$

At the RDE, the anodic current and cathodic current can be given, respectively, by

$$i = FA \frac{D_{Fe^{2+}}}{\delta_{Fe^{2+}}} (C^*_{Fe^{2+}} - C_{Fe^{2+}}(x=0)) \qquad (2.3.1)$$

and

$$i = -FA \frac{D_{Fe^{3+}}}{\delta_{Fe^{3+}}} (C^*_{Fe^{3+}} - C_{Fe^{3+}}(x=0)) \qquad (2.3.2)$$

Let $A_R = FA \frac{D_{Fe^{2+}}}{\delta_{Fe^{2+}}}$ and $A_O = FA \frac{D_{Fe^{3+}}}{\delta_{Fe^{3+}}}$ for convenience, then substitute A_R and A_O into (2.3.1) and (2.3.2) and rearrange them to

$$\frac{C_{Fe^{2+}}(x=0)}{C^*_{Fe^{2+}}} = 1 - \frac{i}{A_R C^*_{Fe^{2+}}} \qquad (2.3.3)$$

and

$$\frac{C_{Fe^{3+}}(x=0)}{C^*_{Fe^{3+}}} = 1 + \frac{i}{A_O C^*_{Fe^{3+}}} \qquad (2.3.4)$$

which may be substituted into (2.1.35), with $f = \frac{F}{RT}$,

$$i = i_o \left\{ \left(1 - \frac{i}{A_R C^*_{Fe^{2+}}}\right) e^{\alpha f \eta} - \left(1 + \frac{i}{A_O C^*_{Fe^{2+}}}\right) e^{-(1-\alpha) f \eta} \right\} \qquad (2.3.5)$$

Solve for i in (2.3.5)

$$i = \frac{e^{\alpha f\eta} - e^{-(1-\alpha)f\eta}}{\frac{1}{i_o} + \left(\frac{e^{\alpha f\eta}}{A_R C^*_{Fe^{2+}}} + \frac{e^{-(1-\alpha)f\eta}}{A_O C^*_{Fe^{3+}}}\right)} \qquad (2.3.6)$$

According to the RDE theory, the ratio of $A_O C^*_{Fe^{3+}}$ to $A_R C^*_{Fe^{2+}}$ must be a constant, independent of potential and current. Let this constant be K.

$$K = \frac{A_O C^*_{Fe^{3+}}}{A_R C^*_{Fe^{2+}}} \qquad (2.3.7)$$

It can be written as:

$$\frac{K}{A_O C^*_{Fe^{3+}}} = \frac{1}{A_R C^*_{Fe^{2+}}} \qquad (2.3.8)$$

Substitute (2.3.8) into the denominator of equation (2.3.6).

$$i = \frac{(e^{\alpha f\eta} - e^{-(1-\alpha)f\eta})}{\frac{1}{i_o} + \frac{1}{A_O C^*_{Fe^{3+}}}(K e^{\alpha f\eta} + e^{-(1-\alpha)f\eta})} \qquad (2.3.9)$$

So far, no approximation has been made, but (2.3.9) can be simplified when η is sufficiently small or sufficiently large. When η is sufficiently small, $e^{\alpha f\eta}$ is expanded as $1 + \alpha f\eta + \frac{(\alpha f\eta)^2}{2!} + \cdots$ the first two terms are taken as in most textbooks[5,25]. Equation (2.3.9) becomes

$$i = \frac{f\eta}{\frac{1}{i_o} + \frac{1}{A_O C^*_{Fe^{3+}}}[(1+K) + (1-\alpha-K\alpha)f\eta]} \qquad (2.3.10)$$

When $\eta = \pm$ 0.005 V, $f\eta$ has a value of 0.19. In this case, a value of K may be obtained from the Levich equation.

$$K = \frac{A_O C^*_{Fe^{3+}}}{A_R C^*_{Fe^{2+}}} = \frac{0.62\, F A\, D_{Fe^{3+}}^{\frac{2}{3}} \nu^{-\frac{1}{6}} \omega^{\frac{1}{2}} C^*_{Fe^{3+}}}{0.62\, F A\, D_{Fe^{3+}}^{\frac{2}{3}} \nu^{-\frac{1}{6}} \omega^{\frac{1}{2}} C^*_{Fe^{2+}}} \qquad (2.3.11)$$

The bulk concentrations for Fe^{2+} and Fe^{3+} were prepared to be equal. From results

of limiting current measurements to be given in Chapter 3 Section (f), $K = 0.894$. If $\alpha \sim 0.5$, the term $(1-\alpha-K\alpha)f\eta$ may be ignored by comparison with $(1+K)$ in the denominator, allowing equation (2.3.10) to be rewritten as

$$\frac{\eta}{i}\,\frac{F}{RT} = \frac{1}{i_o} + \frac{(1+K)}{A_O\, C^*_{Fe^{3+}}} \qquad (2.3.12)$$

Applying the Levich equation to (2.3.12) one has

$$\frac{\eta}{i}\,\frac{F}{RT} = \frac{1}{i_o} + \frac{(1+K)}{0.62\, FA\, D^{\frac{2}{3}}_{Fe^{3+}}\, \nu^{-\frac{1}{6}}\, C^*_{Fe^{3+}}}\, \omega^{-\frac{1}{2}} \qquad (2.3.13)$$

When the rotation speed ω is extrapolated to infinity by plotting $\frac{\eta}{i}$ vs. $\omega^{-\frac{1}{2}}$ and determining the intercept at $\omega^{-\frac{1}{2}} = 0$, the corresponding exchange current is $(i_o)_{\omega\to\infty}$ which is free from mass transfer limitations. Then the linear characteristic of small η can be applied as

$$\frac{\eta}{(i)_{\omega\to\infty}} = \frac{RT}{F}\,\frac{1}{i_o} \quad \text{or} \quad (i)_{\omega\to\infty} = i_o\,\frac{R}{RT}\eta \qquad (2.3.14)$$

The charge transfer exchange current i_o is found directly from the plot. If the solution is prepared with equal bulk concentrations of ferric and ferrous ions, the exchange current gives the rate constant

$$i_o = FAk^oC^* \qquad (2.3.15)$$

where C^* is the common concentration for both Fe^{2+} and Fe^{3+}.

(b) Measurements at High Overpotentials

The Tafel plot may be used to obtain the rate constant and transfer coefficient. However, the measured current at the experimental rotation speed is partially controlled by mass transport. In order to eliminate mass transfer effects to find the pure charge transfer rate, the RDE is a useful tool. The theoretical treatment is similar

to that of Jahn and Vielstich[23]. The net current i is the difference between anodic and cathodic currents:

$$i = i_a - i_c = FAk_f C_{Fe^{2+}}(x=o) - FA\, k_b\, C_{Fe^{3+}}(x=o) \qquad (2.3.16)$$

The measured current i in the equation above is controlled by mass transfer if the surface concentrations $C_{Fe^{2+}}(x=o)$ and $C_{Fe^{3+}}(x=o)$ differ from the bulk concentrations. When the rotation speed is so high that the surface concentrations are identical to the bulk concentrations, the net current obtained by extrapolation represents pure charge transfer without mass transport effects. Defining the current

$$(i)_{\omega\to\infty} = FA\left[k_f C^*_{Fe^{2+}} - k_b C^*_{Fe^{3+}}\right] \qquad (2.3.17)$$

solving equations (2.2.19) and (2.2.20) for $C_{Fe^{2+}}(x=o)$ and $C_{Fe^{3+}}(x=o)$ and substituting them into (2.3.16) gives

$$i = FA\left[k_f\left(C^*_{Fe^{2+}} \frac{-i}{A_R}\right) - k_b\left(C^*_{Fe^{3+}} + \frac{i}{A_O}\right)\right] \qquad (2.3.18)$$

Rearranging (2.3.18), solving for i and inverting gives

$$\frac{1}{i} = \frac{1}{FA(k_f C^*_{Fe^{2+}} - k_b C^*_{Fe^{3+}})}\left[1 + FA\left(\frac{k_f}{A_R} + \frac{k_b}{A_O}\right)\right] \qquad (2.3.19)$$

Again, according to RDE theory, the ratio of A_O to A_R is the constant K if common concentrations of Fe^{2+} and Fe^{3+} are used so that

$$\frac{K}{A_O} = \frac{1}{A_R}$$

and (2.3.19) can be rewritten as

$$\frac{1}{i} = \frac{1}{FA(k_f C^*_{Fe^{2+}} - k_b C^*_{Fe^{3+}})}\left[1 + \frac{FA}{A_O}(K k_f + k_b)\right] \qquad (2.3.20)$$

If the Levich equation is applied to evaluate

$$A_O = FA\frac{D_{Fe^{3+}}}{\delta_{Fe^{3+}}} = 0.62\, FA\, D_{Fe^{3+}}^{\frac{2}{3}} \nu^{-\frac{1}{6}} \omega^{\frac{1}{2}}$$

for substitution into (2.3.20) one gets

$$\frac{1}{i} = \frac{1}{FA\,(k_f C^{\circ}_{Fe^{3+}} - k_b C^{\circ}_{Fe^{3+}})} \left[1 + \frac{(K k_f + k_b)}{0.62\, D_{Fe^{3+}}^{\frac{2}{3}} \nu^{-\frac{1}{6}}} \omega^{-\frac{1}{2}} \right] \qquad (2.3.21)$$

which shows the observed dependency of $(i)^{-1}$ on $\omega^{-\frac{1}{2}}$. Using the definition of pure charge transfer current of equation (2.3.17) then (2.3.21) yields

$$\frac{1}{i} = \frac{1}{(i)_{\omega\to\infty}} \left[1 + \frac{(K k_f + k_b)}{0.62\, D_{Fe^{3+}}^{\frac{2}{3}} \nu^{-\frac{1}{6}}} \omega^{-\frac{1}{2}} \right] \qquad (2.3.22)$$

This is evident if one plots $\frac{1}{i}$ vs. $\omega^{-\frac{1}{2}}$ and extrapolates the line to $\omega^{-\frac{1}{2}} = 0$, or $\omega \to \infty$, then $(i)_{\omega\to\infty}$ is obtained from the intercept. A series of measurements is carried out at constant potentials. After extrapolation of reciprocal currents to $\omega \to \infty$, plotting them in the form of a Tafel plot of logarithm of currents at effectively infinite rotation speed versus potential enables the exchange current for charge transfer and the transfer coefficient to be determined. As is well known, the Tafel equation is applicable for large overpotentials where the Butler-Volmer equation becomes

$$(i)_{\omega\to\infty} = i_o\, e^{\alpha f \eta} \qquad (2.3.23)$$

and taking logarithms

$$\ln (i)_{\omega\to\infty} = \ln i_o + \frac{\alpha F}{RT} \eta \qquad (2.3.24)$$

If $(i)_{\omega\to\infty}$ is the charge transfer current, the exchange current, i_o, yields the rate constant as before, and the slope gives the transfer coefficient.

The equation (2.3.23) may be derived from equation (2.3.9). When the η is either highly positive or negative, one of the terms in the numerator of (2.3.9)

becomes negligible, *e.g.* if η has a high positive value, then $e^{-(1-\alpha)f\eta} \rightarrow 0$; the equation (2.3.9) is rewritten as

$$i = \frac{e^{\alpha f\eta}}{\frac{1}{i_o} + \frac{1}{A_O C_{Fe}^{*}} (K\, e^{\alpha f\eta})} \qquad (2.3.25)$$

Rearranging (2.3.25) and taking the reciprocal of i gives

$$\frac{1}{i} = \frac{e^{-\alpha f\eta}}{i_o} + \frac{K}{A_O C_{Fe^{3+}}^{*}} \qquad (2.3.26)$$

If the Levich equation is applied

$$\frac{1}{i} = \frac{e^{-\alpha f\eta}}{i_o} + \frac{\omega^{-\frac{1}{2}}}{0.62\, F A\, D_{Fe^{3+}}^{\frac{2}{3}} \nu^{-\frac{1}{2}}} \qquad (2.3.27)$$

It also shows when the rotation speed has infinite value, $\omega \rightarrow \infty$, the equation (2.3.27) becomes

$$\frac{1}{(i)_{\omega\rightarrow\infty}} = \frac{e^{-\alpha f\eta}}{i_o} \qquad (2.3.28)$$

This is of the same form as (2.3.23), then the exchange current and transfer coefficient can be obtained by plotting the logarithm of $(i)_{\omega\rightarrow\infty}$ vs. η.

(c) Measurements at Moderate Overpotentials

When the applied overpotentials are not very high, the Butler-Volmer equation cannot be simplified as (2.3.23) but it could have the form

$$(i)_{\omega\rightarrow\infty} = i_o\, e^{\alpha f\eta} [1 - e^{-f\eta}] \qquad (2.3.29)$$

Rearranging (2.3.29) and taking logarithms of both sides gives

$$\ln \left[\frac{(i)_{\omega\rightarrow\infty}}{1 - e^{-f\eta}}\right] = \ln i_o + \alpha f\eta \qquad (2.3.30)$$

The exchange current i_o is obtained by plotting $\ln \left[\frac{(i)_{\omega\to\infty}}{1-e^{-f\eta}}\right]$ vs. η and extrapolating to $\eta = 0$, the intercept and slope giving the exchange current and transfer coefficient, respectively. The equation (2.3.30) is essentially that of Allen and Hickling[17].

Chapter 3 Experimental

3.1 Materials

The materials used in the kinetic measurements had been carefully chosen to avoid unwanted catalytic effects and/or inhibitive effects.

The platinum rotating disc electrode was manufactured from 0.2 cm diameter rod Johnson, Matthey and Mallory (J.M. & M.) Grade 1 platinum. The purity of the platinum is tabled below:

1 ppm	each Ca, Mg, Pd
1 ppm	each Ag, Au
2 ppm	each Fe, Ni, Si
3ppm	Cu

The same grade of platinum foil was used for the reference and counter electrodes. The 96.5% Ultrex concentrated sulphuric acid was diluted to 0.5 mol·L^{-1} H_2SO_4 as the tested solution. The impurity concentrations in the concentrated H_2SO_4 are: As $<$ 0.001 ppm; Cl^-, 0.04 ppm; NO_3^-, PO_4^{3-}, each 0.05 ppm; Si, 0.03 ppm; Se, 0.4 ppm; NH_4^+, 0.3 ppm; Be $<$ 0.02 ppb; Ag $<$ 0.05 ppb; Cu and Mn, each 0.07 ppb; Bi, Co, each $<$ 0.1 ppb; Ni, 0.2 ppb; Cr, Pb, Mg and Ti, each 0.3 ppb; Sn $<$ 0.5 ppb; Zn, Sr, Hg and Cd $<$ 1 ppb; Al and Ca each 3 ppb; K $<$ 5 ppb; Ba $<$ 10 ppb. The highest metallic impurities are Fe and Na with concentrations 30 and 60 ppb, respectively. Johnson Matthey Chemicals Ltd., Puratronic Grade I iron(II) sulphate heptahydrate and iron(III) sulphate anhydrous (10 ppm total metallic impurities each) were used after dissolution in 0.5 mol·L^{-1} H_2SO_4. Some iron sulphate solutions were prepared by dissolving G.F. Smith Chemical Co. 100.00% electrolytic pure iron (ignited into moist hydrogen) in ca. 6 mol·L^{-1} sulphuric acid at room temperature for 20 hours. Then the solution containing Fe^{2+} was oxidized electrolytically to produce

equal concentrations of Fe^{3+} and Fe^{2+}.

Triple distilled water was used throughout the kinetic measurements. Tap water was distilled in a glass still. It was then redistilled over alkaline potassium permanganate and a final distillation in which carbon dioxide was prevented from entry by a soda lime trap.

Argon was used for the best measurements. The Canadian Liquid Air argon (Ar, 99%) was further purified by passing through a furnace at 140 °C containing pre-reduced BTS catalyst from Badische-Anilin-und-Soda Fabrik. This material is composed of 30% finely dispersed copper oxide, stabilized on a carrier and activated by reduction with hydrogen at 140 °C. It diminishes oxygen to less than 0.1 ppm. The argon was then passed through a solid carbon dioxide-ethanol trap and through a pre-saturator filled with triple distilled water and finally into the cell.

3.2 Apparatus

The apparatus consisted of 3 parts: the electronic equipment, the RDE and its accessories, and finally the cell and gas-supply lines.

(a) The Electronic Equipment

The most important electronic equipment was the potentiostat. A custom built potentiostat was used throughout to determine the current-overpotential relations close to equilibrium with a precision of ±0.01 mV, the maximum output being ± 99.99 mV obtained from a push button digital potentiometer with a linearity of 0.1%. For the rate constant and transfer coefficient measurements which have to be carried out at high overpotentials, a maximum of ±600 mV was applied to the potentiostat from a separate D.C. power supply with an accuracy ±0.5 mV. The cell currents were measured with a Keithley 172A multimeter. The digital current readout was printed simultaneously on a Hewlett-Packard HP 5150A thermal printer. At the same time the period of rotation was printed next to the

corresponding current, as will be discussed later.

A Wavetek Model 182 2 MHz Function Generator was used to provide the linear sweep signal to the potentiostat, it was added to the desired equilibrium potentials by the potentiostat. The applied potentials were measured with a Keithley 616 digital electrometer which had an accuracy of 0.01 mV.

A Hewlett-Packard 7046 A, X-Y Recorder was used to record current-potential scans during activation. The RDE rotation speed was measured using a Tektronix DC 505A Universal Counter utilized to give the time period in microseconds between two pulses from the phototransistor. This phototransistor received 30 light pulses per revolution of the RDE from the stationary light source through the holes punched in the ring rotating with the RDE motor. Displayed time periods ranged from 6000 μs to 500 μs with a precision of 1 or 0.1 μs, respectively. The time periods may be converted to rotation speeds in radians per second ($rad \cdot s^{-1}$).

(b) The Rotating Disc Electrode

The rotating disc electrode consisted of a platinum active disc area (at the bottom end of a platinum rod) and an insulating mantle of Kel-F covering all other parts of the electrode. The precision of measurements with a disc electrode depends primarily on the quality of its construction and on the uniformity and reproducibility of its rotation. It has been found that the requirements placed on the shape of the electrode are best met by the bell shaped electrode (BEL) favoured by Riddiford and Blurton[26]. The BEL shaped electrode was therefore chosen for the experiments. With this electrode the interaction between the flow under and above the electrode active surface is minimal and the electrolyte is stirred only minimally by the insulating mantle. The deviation from the theoretical current is less than 1% at rotation rates of 50 to 240 $rev.min^{-1}$ [27]. According to Riddiford's suggestion[28], the radius of the platinum disc r_{10} should be at least 100 times greater than the transport boundary layer, $Y_t = 3.61 (\frac{D}{\nu})^{\frac{1}{3}} (\frac{\nu}{\omega})^{\frac{1}{2}}$. But this is an extremely conservative figure. F.

Opekar and P. Beran[27] showed that with $r_{10} >> 2Y_t$ the electrode works well. In the present case, $r_{10} \sim 20Y_t$, the 0.1 cm radius of the platinum is therefore adequate to the demands. The insulating mantle has a thickness of 1.5 cm, this sheath exceeding the laminar boundary layer thickness $Y_l = 2.8(\frac{\nu}{\omega})^{\frac{1}{2}}$ by 30- to 100-fold at rotation speeds from 360 to 3600 rpm if ν is assumed as 0.01 $cm^2 \cdot s^{-1}$.

The RDE was manufactured from an 8" length x 1.25" diameter Kel-F cylindrical rod obtained from Commercial Plastics Limited, Montreal. The 0.2 cm diameter platinum rod was screw threaded into a #49 drill diameter hole in the stainless steel shaft. The platinum - stainless steel piece was then inserted into a very tight press fit inside the Kel-F. The RDE is machined to obtain the BEL shape and the surface of the disc is cut by a precision machine tool. Then the entire electrode was screwed onto the main rotating shift and at the same time, the top end of the stainless steel rod was contacted with a stainless steel spring positioned in a cavity at the end of the main rotating shaft. The resistance between the platinum disc and the lead to the potentiostat was measured to be about 0.1 Ω. All the screw threads were in a clockwise direction but the RDE operated in a counterclockwise fashion to avoid slippage during rotation. The main connecting shaft from the motor was machined down from 1.27 cm to 0.95 cm diameter so that the Kel-F tube could have thicker and stronger walls. The construction of the electrode was done by Randy Thorne at Memorial University, the construction details being shown in Figs. 3.1 and 3.2.

Figures 3.1 and 3.2 on next pages.

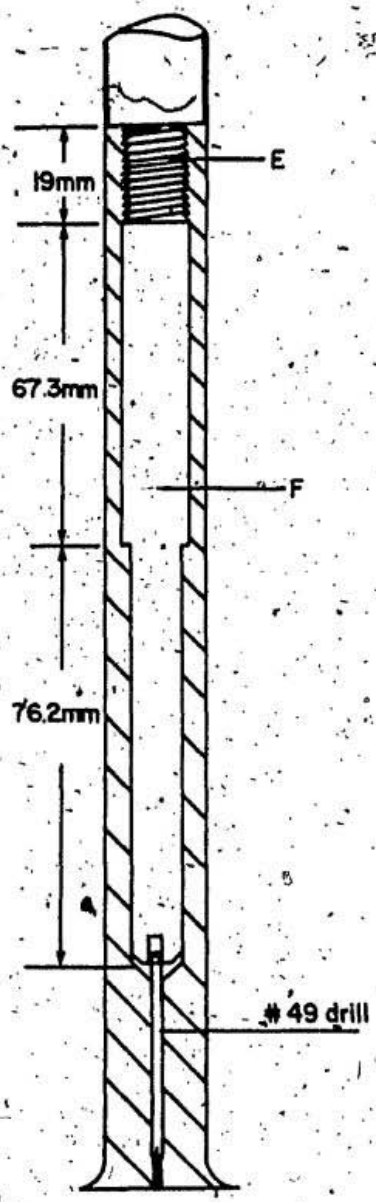

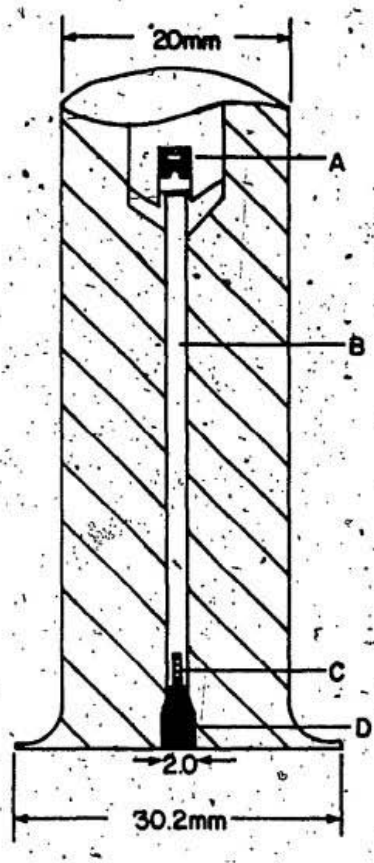

A - spring-loaded stainless steel contact
B - 2 mm stainless steel shaft tapered 1° at upper end
C - stainless steel screw-threaded into noble metal disc
D - platinum rod
E - main shaft threaded opposite to direction of rotation.
F - main shaft machined down to 10 mm

Fig. 3.1 The BEL type rotating disc electrode. (lower portion)

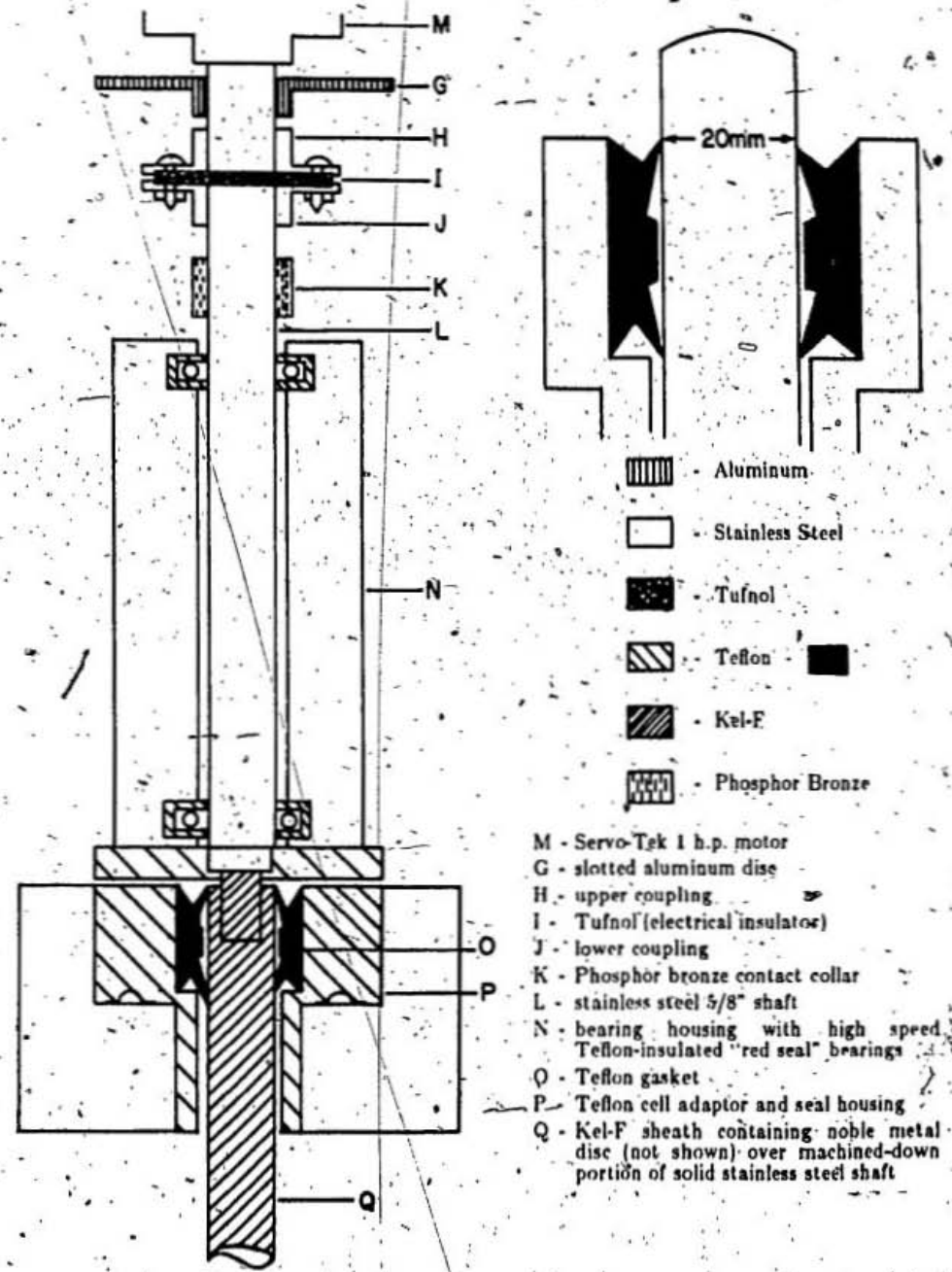

Fig. 3.2 Upper portion of rotating disc electrode.

In order to minimize vibration caused by the motor, the main vertical support was a 9" thick piece of channel iron, which was electric arc-welded to a 9" x 12" x $\frac{1}{4}$" thick steel base plate. Following secure mounting to the working bench, the assembly was further stabilized by the installation of horizontal metal struts, rigidly connecting it to the concrete wall of the laboratory. The RDE was powered by a 7 ampere 1 horsepower motor, Model STE-232-1F, manufactured by Servo-Tek Products Co., New Jersey. Speed control of this unit was attainable to within 0.25%. This was achieved through the coupling of its precision adjustable-speed drive to a solid state tachometer feedback circuit. Constant, accurately known speeds up to 3600 rpm were possible for extended periods of time. Speeds were set on the potentiometer-type control head with resolution to within 0.1%. The Servo-Tek 1 horsepower motor was carefully mounted atop the channel iron assembly and connection to the RDE shaft was made indirectly through a piece of Tufnol, a non-conducting plastic, to ensure that the electrode was electrically insulated from the motor. To keep eccentricities near zero, possible motor-RDE shaft alignment problems were minimized by using suitable flexibility of the coupling material and the coupling bolts were mounted in Teflon for further electrical insulation protection.

The main RDE shaft was mounted in a stainless steel bearing housing using Teflon encased SKF "Red Seal" high speed bearings. This finalized the isolation of the shaft from the main support assembly. A Teflon seal-cup was mounted beneath the bearing support, which also served as an adaptor to the main joint of the experimental glass cell. A "silicone seal" O-ring was used as a gasket between cell and housing. Inside the cup was positioned two Teflon "directional angle seals" tapered to zero thickness with one angled up and the other down. These seals helped prevent air leaking into the cell and minimized possible contact of corrosive acid vapours with the metal interior components of the RDE drive train. This seal system is better than a modern commercial RDE in which sealing the test system from

the atmosphere is still a problem.

A phosphor bronze cylinder key-fitted to the shaft between the Tufnol coupler and the main bearing housing provided electrical contact to the rotating shaft and the platinum disc. This bronze cylinder was dynamically contacted to a brass brush which had to be changed after extensive usage otherwise the output current decreased below that of a normally working brush, especially at high rotation speeds. Using a worn out brush could greatly spoil the linearity for a linear current-potential measurement.

The rotation speed signals were taken from a phototransistor in the RDE assembly. This included a thin slotted circular disc located between the motor and Tufnol coupler. A C-type jaw piece was mounted over this containing the phototransistor on one side and a stationary light source on the other. Thirty holes allowed the light through intermittently to give 30 pulses for each revolution of the disc. The pulse periods in μs were printed on thermal paper with high precision. The time period τ was converted to square root or to reciprocal square root of rotation speed, $\omega^{\frac{1}{2}}$ or $\omega^{-\frac{1}{2}}$, with the following equations.

$$\omega^{-\frac{1}{2}} = 2.185 \times 10^{-3} \sqrt{\tau} \ (\text{rad.s}^{-1})^{-\frac{1}{2}} \qquad (3.2.1)$$

or

$$\omega^{\frac{1}{2}} = 457.7/\sqrt{\tau} \ (\text{rad.s}^{-1})^{\frac{1}{2}} \qquad (3.2.2)$$

(c) Glassware

The main glassware was a test cell and electrodes. The test cell was a single walled Pyrex multi-jointed vessel with a large 'button type' support ring pressed out near the top. The glass support was fused together into one piece. With this sup-

port the cell was able to fit neatly into a thermostatically controlled jacket fitted with a ground glass rim. A metal clamp kept the jacket and cell securely fastened together with two rubber gaskets for a water-tight seal. The jacket was provided with water pumped from a Tamson TE-Z9 water bath controlled to $\pm 0.05\,^{\circ}C$. The thermostatted cell allowed the RDE to enter through an O-ring joint in the centre of the cell. This joint was not off-centered because vortexing was not a problem at the experimental rotating speeds and because it was more convenient to assemble from time to time. On either side of the opening were two B10/19 cup cones for reference and counter electrode entry ports. A third B10/19 cup cone was positioned between these two for the possible inclusion of other auxiliary electrodes. A final B10/19 cone opposite permitted entry of an argon degassing tube. This tube was fitted with a two-way tap for bubbling through the solution or flowing over the surface during the measurements. A B14 socket with a thermometer well allowed the entry of a thermometer which measured the temperature of the test solution. An Ertco F series ($-1\,^{\circ}C$ to $+51\,^{\circ}C$) mercury in glass thermometer was used for this purpose. It had been previously calibrated against a platinum resistance thermometer using a Tinsley Wheatstone bridge. The Pyrex cell and its thermojacket were raised and lowered by mounting it on a small scissors-jack support.

All the electrodes and degassing tube were constructed in Pyrex. The platinum counter and reference electrodes were prepared from 1 cm^2 J.M. & M. Grade 2 platinum foils rolled in a cylindrical fashion, and pinch sealed through the Pyrex. Apparatus grade platinum (*i.e.* Grade 4, J.M. & M.) was employed as connecting leads to the counter and reference electrodes through Pyrex glass tubes with an outer diameter of 4 mm.

3.3 Procedures

(a) Cleaning

All the glassware and RDE were cleaned with ACS grade sodium hydroxide concentrated solution and ACS grade concentrated nitric acid. The RDE was soaked in concentrated NaOH at 80° C for 30 to 60 minutes with low speed rotation followed by washing with triple distilled water at least 5 times to remove organic impurities. This procedure was concluded by spinning the electrode at high speed for several minutes to dry it. The cell was filled with hot (about 80° C) concentrated NaOH with the reference electrode and counter electrode, gas entry tube and the wall of the thermometer tube inserted in the cell for about 4 hours. Then the cell and glassware and electrodes were washed with triple distilled water. After rinsing thoroughly, the cell was filled with boiling concentrated HNO_3 with all electrodes (except the RDE) and glassware in it, the acid was usually left in the cell throughout the night. The electrodes and glassware were then thoroughly rinsed with triple distilled water. The final cleaning procedure was by steaming as follows: each piece of glassware and each electrode was immersed in steam by placement above a sprayer under which triple distilled water was boiled. All the volumetric flasks and weighing bottles and beakers were treated in the same way as the cell.

(b) Preparation of Fe^{2+} and Fe^{3+} Solution

The Fe^{2+} and Fe^{3+} solution in 0.5 mol·L^{-1} H_2SO_4 was prepared either by dissolving ultra-pure Puratronic $FeSO_4 \cdot 7H_2O$ and $Fe_2(SO_4)_3$ in 0.5 mol·L^{-1} H_2SO_4 or by potentiostatically oxidizing $FeSO_4$ to bring the ferrous and ferric ions to equal concentrations. In the latter case, the current was measured as a function of time during the electrolysis so that an estimate of the total charge passed could be made. The concentrations of Fe^{2+} and Fe^{3+} were measured by using the Levich mass transport limiting current and concentration relations. The concentrations could be adjusted to be equal by adding the desired amount of Fe^{2+} solution from the

volumetric flask to the test cell in the case of some over-oxidization.

The concentration measurements had been calibrated by potentiometric titrations against a standard Ce^{4+} titrant solution, which has been discussed in Part I of the thesis. The applied overpotential for the purpose of concentration measurements was ±550 mV to bring the currents to the limiting current region and usually nine evenly distributed rotation speeds were chosen from the lowest ω to the highest ω to achieve a good linearity with $\sqrt{\omega}$.

(c) Activation of the Test Electrode

The RDE was activated either by cyclic linear sweep recommended by some previous workers[6,8,29,30] or by oxidation and chemical reduction recommended by Galus and Adams[7], and by Rao and Rangarajan[31]. For the first method, the sweep rate was always set at 40 $mV \cdot s^{-1}$. Cathodic and anodic limits of activation were tried from 0.1 V to 0.41 V vs. SHE for the cathodic limit and 1.05 V to 1.45 V vs. SHE as the anodic limit. The activation was usually carried out for a period of one and a half hours at 25.0 °C. The X-Y recorder was used to obtain the sweep diagram for the surface information. The activation procedure was always halted on the cathodic limit potential of the scan, so that oxide films present on the surface would be minimal.

The oxidation-chemical reduction method was carried out in two steps. The platinum was first oxidized at a high positive potential (about +1.3 V vs. SHE) for about 4 minutes, then it was soaked in 0.1 $mol \cdot L^{-1}$ $FeSO_4$ solution in 0.5 $mol \cdot L^{-1}$ H_2SO_4 for 1 to 12 hours to reduce the formed oxide films.

(d) Measurement of Rate Constant with Low Overpotentials

The kinetic parameter rate constant was obtained by applying overpotentials from -5.0 mV to +5.0 mV to the RDE at a constant rotation speed. The chosen rotating speeds were evenly distributed from 360 rpm to 3600 rpm, and usually 8 to 11 speeds were chosen to have sufficient points. The corresponding currents were

measured and printed after applying a particular overpotential for 10 seconds, after which the potential was step-changed with a push-button digital potentiometer. Then the currents were plotted versus potential to obtain a slope $(\frac{\partial i}{\partial \eta})_\omega$. The linearity of the curve was determined from the correlation coefficient calculated by the least squares method. The obtained slopes $(\frac{\partial i}{\partial \eta})_\omega$ at each rotation speeds were then plotted against $\omega^{-\frac{1}{2}}$. The intercepts gave the exchange current enabling the rate constant to be calculated. The slope reflects the mass transport condition and it has been found to be essentially constant. All the intercepts, slopes and inherent errors were also determined by a weighted least squares analysis using a VAX (model 11/780) computer.

(e) Measurement of Rate Constant with Higher Overpotentials

Higher overpotentials from -250 mV to +250 mV were applied to the RDE with points taken every 25 mV. The currents at one of these overpotentials were measured at different rotation speeds. The reciprocal currents were plotted versus $\omega^{-\frac{1}{2}}$ from 360 rpm to 3600 rpm to obtain the intercept by extrapolation (the reciprocal current under this potential), the obtained current $(i)_{\omega\to\infty}$ would then be free of mass transfer effects. According to the Allen and Hickling[17] approach, the logarithm $(i)_{\omega\to\infty} / (1-e^{f\eta})$ was plotted versus the corresponding overpotentials to find the exchange current from the curve extrapolated to $\eta = 0$ and the transfer coefficient α from the slope of the curve. Intercepts, slopes and inherent errors were also determined by the least squares method with aid of a computer program, also using the VAX computer.

(f) Ferrous and Ferric Ion Concentration Measurements from Limiting Current Measurements

The Levich equation for the limiting current at a rotating disc electrode may be

used to determine the concentrations of Fe^{2+} and Fe^{3+} ions by choice of suitable potentials and a single rotation speed measurement:

$$i_l = 0.62\, n\, F A D^{\frac{2}{3}} \nu^{-\frac{1}{6}} C^* \omega^{\frac{1}{2}} \qquad (3.3.1)$$

A better method is to measure the limiting current as a function of rotation speed, whereupon the first derivative at constant redox ion concentration is

$$\left(\frac{\partial i_l}{\partial \omega^{\frac{1}{2}}} \right)_{C^*} = 0.62\, n\, F A D^{\frac{2}{3}} \nu^{-\frac{1}{6}} C^* \qquad (3.3.2)$$

Even better, since it places the relationships firmly on an empirical basis, no longer dependent on the adequacy or otherwise of the Levich equation, is to experimentally determine the second derivative:

$$\frac{d\left(\frac{\partial i_l}{\partial \omega^{\frac{1}{2}}} \right)_{C^*}}{dC^*} = 0.62\, n\, F A D^{\frac{2}{3}} \nu^{-\frac{1}{6}} = K' \qquad (3.3.3)$$

Use of a series of precisely known concentrations of Fe^{2+} and Fe^{3+} and precisely measured rotation speeds enabled two constants K' to be determined, one for ferrous iron and the other for ferric iron. Then, the Levich-equation simplifies to the form

$$i_l = K' C^* \omega^{\frac{1}{2}} \qquad (3.3.4)$$

so that the empirical equations

$$\frac{d i_{l,Fe^{2+}}}{d\omega^{\frac{1}{2}}} = K'_{Fe^{2+}} C^*_{Fe^{2+}} \qquad (3.3.5)$$

and

$$\frac{d i_{l,Fe^{3+}}}{d\omega^{\frac{1}{2}}} = K'_{Fe^{3+}} C^*_{Fe^{3+}} \qquad (3.3.6)$$

allow determination of the Fe^{2+} and Fe^{3+} concentrations in the same supporting electrolyte and with the same rotating disc electrode.

The calibration of the RDE for the measurement of $K'_{Fe^{2+}}$ was carried out by adding the desired amount of standardized Fe^{2+} solution to the test cell already containing 0.50 mol·L^{-1} H_2SO_4 solution of which the volume had been exactly measured so that the total volume could be calculated. The added Fe^{2+} solution had been standardized by potentiometric titration with standard $Ce(NH_4)_2(NO_3)_6$ as described in Part I. The limiting current measurements at an overpotential of ±550 mV were applied to each known concentration to obtain the corresponding slope $(\frac{\partial i_{l,Fe^{2+}}}{\partial \omega^{\frac{1}{2}}})_{C^*_{Fe^{2+}}}$, the data being presented in Table 3.1.

Table 3.1 Calibration of R.D.E. for Fe^{2+} Concentration Measurement.

Volume of known Fe^{2+}/solution added/mL	20.00	22.00	24.00	26.00	28.00	30.00
$[Fe^{2+}] \times 10^3$/mol·L^{-1}	8.686	9.527	10.36	11.19	12.02	12.84
$(\frac{\partial i_{l,Fe^{2+}}}{\partial \omega^{\frac{1}{2}}})_{C^*_{Fe^{2+}}}$/mA·$s^{\frac{1}{2}}$	0.0115	0.0126	0.0137	0.0147	0.0159	0.0168

The overall constant $K'_{Fe^{2+}}$ is obtained by plotting $(\frac{\partial i_{l,Fe^{2+}}}{\partial \omega^{\frac{1}{2}}})_{C^*_{Fe^{2+}}}$ versus $C^*_{Fe^{2+}}$, expressed as mol·cm^{-3}, as shown in Figure 3.3. The plot is reasonably linear and yields the value $K'_{Fe^{2+}} = 1.304$ A·$s^{-\frac{1}{2}}$·cm^3·mol^{-1}.

Figure 3.3 on next page

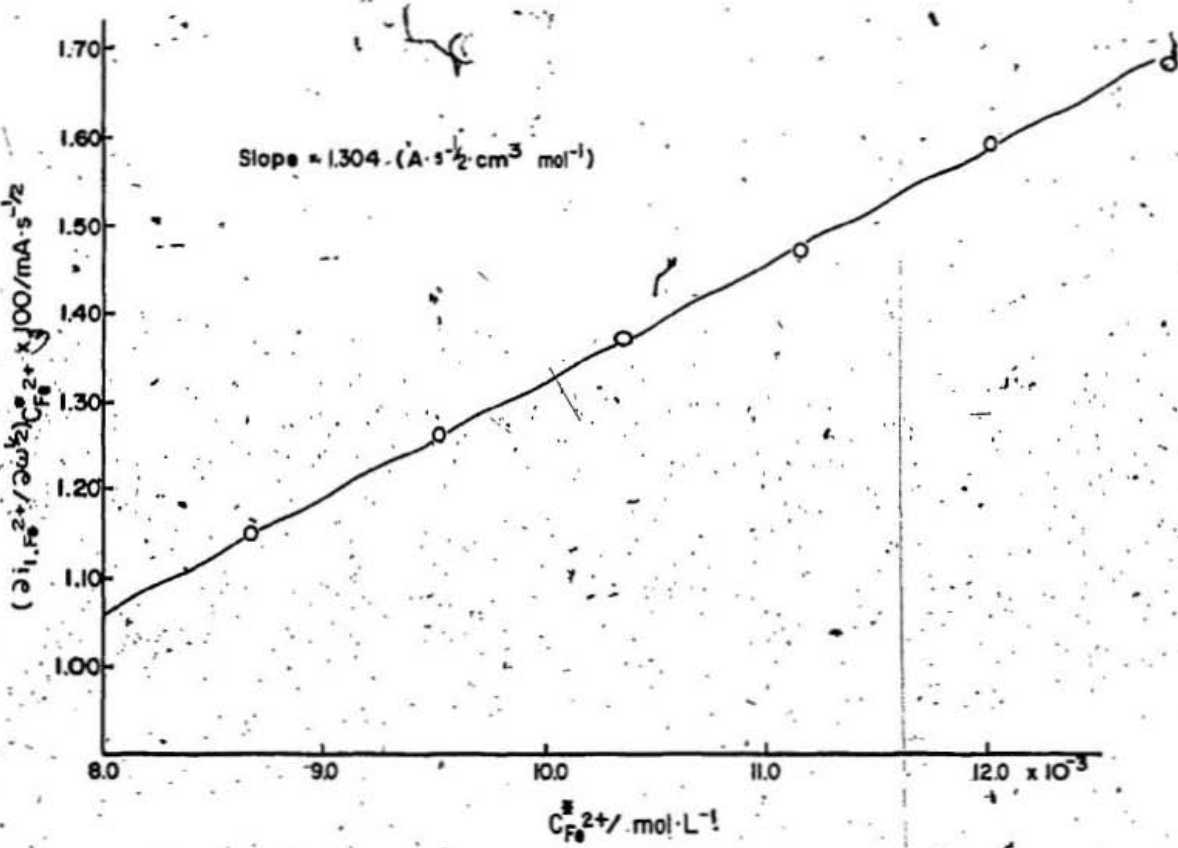

Fig. 3.3 A plot of $\left[\frac{\partial i_{l,Fe^{2+}}}{\partial \omega^{1/2}}\right]$ vs. $C^*_{Fe^{2+}}$ to find the overall constant $K'_{Fe^{2+}}$.

The calibration of the RDE for the measurement of $K'_{Fe^{3+}}$ was carried out in the same way, except that the Fe^{3+} solution was standardized by a photometric titration[32] with EDTA using a Thorn-Smith circulating system enabling the contents of the titration-flask to flow through a cuvette in the light path of a Bausch and Lomb Spectronic 20. Salicylic acid was used to generate a highly coloured compled with Fe(III) before the end-point, the spectrophotometer being set at 525 nm and the solutions were buffered with chloroacetic acid and its sodium salt at pH 2.2. Electrolytic iron (100.00%) from G.F. Smith and Co., dissolved in 6 $mol \cdot L^{-1}$ H_2SO_4 was used as primary standard, after oxidation with the aid of hot concentrated nitric acid. Table 3.2 illustrates the calibration results.

Table 3.2 Calibration of R.D.E. for Fe^{3+} Concentration Measurement.

Volume of known Fe^{2+} solution added/mL	20.00	22.00	24.00	26.00	28.00	30.00
$[Fe^{3+}] \times 10^3$/mol·L^{-1}	8.072	8.852	9.628	10.40	11.17	11.93
$(\frac{\partial i_{l,Fe^{3+}}}{\partial \omega^{\frac{1}{2}}})_{C^*_{Fe^{3+}}}$/mA·s$^{-\frac{1}{2}}$	0.0098	0.0107	0.0116	0.0125	0.0134	0.0142

The overall constant $K'_{Fe^{3+}}$ is obtained by plotting $(\frac{\partial i_{l,Fe^{3+}}}{\partial \omega^{\frac{1}{2}}})_{C^*_{Fe^{3+}}}$ versus $C^*_{Fe^{3+}}$, expressed as $mol \cdot cm^{-3}$, as shown in Figure 3.4. Again the plot is reasonably linear and yields the value $K'_{Fe^{3+}} = 1.166\ A \cdot s^{-\frac{1}{2}} cm^3 \cdot mol^{-1}$. The simplified Levich equations for the two cases are

$$i_{l,Fe^{3+}} = 1.304\ C^*_{Fe^{3+}}\ \omega^{\frac{1}{2}} \qquad (3.3.7)$$

Figure 3.4 on next page

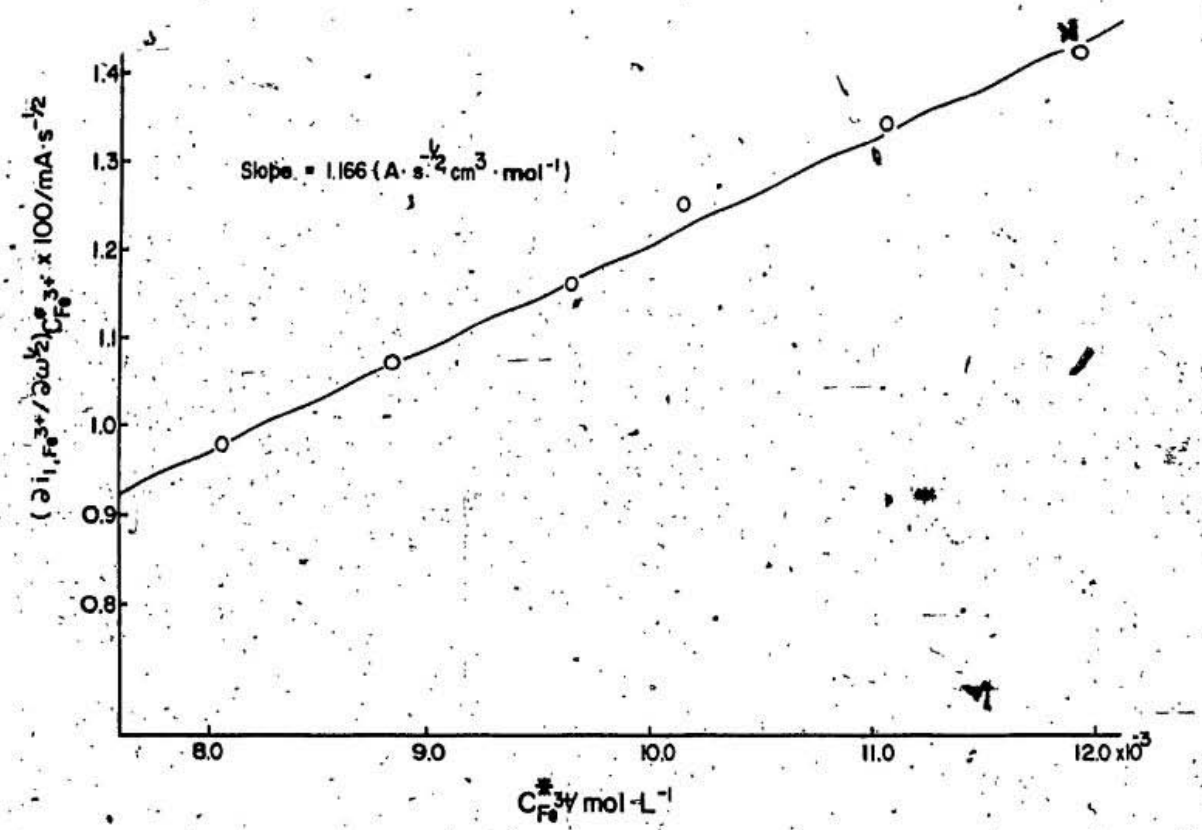

Fig. 3.1 A plot of $\left\{\frac{\partial i_{l,Fe^{3+}}}{\partial \omega^{1/2}}\right\}$ vs. $C^*_{Fe^{3+}}$ to find the overall constant $K'_{Fe^{3+}}$.

and

$$i_{l,Fe^{3+}} = 1.166\, C^{*}_{Fe^{3+}}\, \omega^{\frac{1}{2}} \qquad (3.3.8)$$

It is to be expected that the coefficients in these two equations should be related as $D_{Fe^{2+}}^{2/3}/D_{Fe^{3+}}^{2/3}$. Data for these diffusivities in aqueous H_2SO_4 do not appear to be available from the literature, although two sources give values for aqueous $HClO_4$. Wadden's results[12] at 298.2 K have mean values of $D_{Fe^{2+}} = 0.88 \times 10^{-5}\ cm^2 \cdot s^{-1}$ and $D_{Fe^{3+}} = 0.69 \times 10^{-5}\ cm^2 \cdot s^{-1}$ giving a ratio of 1.175 while the ratio of $K'_{Fe^{2+}}/K'_{Fe^{3+}}$ for aqueous H_2SO_4 from the above results is 1.118, fair agreement considering the change of medium.

Table 3.3 and Figure 3.5 illustrate the practical application of these results to the determination of concentrations of Fe^{2+} and Fe^{3+} in a working solution. These concentrations were the ones used in subsequent calculations. In all cases they were satisfactorily in accord with expectations from the quantities of salts weighed out for preparation of the experimental solutions.

Figure 3.5 on next page

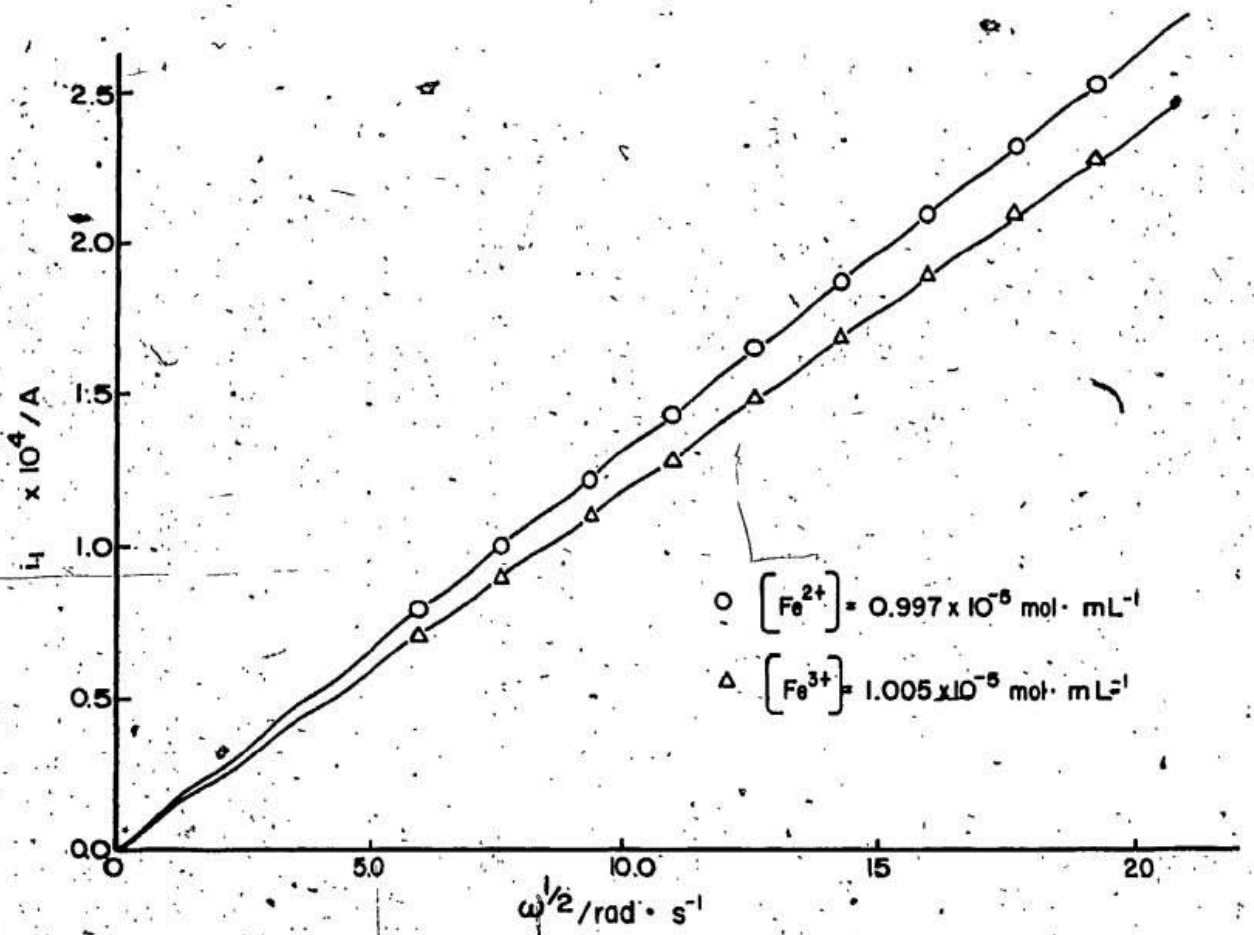

Fig. 3.5 Plots of limiting current measurements.

Table 3.3 Limiting Current Measurements on a Typical Solution at Nine Rotation Speeds

(Rotation Speed) $^{\frac{1}{2}}$	Anodic Limiting Current	Cathodic Limiting Current
$\omega^{\frac{1}{2}}$/rad·s$^{-\frac{1}{2}}$	$i_{l,Fe^{2+}}$/A x 10^4	$i_{l,Fe^{3+}}$/A x 10^4
6.094	0.787	0.704
7.707	0.994	0.894
9.399	1.214	1.092
10.97	1.419	1.275
12.62	1.638	1.467
14.36	1.859	1.674
16.03	2.077	1.877
17.76	2.307	2.075
19.32	2.511	2.263

In this particular example, $C^*_{Fe^{2+}} = 0.997 \times 10^{-5}$ mol·cm^{-3} and $C^*_{Fe^{3+}}$ 1.005×10^{-5} mol·cm^{-3}.

(g) Electrode Area Measurement

Rotating disc electrodes were constructed of 2 mm diameter platinum rod and geometric measurement confirmed this diameter and hence a circular cross sectional area of 0.0314 cm^2. True surface areas may be ascertained using methods surveyed by Woods[33]. Two methods are available for platinum, measurement of the charge required to adsorb a monolayer of hydrogen atoms or to desorb a monolayer of oxygen atoms. Using a triangular sweep voltammogram, the area under the peaks for hydrogen adsorption or under the peak for oxygen desorption may be measured and converted to an equivalent charge through knowledge of the experimental conditions.

The measurement error may be diminished by use of the oxygen desorption peak rather than the hydrogen adsorption peaks because the area of the oxygen peak is much larger; therefore, the result from the oxygen peak was preferred in this work. The real surface area was calculated by dividing the integrated charge by 420 $\mu C \cdot cm^{-2}$ for oxygen desorption or by 210 $\mu C \cdot cm^{-2}$ for hydrogen adsorption.

In working out the areas under the curves, the peaks were cut out and weighed on an analytical balance. The mass of an integral number of square inches was also determined, using 2 and 4 in^2 squares of graph paper, the masses being in the range of tenths of a gram in every case. The experimental conditions for the area determinations on the best platinum RDE were as follows:

Sweep rate: 0.415 $V \cdot s^{-1}$

Potential scale: 0.10 $V \cdot in^{-1}$

Current scale: 1.577 $\mu A \cdot in^{-1}$

The charges for hydrogen and oxygen were, respectively, $Q_H = 15.89\ \mu C$; $Q_O = 29.08\ \mu C$ yielding real areas of 0.0757 cm^2 and 0.0692 cm^2, respectively. These results indicate surface roughness factors of 2.205 from the oxygen determination, or 2.4 from the hydrogen determination. Considering that the platinum surface had been machined but was not polished with abrasive materials, a surface roughness factor of 2.2 is quite satisfactory. Earlier, less precise measurements of the real area of a well-used platinum electrode (in the less satisfactory plastic sheath) had indicated a roughness factor of 3 or more in that case.

Chapter 4 Results

The experiments for the kinetic measurements were done in several stages, preliminary work and then later work with various levels of cleaning. Except where indicated otherwise, rate constants refer to platinum electrodes in the ferrous sulphate-ferric sulphate system at concentrations of approximately 0.01 mol·L^{-1} $FeSO_4$ and 0.005 mol·L^{-1} $Fe_2(SO_4)_3$ in 0.5 mol·L^{-1} H_2SO_4.

4.1 Preliminary Investigation of Activation

In earlier work from this laboratory,[11,12] studies of anodic activation of platinum (as well as of palladium and gold) were inconclusive as to the relative merit of activation in the presence or absence of iron salts and as to the most suitable potential range to be used. The first step, therefore, was to investigate this question. In the experiments in the early stage less pure $FeSO_4$ and $Fe_2(SO_4)_3$ salts and sulphuric acid were used. The RDE was by error insulated by a piece of polystyrene or lucite plastic instead of Kel-F. Solutions were made up with single distilled water and the cleaning of the whole system was not as thorough as in the later stages. The rate constants were measured in this stage by applying overpotentials (relative to a platinum reference electrode in the redox system) every 1.0 mV over the range -10.0 to +10.0 mV. The corresponding currents at each rotation speed were plotted versus overpotential to obtain a slope $(\frac{\partial i}{\partial \eta})_\omega$, two examples of which are shown in Fig. 4.1.

Figure 4.1 on next page

The relation between i and η is a pure resistance characteristic since the curves are linear and go through the origin. To eliminate mass transport effects, the slopes were plotted versus the reciprocal square root of rotation speed, $\omega^{-\frac{1}{2}}$, according to

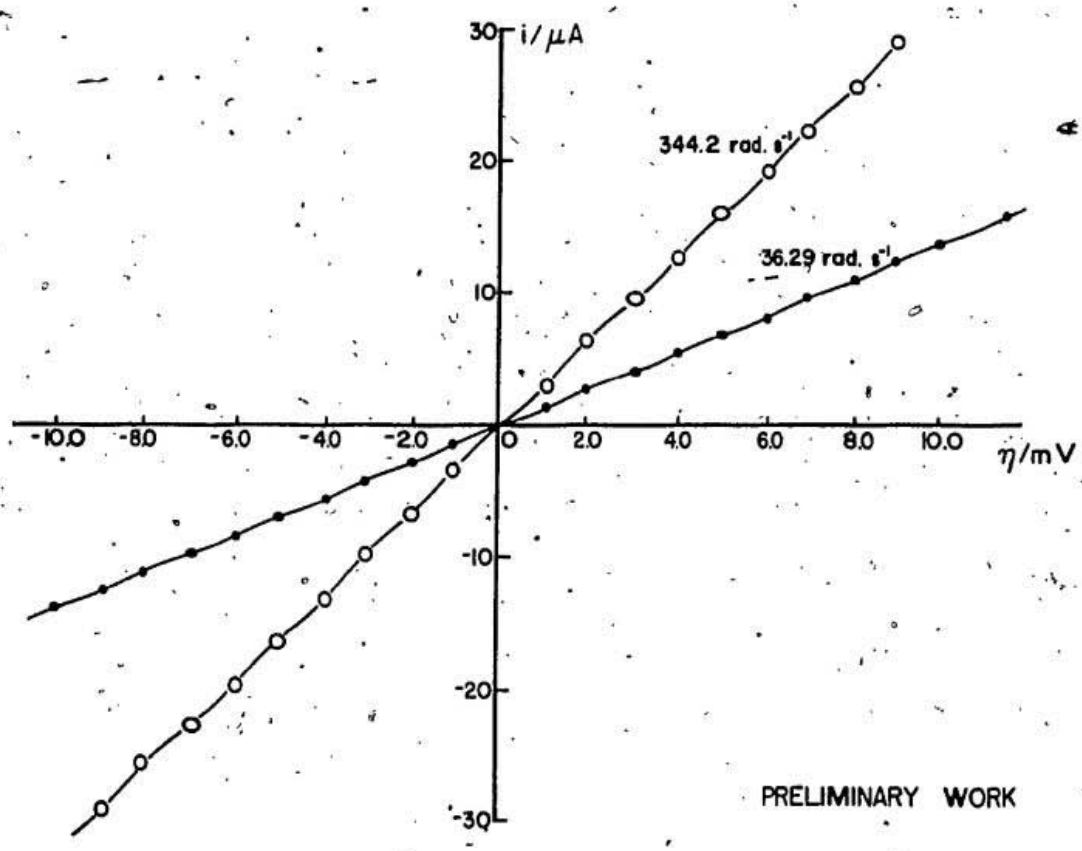

Fig. 4.1 Linear plots of current vs. overpotential at two rotation speeds.

equation (2.3.13). The true exchange current was obtained from the intercept by the extrapolation to infinite rotation speed; an example of such a curve is shown in Fig. 4.2.

Figure 4.2 on next page

The measurements of rate constant gave information about electrode activity, allowing comparison of the rate constants before activation and after activation under the same experimental conditions. A series of experiments was designed to find the best conditions for activation, whether to use aqueous H_2SO_4 alone or containing Fe^{2+} and Fe^{3+} salts and what was the best potential range to employ. As many workers have done[34,35], the activation was carried out in 0.5 mol·L^{-1} H_2SO_4 (or some other acid solution) in the absence of iron salts. For this purpose a previously hydrogen-charged α/β palladium hydride reference electrode[36] (potential +50 to +60 mV vs S.H.E.) was used. It was not very convenient to change solutions from the activation solution to the test solution; especially since the electrode and the cell system could be contaminated if a specially designed cell system were not used. S. Gilman[37] mentioned that if even for an instant the platinum electrode is exposed to the air, its activity could greatly decrease and it could be assumed to be contaminated. The objective here was to try to activate the platinum RDE in the test solution without changing the solution before measurements. The following table shows that in this case the rate constant increased even more than it did after activation in pure 0.5-mol·L^{-1} H_2SO_4 solution.

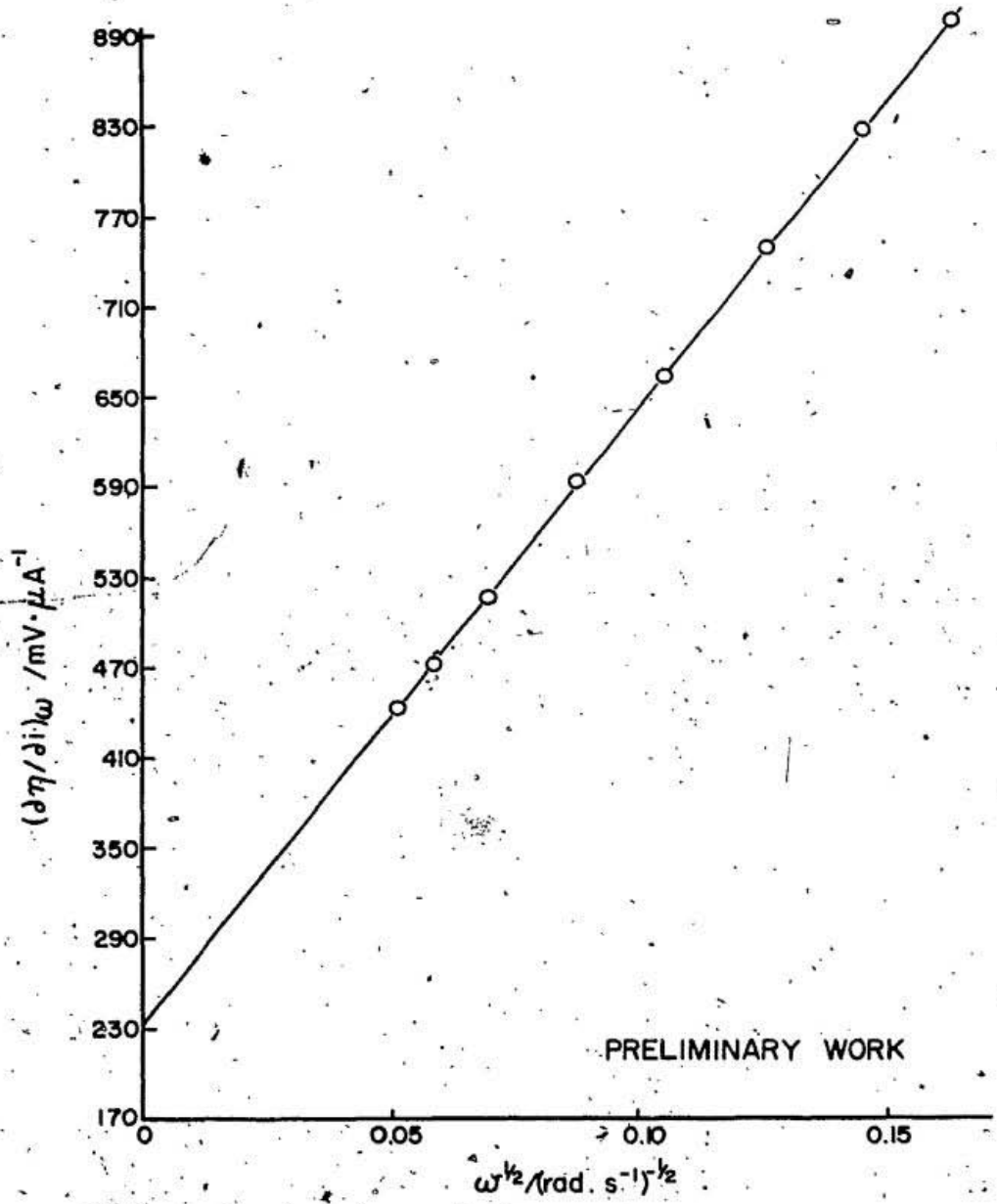

Fig. 4.2 A plot of $(\frac{\partial \eta}{\partial i})_\omega$ vs $\omega^{-\frac{1}{2}}$

Table 4.1 - A Comparison of Activation in Different Solutions - Preliminary Work: Pt RDE

Activation Conditions	Test No.	Electrode Conditions	Rate Const. $k^0 \times 10^3/cm \cdot s^{-1}$	Percentage increase of rate constant
In solution A*	001	before activation	4.67	
	002	after activation	7.01	+50%
In solutionB**	005	before activation	5.17	
	007	after activation	6.87	+32%
In solution A	008	before activation	4.94	
	009	after activation	12.6	+155%
In solution B	011	before activation	4.94	
	012	after activation	8.89	+80%

* Solution A contains 0.01 M Fe^{2+} and Fe^{3+} in 0.5 $mol \cdot L^{-1}$ H_2SO_4.

** Solution B contains only 0.5 $mol \cdot L^{-1}$ H_2SO_4.

The presence of Fe^{2+} and Fe^{3+} does not hinder the activation but does seem to enhance it. Similar results were found in later experiments. Fig. 4.3 and Fig. 4.4 show the cyclic voltammograms for the activation in 0.5 $mol \cdot L^{-1}$ H_2SO_4 above and in Fe^{2+} and Fe^{3+}-containing solution, respectively.

Figures 4.3 and 4.4 on next page

4.2 Preliminary Work with Improved Platinum Disc Electrode

After the preliminary experiments, two series of more precise work were done For the first series, the platinum disc electrode had been replaced with a newly made one with the correct Kel-F mantle and all electrodes and glassware were cleaned by

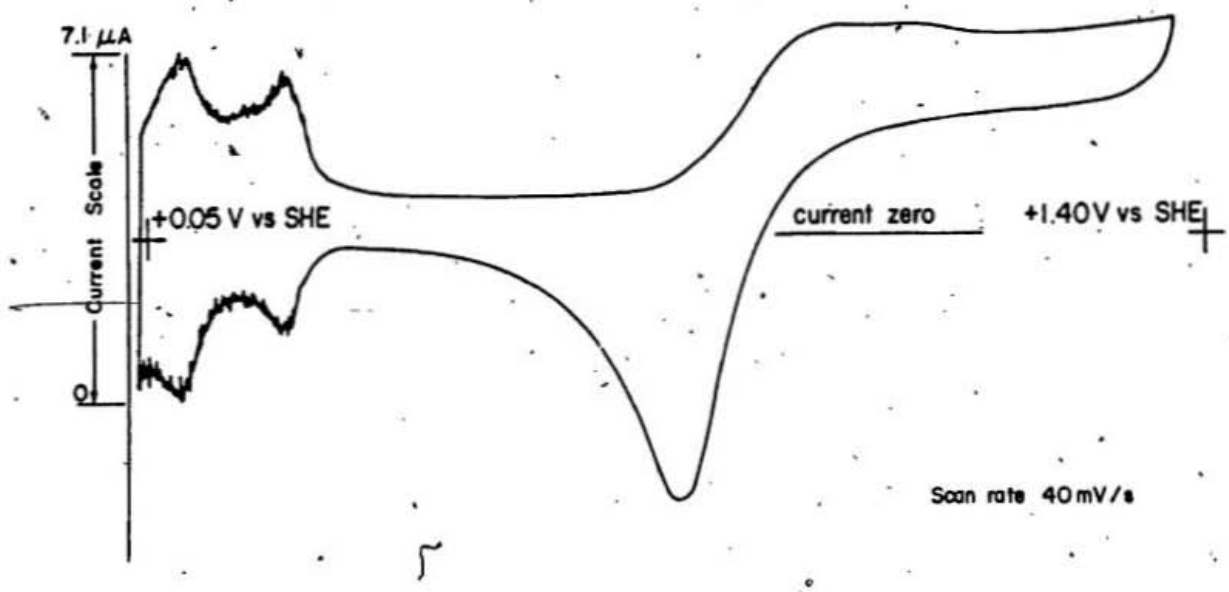

Fig. 4.3 The triangular sweep voltammogram for activation in pure 0.5 mol·L^{-1} H_2SO_4 under stationary conditions.

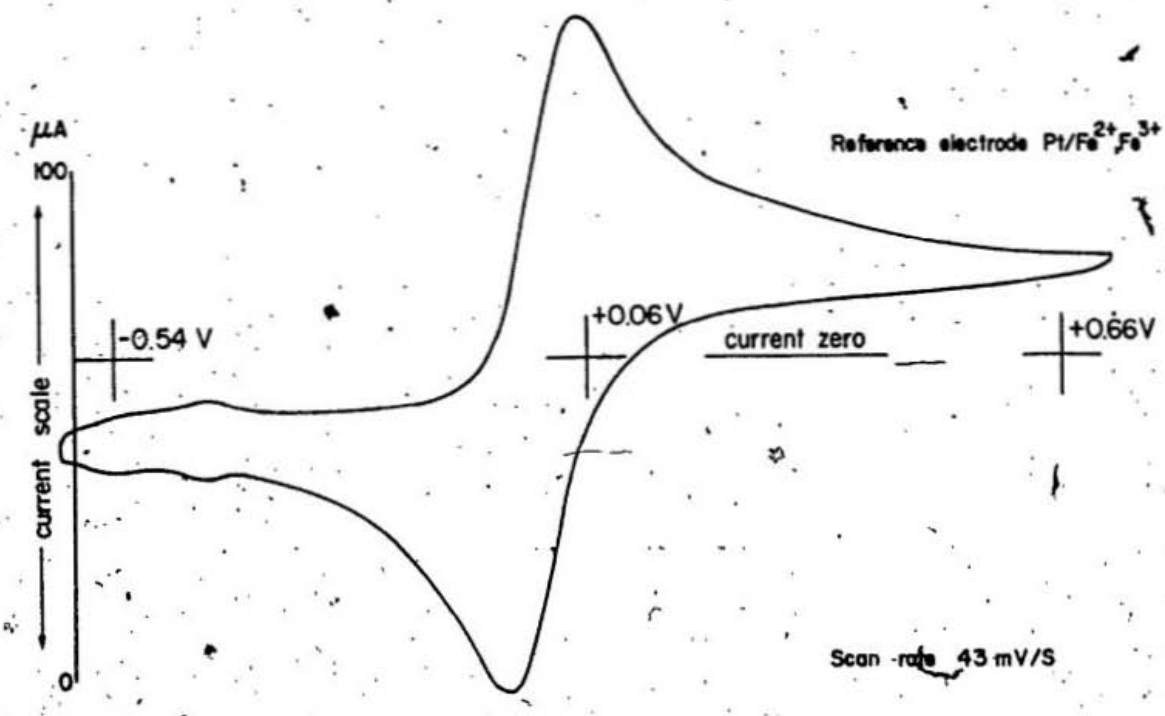

Fig. 4.4 The triangular sweep voltammogram for activation in 0.5 mol·L^{-1} H_2SO_4 solution containing Fe^{2+} and Fe^{3+} under stationary conditions.

procedures similar to those that have been described in Chapter 3 except that steaming treatment was not used and cold HNO_3 was used to wash the cell; furthermore, the cell was dried in a possibly unclean oven before use. Many measurements show that the platinum activity increased slightly after activation but the rate constants are all small as Table 4.2 shows:

Table 4.2 The Activation Effects on the Rate Constant for $Fe^{2+} \rightleftharpoons Fe^{3+} + e^-$ Using a New Pt RDE

Test No.	Pt RDE and Activation Conditions*	Rate Const. $k^\circ \times 10^3$/cm·s^{-1}	Percentage increase of rate constant
100	before activation	2.8	
101	after activation in solution A	3.0	6%
104	before activation	1.7	
105	after activation in solution A	2.7	37%
106	before activation	1.4	
107	after activation in solution B	2.3	39%
112	before activation	1.6	
113	after activation in solution A	2.5	36%

* Solutions A and B are as in Table 4.1.

Those results above are similar to the preliminary results, but the activation seems less efficient than in the preliminary measurements.

4.3 The Effect of Improved Cleaning Techniques

A second series of experiments was performed with great attention to the cleaning steps. However, the steaming treatment was not yet applied. The procedures followed those described in Chapter 3 with this one exception and the cleaning preparation took about one week each time. Unfortunately the results obtained were disappointing as Table 4.3 shows.

Table 4.3 Results From Clean System

Test No.	Pt RDE and Activation Conditions*	Rate Const $k^o \times 10^3/cm \cdot s^{-1}$	Percentage increase rate constant
060	before activation	9.5	
061	after activation in solution A potential range 0.41 - 1.46 V vs SHE	6.8	-28%
064	before activation	7.5	
065	after activation in A potential range 0.41 - 1.46 V vs SHE	5.3	-29%
067	before activation	7.8	
068	after activation in A E range 0.31 - 1.07 V vs SHE	5.4	-30%
069a	before activation	6.7	
069b	after activation in A E range 0.32 - 1.16 V vs SHE	5.4	-19%
070	before activation	7.1	
071	after activation in A E range 0.32 - 1.26 V vs SHE	5.4	-24%
072	before activation	7.0	
073	after activation in A E range 0.32 - 1.36 V vs SHE	6.0	-14%
080	before activation	8.4	
081	after activation in A E range 0.41 - 1.46 V vs SHE	5.4	-36%

* Solution A is as in Table 4.1, and contains both Fe^{2+} and Fe^{3+} ions.

Apparently a *deactivation* of the platinum surface occurred instead of activation. A fairly good reproducibility may be found in which the initial rate constant is about 7.5×10^{-3} $cm \cdot s^{-1}$, the rate constants after activation are *ca.* 5.4×10^{-3} $cm \cdot s^{-1}$. Great efforts have been made to find the reason for the decrease of activity after activation. Observing Table 4.3, even though the anodic potential limits were changed from 1.07 V vs SHE to 1.46 V vs SHE, the situation still remained the same.

4.4 Further Improvements in Technique

In order to explain the unexpected results, extreme care was taken in the cleaning procedures, thus the steaming treatment was applied to every piece of experimental material. Puratronic 99.999% pure $FeSO_4 \cdot 7H_2O$ and 99.999% pure anhydrous $Fe_2(SO_4)_3$ were used instead to avoid possible contamination before and during the electrolytic oxidation of Fe^{2+} to Fe^{3+}. About 2 to 3 days had to be spent on dissolving the metallic iron and oxidizing Fe^{2+} to Fe^{3+} in that case. Thus the sintered glass separator and a tube of 3 $mol \cdot L^{-1}$ H_2SO_4 solution and a large area platinum anode were not used in preparing the solution for this work. The rate constant could now be measured immediately after the preparation of the test solutions.

By changing the procedures and reagents as mentioned above, large differences of rate constant were found between the measurements before and after activation as shown in Table 4.4.

Table 4.4 Results of Activation in Very Pure Solution

Test No.	Pt RDE and Activation Conditions	Rate Const $k^o \times 10^3/cm \cdot s^{-1}$	Percentage increase in rate constant
124	Before activation, the RDE and cell were extremely cleaned.	9.0	
125	After activation, in solution A at potential range 0.01 - 1.35 V vs SHE	2.0	-78%
150	Before activation, the RDE and cell were extremely cleaned.	8.8	
151	After activation in solution A at potential range 0.07 - 1.41 V vs SHE	2.2	-68%
161a	Before activation, the RDE and cell were extremely cleaned.	9.0	
161b	After activation in solution A at potential range 0.07 - 1.41 V vs SHE	2.0	-78%

The rate constant of the platinum RDE was increased to about 9.0 x 10^{-3} cm·s^{-1} by the thorough cleaning procedures but the rate constants were decreased to about 2.0 x 10^{-3} cm·s^{-1} by the "activation" and this phenomenon had fairly good reproducibility in different experiments. The results above give the impression that the cyclic sweep may build up some oxide film on the very clean platinum surface and the electrode activity was thereby decreased.

In order to avoid the error which may be caused by using only low overpotential methods, high overpotential methods were employed which enabled comparison of rate constants from several methods and also determination of α. Fig. 4.5 shows the extrapolation plots for several high negative overpotentials. The intercepts give the reciprocal currents which are free of mass transport effects. Fig. 4.6(a) shows the Tafel plot of these extrapolated currents for overpotentials from -50 to -200 mV; the intercept extrapolated to zero overpotential gives the exchange current freed from mass transport hindrance and the slope gives the transfer coefficient. Fig. 4.6(b) shows the same data treated by the preferable Allen and Hickling plot - the linearity is somewhat improved.

Figures 4.5, 4.6(a) and 4.6(b) on next pages

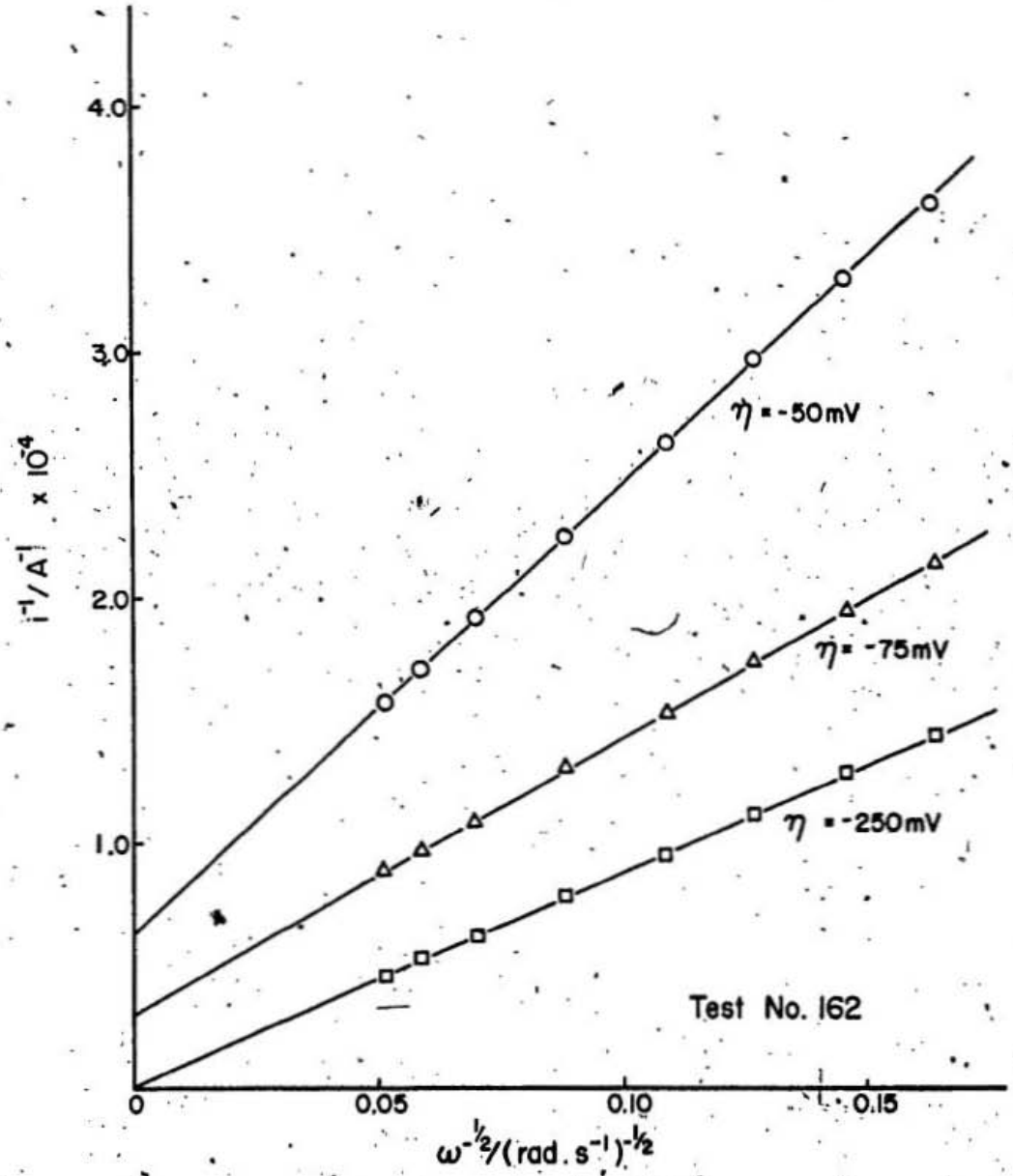

Fig. 4.5 Inverse Levich plots for negative overpotentials. Pt RDE soaked in 0.1 mol·L^{-1} $FeSO_4$ for 4 h before measurements.

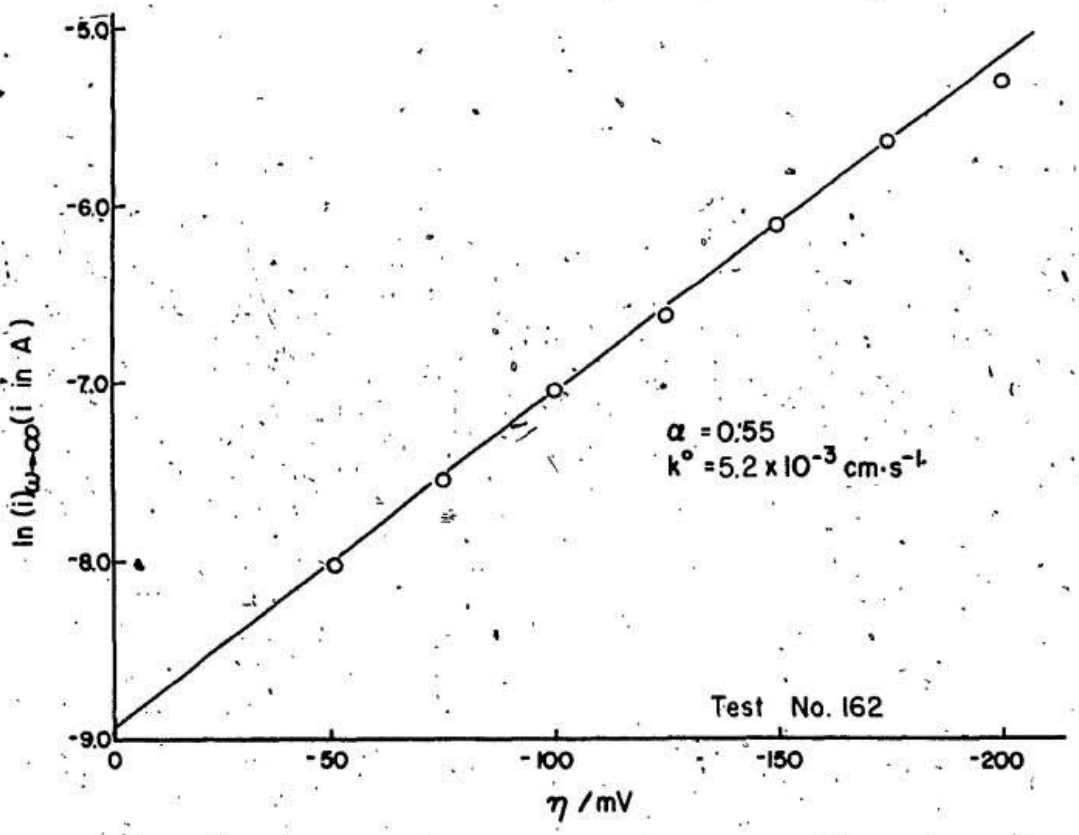

Fig. 4.6(a) Tafel plot of infinite rotation speed currents for negative overpotentials

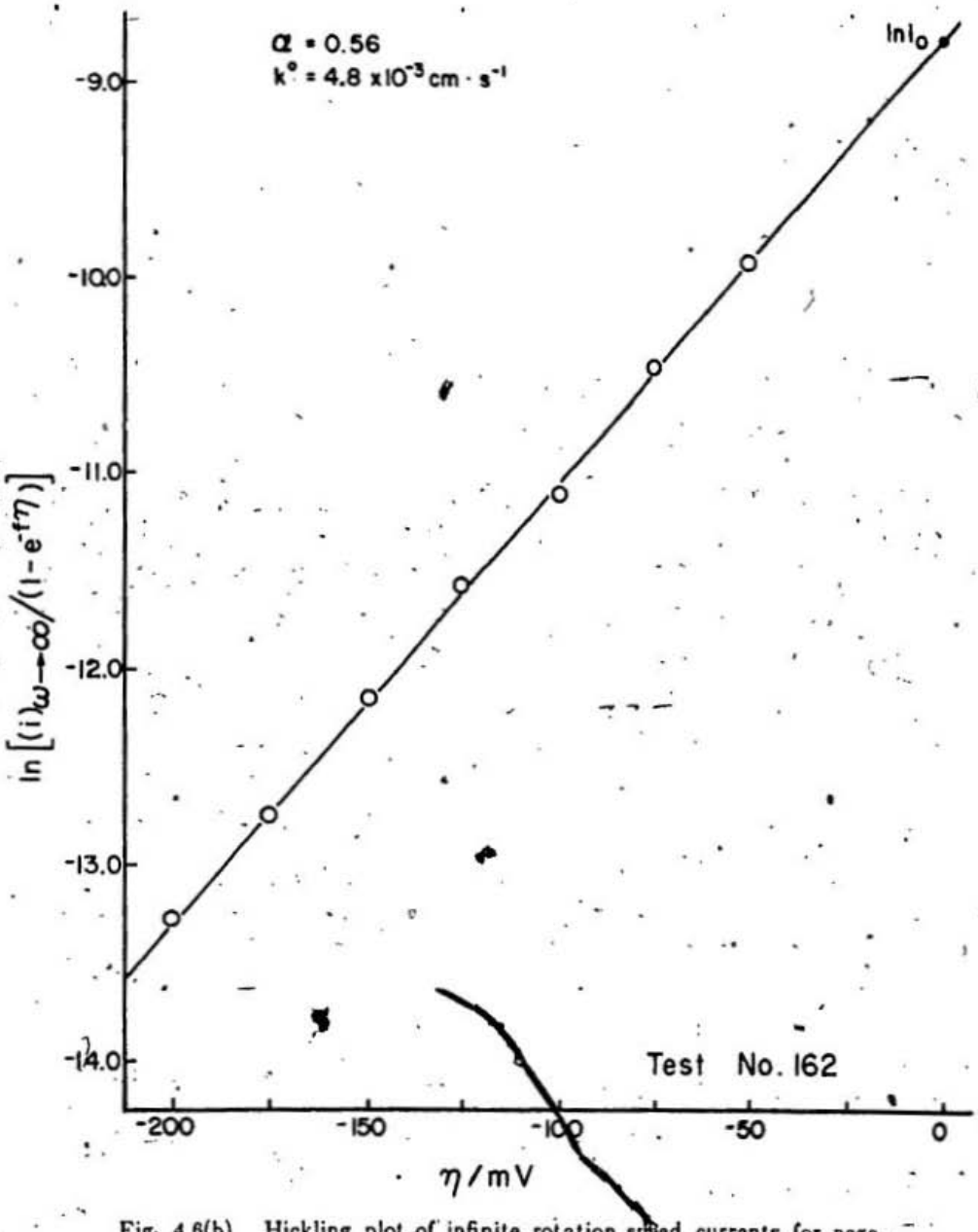

Fig. 4.6(b) Hickling plot of infinite rotation speed currents for negative overpotentials.

Many measurements were carried out using high negative overpotentials as in Figs. 4.5, 4.6(a) and 4.6(b) and in Table 4.5.

Table 4.5 Rate Constants and Transfer Coefficients Measured from Tafel Plots at High Negative Overpotentials

Test No.	High Negative Overpotential Result $k^\circ \times 10^3/cm \cdot s^{-1}$	α (anodic)	Correlation Coefficient of Tafel Plot	Corresponding Low Overpotential Measurement Result $k^\circ \times 10^3/cm \cdot s^{-1}$
151	2.1	0.59	0.9999	2.2
152	5.6	0.57	0.9997	7.7
153	5.0	0.55	0.9995	7.0
156	1.8	0.60	0.9999	1.6
162	5.2	0.55	0.9994	6.5
164	8.2	0.54	0.9970	9.3

The overpotential range was usually from -50 mV to -250 mV: with points taken at -50 mV, -75 mV, -100 mV, -125 mV, -150 mV, -175 mV, -200 mV and -250 mV. The corresponding currents $(i)_{\omega \to \infty}$ were extrapolated for each of the overpotentials and all the results were calculated with the least squares method by computer. The variation of rate constants was presumably caused by differing RDE surface conditions. The measured transfer coefficients have an average value of 0.57. Comparing the rate constants measured in the high negative overpotentials with low overpotential methods, they are mostly smaller than the corresponding low η methods. The linearities reflected by the correlation coefficients are fairly good.

The rate constants were also measured by applying high positive overpotentials. The applied overpotential range was from +50 mV to + 250 mV and points were taken every 25 mV. Similarly, the current $(i)_{\omega \to \infty}$ was extrapolated versus the

reciprocal square root of rotation speed to infinite value at each constant overpotential. Fig. 4.7 shows some of these extrapolations (so-called inverse Levich plots). The exchange current and transfer coefficient were found by Tafel plots or by using Allen and Hickling's improved Tafel equation. Fig. 4.8 shows the somewhat scattered linear relation between $\ln\left[\frac{(i)_{\omega\to\infty}}{1-e^{-f\eta}}\right]$ and overpotential η. Table 4.6 gives some of the results. The poor correlation coefficients suggest that a linear treatment is inappropriate.

Table 4.6 Results of k° and α Measurments at High Positive Overpotentials

Test No.	High Positive Overpotential Result $k^\circ \times 10^3/cm\cdot s^{-1}$	α (anodic)	Correlation Coefficient of Tafel Plot	Corresponding Low Overpotential Measurement Result $k^\circ \times 10^3/cm\cdot s^{-1}$
150	6.4	0.68	0.9919	8.8
151	9.1	0.74	0.9933	2.2
152	13.6	0.79	0.9775	7.7
153	5.7	0.74	0.9288	7.0

In Fig. 4.10 the large negative deviations from linearity of the Hickling plot suggest a buildup of oxide film on the platinum surface, hindering the electron transfer process, as the potential is shifted to more and more positive values.

Figures 4.7, 4.8, 4.9 and 4.10 on next pages

The rate constant was also measured by applying both positive and negative overpotentials to the RDE. The procedures to find the infinite rotating speed current were the same as discussed above. Fig. 4.9 is one of the Hickling plots for overpotentials from +100 mV to -100 mV. A reasonably good linear relation is

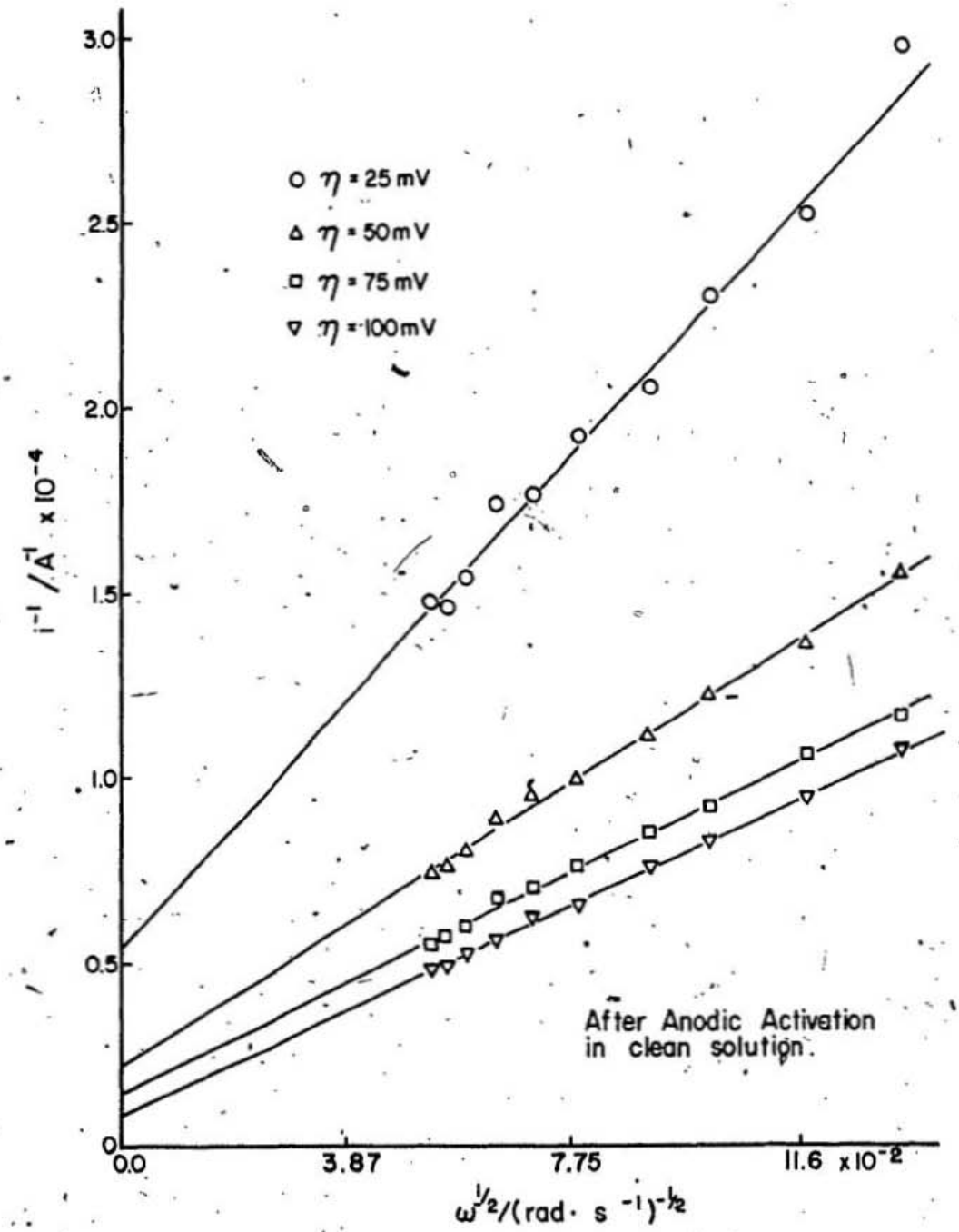

Fig. 4.7 Inverse Levich plots for positive overpotentials.

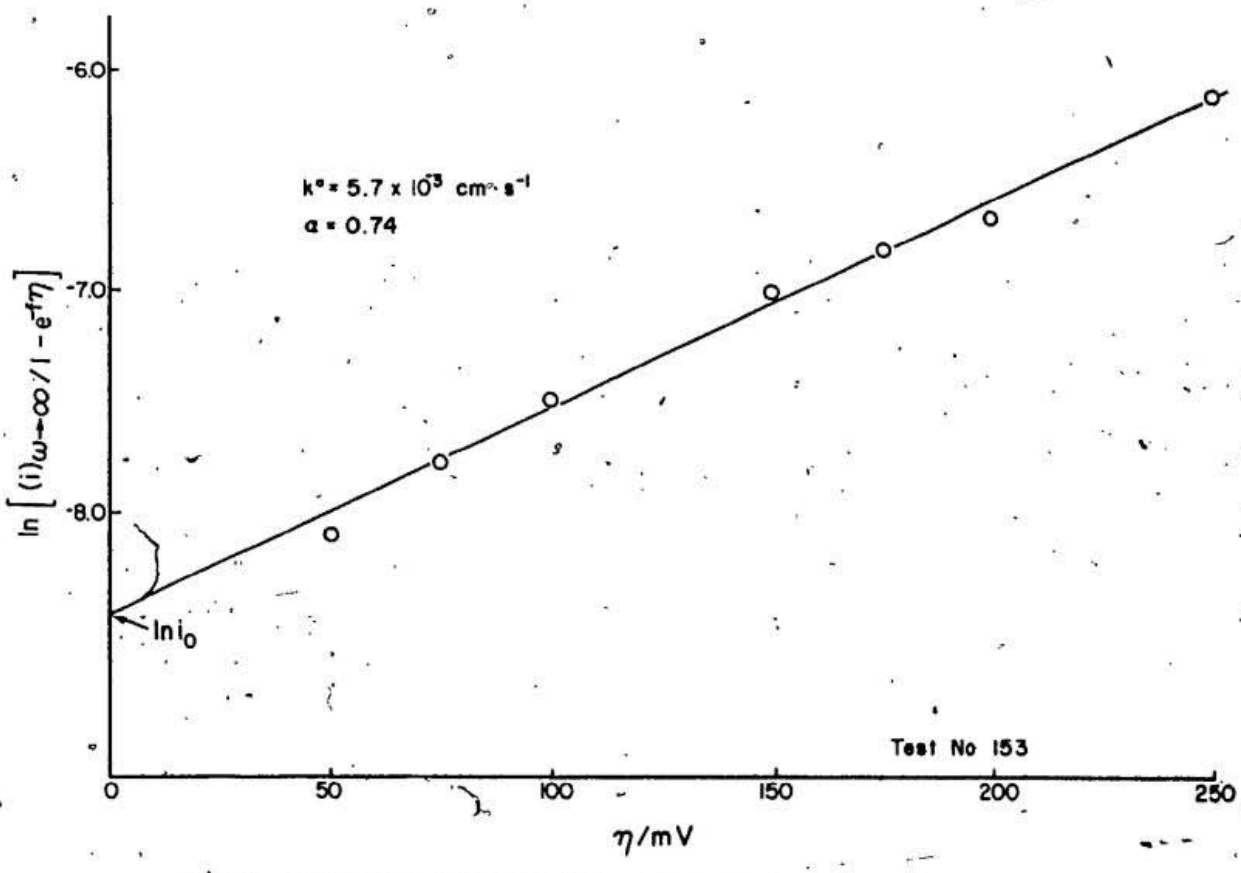

Fig 18 Hickling plot of infinite rotation speed currents for positive overpotentials

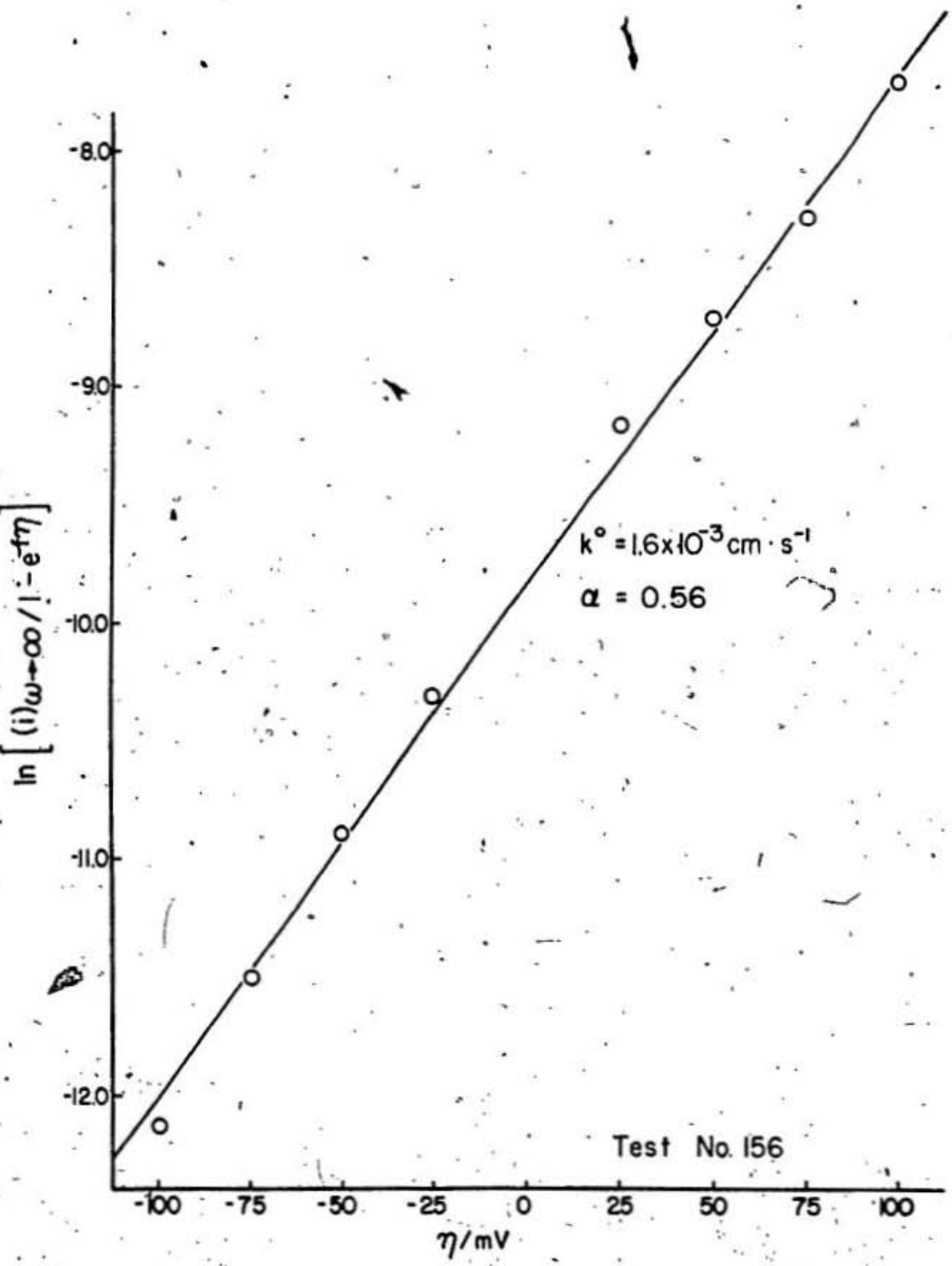

Fig. 4.9 Hickling-plot of infinite rotation speed currents for positive and negative overpotentials.

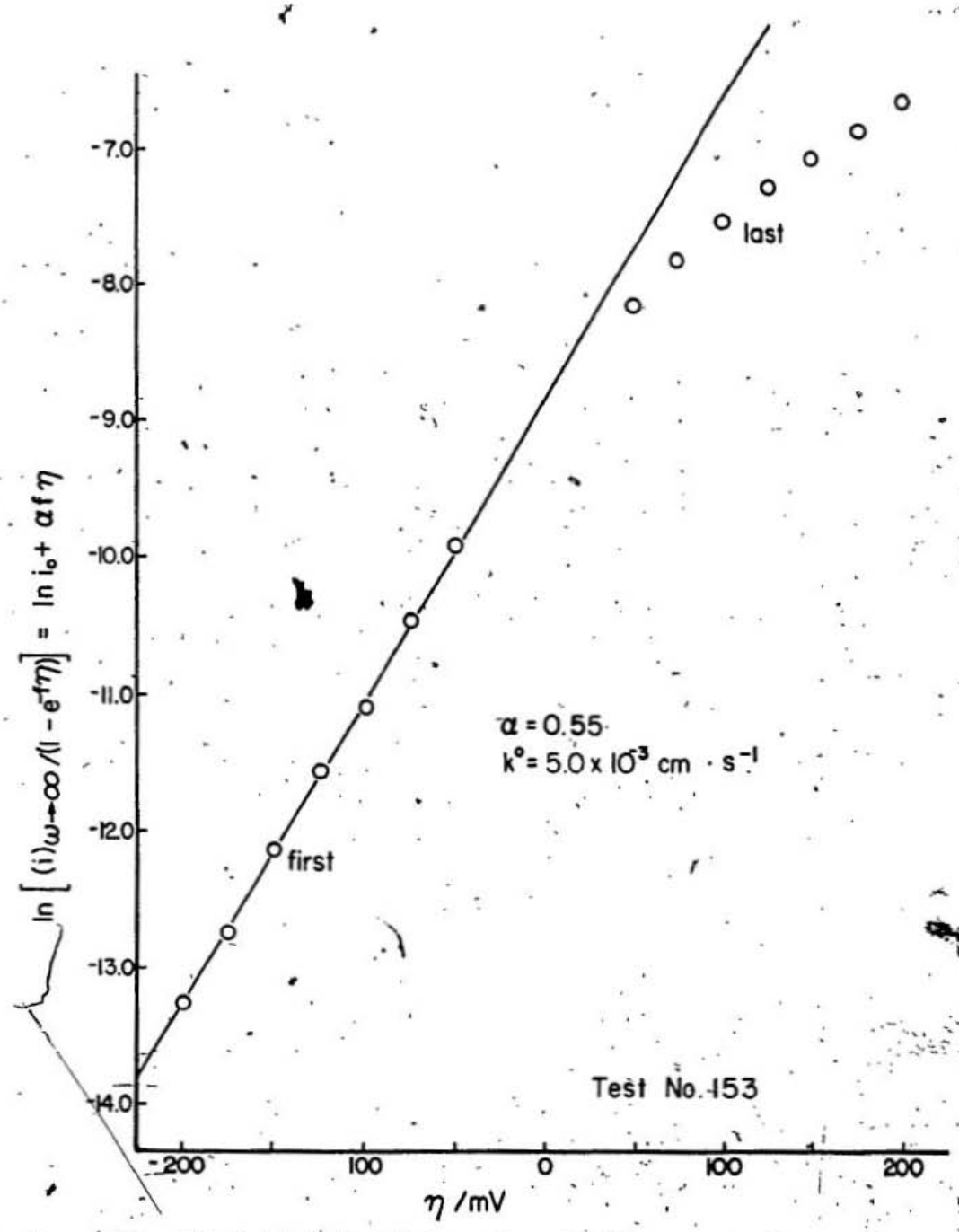

Fig. 4.10 Hickling plot at high negative and positive overpotentials.

displayed. The exchange current is decided by the line intersecting zero overpotential. However, if even higher overpotentials were applied to the platinum, the linear relation deviated negatively on the side of high positive overpotential. This effect, shown in Fig. 4.10, was always observed with such positive potential values. The following table shows some results of measurements using both negative and positive overpotentials.

Table 4.7 Results of k^o and α Measurements at Moderate Positive and Negative Overpotentials ($|\eta| \leq 100$ mV).

Test No.	Moderate Positive and Negative Overpotential Result $k^o \times 10^3/cm \cdot s^{-1}$	α (anodic)	Correlation Coefficient of Hickling Plot	Corresponding Low Overpotential Measurement Result $k^o \times 10^3/cm \cdot s^{-1}$
155	2.2	0.55	0.9980	4.0
156	1.6	0.56	0.9970	1.8
160	1.9	0.55	0.9978	3.6

The rate constants measured with this method are lower than the corresponding results from the low overpotential method but the transfer coefficients have good agreement. The average value is about 0.55, compared with 0.57 from negative overpotentials alone.

It is clear that a high positive overpotential applied to an extremely clean electrode decreases the platinum activity for the Fe^{2+}, Fe^{3+} redox reaction no matter how the high positive potential is applied, such as by trangular sweeping or during the rate constant measurement. Many efforts were made to recover the activity of the RDE. The most significant way is soaking platinum electrode in a 0.1 $mol \cdot L^{-1}$ $FeSO_4$ in 0.5 $mol \cdot L^{-1}$ H_2SO_4 solution. Furthermore, once the activity is increased, the RDE can retain the high activity in Fe^{2+}, Fe^{3+}-containing solution. The follow-

ing table shows the results of this soaking.

Table 4.8 Experiments Including Soaking Platinum RDE in 0.1 mol·L^{-1} $FeSO_4$ Solution

Test No.	Procedures	$k^\circ \times 10^3$ /cm·s^{-1}	Correlation Coefficient of k° Determination
160	Initial rate constant k° measured at low η	3.6	0.9999
	k° measured at high negative η	1.7	0.9948
	k° measured at moderate - η and + η	1.9	0.9978
	After the RDE was soaked in 0.1 mol·L^{-1} $FeSO_4$ solution for 3 hours, k° measured at low η	3.7	1.0000
161	Right after cleaning and k° was measured at low η	9.0	1.0000
	Right after anodic activation E = -0.61 to +0.73 V vs Pt, Fe^{2+}/Fe^{3+} and k° was measured at low η	2.0	0.9995
162	After soaking RDE in 0.1 mol·L^{-1} $FeSO_4$ for 4 hours, k° measured at low η	6.5	1.0000
	k° measured at high negative η	5.2	0.9994
	k° measured at moderate - η and + η	1.9	0.9963
	After soaking RDE in 0.1 mol·L^{-1} $FeSO_4$ for 3 hours, k° measured at low η	6.0	1.0000
163	Pt RDE left in cell solution 24 h k° measured at low η	7.1	1.0000
	After RDE was soaked in $FeSO_4$ for 12 hours, k° measured at low η	9.1	1.0000

The activity of the RDE recovered after the chemical reduction of the oxide film on the surface of RDE which must have been formed by the application of high positive

overpotentials. It has to be mentioned that the soaking solution was made up using the same highly pure salt (99.999% $FeSO_4 \cdot 7H_2O$) as in the test solution and the container for preparation of the solution was also thoroughly cleaned.

Chapter 5 Conclusions

5.1 Low Overpotential Measurements

Most of the measurements of rate constant in the present work were carried out using the low overpotential method. The reliability of the method may be estimated by considering its intercept and its slope. The rate constants by the method were compared with the literature values and an adequate agreement was found (see Section 5.4). Secondly, the experimental slopes are compared with the theoretical value evaluated from equation (2.3.13) using $K = 0.894$, $A_O = 1.166\ \omega^{1/2}$ A·cm^3·mol^{-1} and $C^*_{Fe^{3+}} = 1.0 \times 10^{-5}$ mol·cm^{-3}. Table 5.1 contains thirteen low overpotential measurements under different RDE surface conditions.

Table 5.1 The Slopes of $(\frac{\eta}{i} \cdot \frac{F}{RT})$ versus $\omega^{-1/2}$ from Low Overpotential Measurements.

Test No.	Slope x 10^{-5}/ $A^{-1}\cdot s^{-1/2}$	Rate Constant/ $cm\cdot s^{-1}$	Correlation Coefficient
155A	1.61	0.0040	1.0000
155B	1.61	0.0039	1.0000
157	1.62	0.0031	1.0000
159	1.57	0.0017	0.9999
160A	1.60	0.0036	0.9999
160B	1.59	0.0037	1.0000
161	1.61	0.0090	1.0000
162A	1.59	0.0065	1.0000
162B	1.60	0.0060	1.0000
163A	1.60	0.0071	1.0000
163B	1.62	0.0091	1.0000
163C	1.60	0.0071	1.0000
164	1.62	0.0093	1.0000

The average slope is 1.60×10^5 $A^{-1}\cdot s^{-1/2}$. This result shows that no matter how the

rate constant varies from 1.7×10^{-3} to 9.3×10^{-3} $cm \cdot s^{-1}$, the experimental slopes of $(\frac{\eta}{i})$ versus $\omega^{-\frac{1}{2}}$ plots remain $1.60 \pm 0.02 \times 10^{5}$ $A^{-1} \cdot s^{\frac{1}{2}}$. This result also means that the equation used for the measurements is best divided into two parts; one dealing with the kinetic parameter and the second only responding to the mass transport conditions. It could be written as:

$$\left(\frac{\partial \eta}{\partial i}\right)_{\omega} \frac{F}{RT} = \left(\frac{1}{i}\right)_{Kin} + \left(\frac{1}{i}\right)_{Diff} \qquad (5.1)$$

where $(\frac{1}{i})_{Kin}$ is the kinetic part and $(\frac{1}{i})_{Diff}$ is the diffusion or mass transfer part. From equations (2.3.11), (2.3.12), (2.3.13), (3.3.7) and (3.3.8) the theoretical slope is

$$\frac{1+K}{0.62\, F A D_{Fe^{3+}}^{\frac{2}{3}} \nu^{-\frac{1}{6}} C_{Fe^{3+}}^{*}} = \frac{1 + 0.894}{1.166 \cdot 1.0 \times 10^{-5}} = 1.62 \times 10^{5} A^{-1} s^{-\frac{1}{2}}$$

Comparing this value with the experimental data, the relative error is only 1.2%. Therefore the kinetic parameter could be determined without mass transport effects.

In the previous work by Su[11] and Wadden[12], the left side of equation (5.1) was called the reciprocal exchange current, using the linear characteristic relation

$$i = i_o\, nf\, \eta \qquad (5.2)$$

to give $\frac{1}{i_o} = nf \frac{d\eta}{di}$. Also, from Bard and Faulkner's book[38] the equation (5.2) could be used as long as the solution is well stirred. It may be correct for a slow reaction. But in the case of a fast reaction, *e.g.* the heterogenous reaction of Fe^{3+} and Fe^{2+}, this conclusion is not true. Since the exchange current i_o refers to the charge transfer process it is independent of rotation speed, and therefore the slope $(\frac{d\eta}{di})$ should not change with rotation speed. However, the slopes of $\frac{d\eta}{di}$ are greatly dependent on the rotation speeds. Table 5.2 shows the change from experiment #164.

Table 5.2 The Changes of Slopes $(\frac{d\eta}{di})_\omega$ With Rotation Speed

rotation speed / rad·s^{-1}	Slope $(\frac{\partial\eta}{\partial i})_\omega$ / V·A^{-1}
37.09	773.4
46.66	700.7
61.90	616.8
84.32	542.1
128.2	457.9
203.5	382.6
284.4	336.9
375.6	306.3

Even though the solution was very well stirred at high rotation speeds, the slopes do not remain constant. Under this circumstance, the equation $i \neq i_o\, nf\eta$ resulted so that i_o is not the charge transfer exchange current but is controlled by mass transport for a fast reaction like the Fe^{2+}, Fe^{3+} redox reaction.

The only approximation made in the theory of the low overpotential method differing from other methods in electrochemistry textbooks is that

$$(1+K) + (1-\alpha(1+K))f\eta = (1+K) + (1-\alpha-\alpha K)f\eta \qquad (5.3)$$

is approximated to be (1 + K). The error in making this approximation may be estimated by letting

$$l = (1-\alpha-\alpha K)\, f\eta \qquad (5.4)$$

with K = 0.89, η = 0.005 V, when α changes from 0.2 to 0.8, then l has the relation shown in Fig. 5.1.

Figure 5.1 on next page

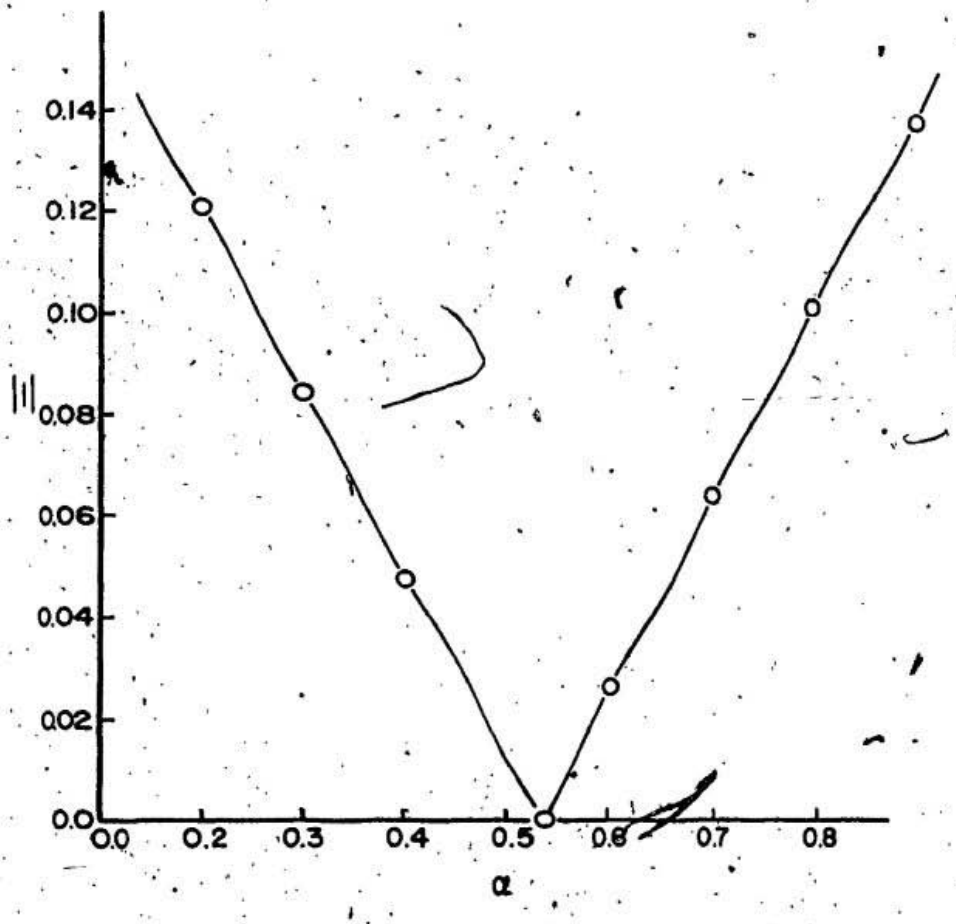

Fig.-5.1 Estimated values of $||$ as a function of α.

At the point $\alpha = 0.53$, $l = 0$, and even the largest values at $\alpha = 0.2$, $l = 0.12$ which is negligible compared with $1 + K = 1.89$ or at $\alpha = 0.8$ $l = 0.10$, also, negligible. If η has a lower value than 5 mV, *e.g.* 1 mV, the maximum value of $|l|$ is 0.020 for $\alpha = 0.8$. Comparing 0.020 with 1.89, the value of l can be ignored without causing significant error. In conclusion the theoretical treatment and the approximation are reasonable.

The advantages of using the low overpotential method for rate constant determination are twofold. Firstly, very low overpotentials are normally required: ± 5.0 mV. These may not cause any changes in the surface condition of the RDE. It was found in this work that high positive overpotentials build up oxide film on the platinum RDE surface. The surface reactivity was thus affected by measurements in which high overpotentials were applied and the linearity in the Tafel or Hickling plot was found greatly ruined by the high overpotential. Secondly, excellent linearities were achieved in the low overpotential measurements for plots of η against i and of $(\frac{\partial \eta}{\partial i})_\omega$ against $\omega^{-\frac{1}{2}}$. The correlation coefficients for these plots often reach to 1.0000. In contrast, the bending of the Hickling or Tafel plot at high and low overpotentials is rarely avoided. Moreover, the perturbation by applying overpotential to the test system is very small because the low overpotential keeps the system very close to the equilibrium point so that the measured exchange current should be more reliable.

5.2 High Overpotential Measurements

High overpotential measurements have been a well known method to obtain both rate constants and transfer coefficients. However, the application of the method to a RDE system is not quite satisfactory. There are two overpotential limits at low and high overpotentials. For example in the Hickling plot

$$\ln \frac{i}{1 - e^{-f\eta}} = \ln i_o + \alpha f\eta$$

if the η is very small $\rightarrow$ 0, a deviation from the linear relation will occur because $e^{-f\eta} \rightarrow 1$. One often has to choose higher overpotentials. In the case when a RDE is used, an inverse Levich plot $\frac{1}{i}$ against $\omega^{-\frac{1}{2}}$ is plotted and then is extrapolated to infinite ω to obtain a charge transfer current at a constant overpotential from the intercept. However, when the overpotential is too high, the intercept of such inverse Levich plot is too close to the origin to precisely determine it, as shown in Fig. 5.2 and 5.3.

Figures 5.2 and 5.3 on next pages

Therefore a high overpotential limits the reliability of this method. In the present case, if the overpotential is larger than 250mV, great error would be caused. It may not be a problem for the kinetic measurement by other techniques, *e.g.* potential step methods, or for a slow rate reaction, but if it is applied to a fast reaction and RDE inverse Levich plots are used, the two limits discussed above have to be considered.

Another problem that may arise in the high overpotential measurement is the formation of oxide film in the high positive branch and the possible plating out of metallic impurities at high negative overpotentials. The present experiments provided ample evidence that once any high positive overpotential was applied to a extremely cleaned platinum RDE, the rate constant decreased dramatically. Further discussion of high positive overpotential effects is given later. The high negative overpotentials have smaller effects on the surface. As shown earlier, better linear relations were obtained in the Hickling plot than in the Tafel plot, but the results of Table 4.5 show that the measured rate constants are essentially slightly lower than the corresponding values measured with the low overpotential method. An

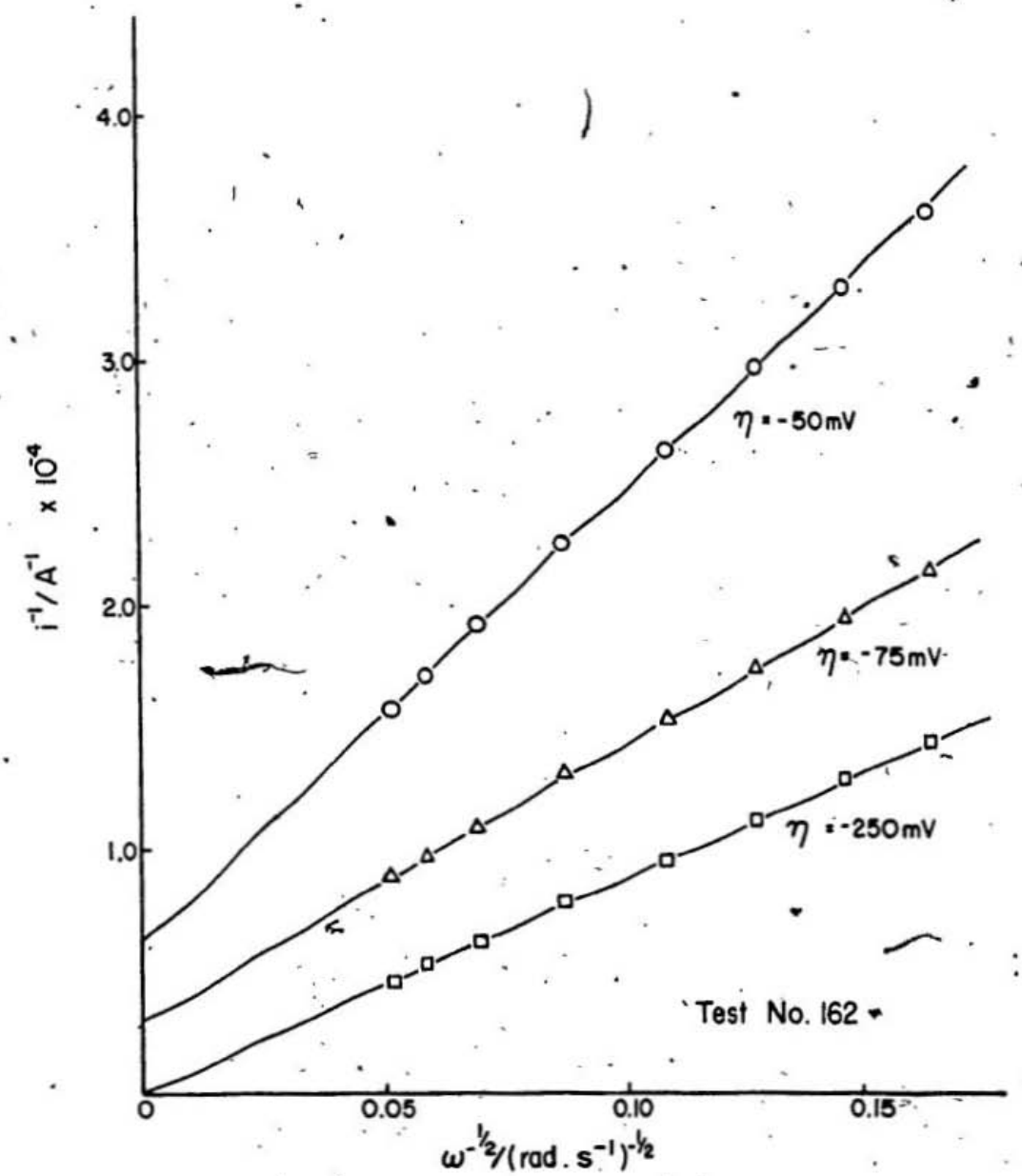

Fig. 5.2 Inverse Levich plots for negative overpotentials. Pt RDE soaked in 0.1 mol·L^{-1} $FeSO_4$ for 4 h before measurements.

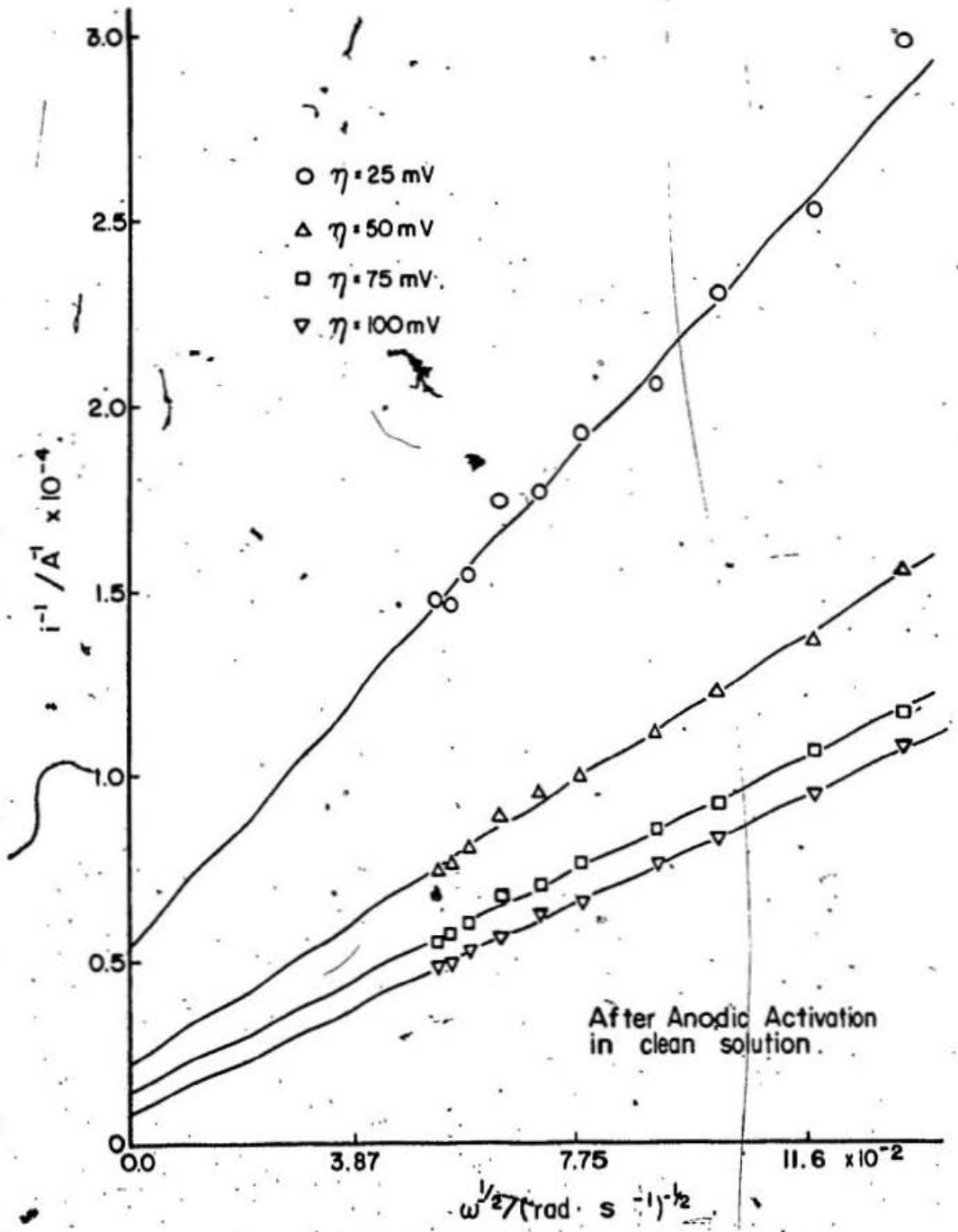

Fig. 5.3 Inverse Levich plots for positive overpotentials.

assumption is made that trace metallic ions may be plated on the surface during the measurement since the potential applied to the platinum RDE was sufficiently low to deposit some metal ions on it. If the overpotential were lower than -480 mV ($\eta < -480$ mV) the reduction of hydronium ion, seen in the activation voltammogram of Fig. 4.3, would become significant and affect the rate constant measurement. In order to avoid all the problems caused by high overpotential, the low overpotential method for the rate constant of a fast reaction is preferred.

5.3 The Activation of an Extremely Cleaned Platinum RDE

All papers searched regarding the activation are certain that the activations with triangular sweeps always increase the surface activity. So as in the preliminary work, the activation in H_2SO_4 alone and in Fe^{3+}, Fe^{2+}-containing solution always increased the activity by observing the rate constants before and after activation. In the second stage of the preliminary work, the rate constants measured after activation did not increase as much as did the rate constant in the preliminary work. The main difference is that the test apparatus was carefully cleaned, especially the platinum RDE. The results in Table 4.2 show that the increase of rate constant after activation only averaged 37%. Comparing the value with the value obtained in the early preliminary work, *ca.* 80%, the activation is not so efficient. The situation of activation by triangular sweep was getting worse after the apparatus was further cleaned in the first stage of the late work. The rate constants decreased about 30% after the triangular sweep activation. In other words, only 70% of the original activity remained after the activation. More careful work had been done to solve the problem by cleaning the apparatus by extreme means. The procedures were discussed earlier. As expected, great deactivation was found in the latest stage of the work. Many runs were carried out to obtain a good reproducibility so that this phenomenon did not happen by chance. The fairly good agreement for the different

runs can be found in Table 4.4. These results in the latest stage give very high rate constants (9.0×10^{-3} cm s^{-1} in average) but they were more sensitive to the activation. The activity decreased about 75% on average, in other words, only 22 ~ 25% activity remained after the activation by triangular sweep. The following table shows a summary for the phenomenon.

Table 5.3 The Effect of Activation

The work carried out	RDE surface and apparatus condition	Rate constant change
early preliminary work	less clean	increase 80% to 150%
late preliminary work	clean	increase ~ 30%
first stage of late work	very clean	decrease 19% to 30%
latest work	extremely clean	decrease ~ 75%

Apparently, the activation had a negative effect on a very clean platinum electrode. The search in the literature to answer this problem was not satisfactory but a possible solution is somewhat as follows. According to Breiter[34], the triangular sweep activation is mainly due to the oxidation of a layer of organic impurities sitting originally on the surface so that the blocking of the surface is slowly removed. Gilman[39] mentioned that some investigators feel that anodic activation operates, not simply through the cleaning of the Pt surface, but through an indirect mechanism as absorption of oxygen, production of "activated oxides" and recrystallization of the surface. In his other work[37], concerned with the problem of solution impurities, highly developed surfaces were used to minimise impurity effects. The fact that on a platinized surface the height of the "hills" is small compared with the steady-state diffusion layer thickness is advantageous. Therefore, the geometric area remains unchanged while the number of adsorption sites per square centimetre of geometric

area is increased. This results in an increase of the reactivity of the electrode. All the workers above give an impression that the purpose of carrying out activation is to remove the impurities sitting on the surface. Another view of the mechanism is the electrochemical roughening of the platinum surface[40-42] by anodic-cathodic triangular sweeps. Biegler[35] suggested that the roughening occurs through weakening of platinum interactions due to formation of the strong platinum oxygen chemisorption bond. The platinum surface atoms are therefore rearranged and the dissolution of platinum-oxygen species occurs. A study by electron microscopy in his work showed that activation by triangular sweep involves structural alteration of the surface but it is a slow process while cleaning of a contaminated surface occurs in fewer cycles. His work suggested that the mechanism of electrode activation seems to involve some kind of redistribution of surface platinum atoms during the triangular sweep. The suggested mechanism for electrode activation is that after rolling or drawing during manufacture, a platinum surface probably contains a large proportion of high index crystal faces and many defects. There is a correspondingly large number of high energy surface platinum atoms with low co-ordination to the underlying lattice. Such a surface is essentially generated by a layer of adsorbed oxygen and when the strong Pt-O chemisorption bond forms, the further weakening of the co-ordination of the high energy platinum atoms allows rearrangement of the atoms or complete separation of the Pt-O entity from the surface. Repetition of this process using one of the nonroughening programs eventually removes most or all of the high energy platinum atoms and leaves a stable surface exposing predominantly low index, high co-ordination faces.

According to this work and the experimental facts, the formation of strong Pt-O chemisorption bond at high positive overpotentials is acceptable. Many experiments showed that the rate constant decreased to about one third or one fourth of the original value after applying a +550 mV overpotential to determine the concentration

of Fe^{2+} by the limiting current method. Presumably, the activation by triangular sweep may have the same effect on the surface as the high overpotential was applied alternately and of course, the negative overpotential was also applied periodically but it is not able to reduce all the platinum oxide because a series of experiments was carried out, holding the potential at high negative overpotential for hours after triangular sweep, then the rate constant was measured. This "held method" did not increase the rate constant nor the activity of electrode. The schematic platinum oxygen structures from Vetter and Schultze's paper[43] are shown in Fig. 5.4.

Figure 5.4 on next page

Although the coverage in our work may not be unity, some of the oxygen atoms may penetrate deeply inside of the extremely clean platinum surface, as shown in Fig. 5.4c.

An hypothesis is that the formation and reduction of an oxide film on the surface is not electrochemically reversible for a completely clean electrode. In general, the oxygen coverage Θ decreases if the applied potential is decreased according to the $E - \Theta$ curve provided in Delahay's book[44]. The oxygen coverage should be lower than 2.5% of a monolayer at a potential of about 0.4 V SHE on a platinum electrode. The oxide film should be essentially removed. However, the failure of holding the RDE at a constant high negative overpotential (η = -0.27 V, -0.47 V, and -0.67 V were tried) for hours suggested that the experimental method recommended by Angell and Dickinson[8] could not remove the formed oxide film. Their pretreatment for a Pt RDE in their work was composed of three parts, the third step was that the electrode was oxidized strongly for 1 min, and then reduced at 0.46 V (SHE) (η = -0.22 V). In this work, the original rate constant for a set of experiments was 7.2 x 10^{-3} $cm \cdot s^{-1}$, but after strong oxidization by triangular sweep in the potential range 1.13 V to 2.13 V SHE, *i.e.* close to Anson's[2] oxidation potential

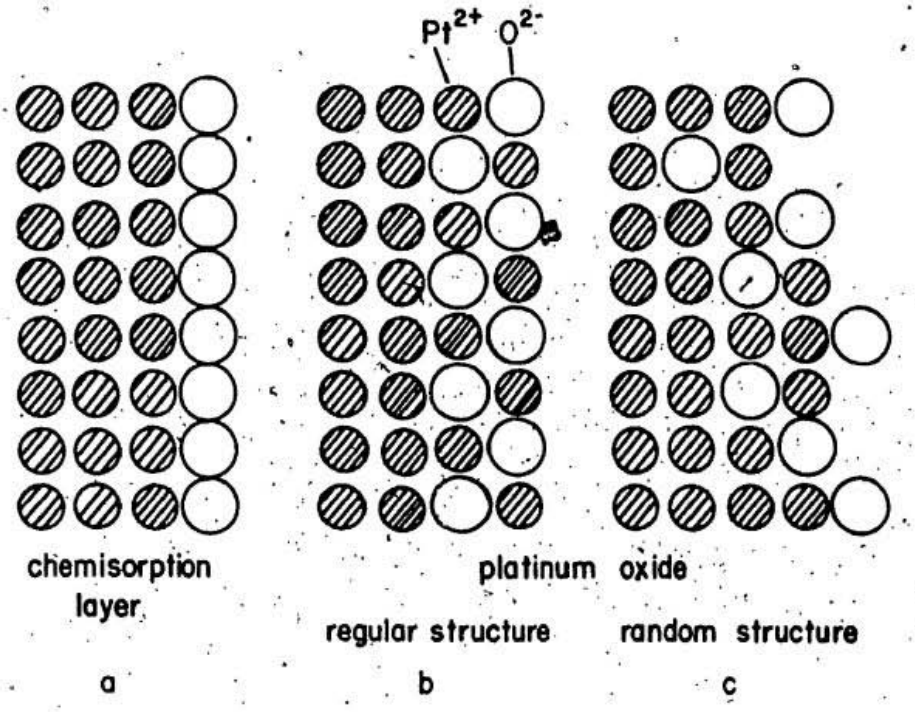

Fig.5.4 Schematic diagram of oxygen layers on the 100- face of platinum at a coverage $\theta = 1$.

(2.04 V), for 80 s, the rate constant decreased to 2.6×10^{-3} cm·s^{-1}. Then the RDE was held at a potential of 0.40 V (SHE), according to Dickinson, for 9 hours, but the measured rate constant by the low overpotential method was still 2.6×10^{-3} cm·s^{-1}.

Many efforts have been made to recover the electrode reactivity. The best method to finally remove the formed film was that recommended by Galus and Adams[7], and Rao and Rangarajan[31], which is soaking the electrode in $FeSO_4$ solution. The rate constant was well recovered to the initial value or at least increased after this soaking procedure. Apparently, the chemical reduction of the film is more efficient to remove the oxide film than the electrolytic method. The chemical reduction of oxide film was carefully studied using the chronopotentiometric method by Anson[2]. He concluded that the oxide film was chemically reduced *rapidly* by Fe(II) in 1F H_2SO_4, and suggested that this reduction gave a layer of freshly formed, finely divided platinum metal on its surface. It may be the reason of the high efficiency of reduction by Fe(II) solution. Also, it may be explained by considering that the potential of platinum soaked in only Fe(II)-containing solution would be very negative according to the Nernst equation,

$$E = E^{\circ} + 0.059 \log \frac{[Fe^{3+}]}{[Fe^{2+}]}$$

when $[Fe^{3+}] \rightarrow$ zero so that the oxide film is more susceptible of reduction under these conditions.

In conclusion, a platinum RDE could achieve a very high activity in two ways as mentioned by Gilman[39]: One is by the careful purification of the solution and related apparatus, although procedures used here were quite different from those of Gilman. Secondly, for an extremely cleaned RDE, the electrode can be oxidized by various means, such as: cathodic-anodic triangular sweep, polarization at the anodic limiting current, kinetic measurements including high positive overpotentials. Then the electrode should be soaked in 0.1 mol·L^{-1} $FeSO_4$, 0.5 mol·L^{-1} H_2SO_4 solution (the

solution must be of the same purity and prepared in clean apparatus) to develop a high reactivity surface by electrolytic and chemical means. However, the detailed, true mechanism of *deactivation* by a triangular sweep for an extremely cleaned system has not been thoroughly studied and an hypothesis for the phenomenon might be a strained interpretation due to the limited time available.

The most significant impurity to affect the rate constant (mentioned in many papers) may be halides, in particular chloride, which may exist in the tested solution as trace impurities and increase the rate constant by catalysis. In the case where $HClO_4$ is used as the support solution, the generation of chloride from the bulk $HClO_4$ leads to actual or potential catalysis. The overall reaction which may be written as

$$4Fe(s) + ClO_4^- + 8H^+ \rightleftharpoons 4Fe^{2+} + Cl^- + 4H_2O \qquad E^\circ = 1.81V$$

is thermodynamically feasible and the generated chloride ions are capable of speeding the reaction of Fe^{2+} and Fe^{3+}.

In the case that H_2SO_4 is used as electrolyte solution, generation of Cl^- is avoided, the only sources of chloride are the reagents or water. The concentration of Cl^- was measured in this work with the spectrophotometric method.[45] The concentration of Cl^- was about 1.0×10^{-6} mol·L^{-1}. It may have some catalysis effect but not very significant according to this work. Wadden[12] mentioned that the Cl^- adsorption on the platinum surface might be one of the reasons that anodic activation increases the rate constant. The results of activation in present work is negative, the rate constant measured after activation did not increase at all. The adsorbed Cl^- did not seem to be significant.

5.4 Comparison of Measured Rate Constant with Literature Values

As a conclusion to Part II, the measured rate constant for the heterogenous reaction $Fe^{2+} \rightleftharpoons Fe^{3+} + e^-$ is compared with the work which has been done by

other workers and all the results found in the literature are tabulated in Table 5.4.

The result from this work quoted in the table is the value divided by the roughness factor; corrections for double layer effects were made by Samec and Weber[6], who obtained $k^{o}_{true} = 0.136$ for Pt in 0.5 mol·L^{-1} H_2SO_4. Other workers have not attempted this, so all k_o values in Table 5.4 are uncorrected. It is difficult to make very meaningful comparisons of the values of the rate constant since this quantity depends on the true surface area of the electrode and of course on its cleanliness. Differences in these two variables presumably account for the range of results obtained. It is unfortunate that surface area measurements have not normally accompanied measurements of the rate constant. Under the circumstances agreement to within a factor of two to three times must be regarded as satisfactory. On this basis, the present work has results which are in agreement with the published work tabulated in Table 5.4. The transfer coefficients lie between 0.39 and 0.61 and values of α from this work is also within this range. The comparison shows that the rate constant obtained by the present technique (low overpotential measurement) is consistent with the literature data and it is a reliable method to determine the rate constant.

Table 5.3 A Comparison of the Measured Rate Constant and Transfer Coefficient at 25 °C with the Literature Values for Platinum in Sulphate Media

Supporting Electrolyte	$[Fe^{2+}]$, $[Fe^{3+}]$ /mol·cm^{-3}	k^o x 10^3 /cm·s^{-1}	α^*	Authors	Reference No.
0.5 mol·L^{-1} H_2SO_4	1.0 x 10^{-5}	3.9 ± 0.2	0.56	This work	-
0.5 mol·L^{-1} H_2SO_4	$[Fe^{2+}] = 3.6 \times 10^{-6}$ $[Fe^{3+}] = 6.5 \times 10^{-6}$	3.2 (at 22 °C)	0.48	Samec and Weber	6
0.5 mol·L^{-1} H_2SO_4	?	3.9		Samec and Weber	49
0.5 mol·L^{-1} H_2SO_4	1.0 x 10^{-5}	7.0	0.5	Angell and Dickinson	8
0.5 mol·L^{-1} H_2SO_4	2.0 x 10^{-6}	3.3	0.42	Agarwal	3
0.1 mol·L^{-1} H_2SO_4	1.0 x 10^{-6}	4.3	0.39	Galus and Adams	7
1.0 mol·L^{-1} H_2SO_4	1.0 x 10^{-6}	4.3	0.53	Galus and Adams	7
1.0 mol·L^{-1} H_2SO_4	$[Fe^{2+}] = 6.4 \times 10^{-5}$ $[Fe^{3+}] = 14.0 \times 10^{-5}$	5.32	0.39	Rao and Rangarajan	31
1.0 mol·L^{-1} H_2SO_4	10^{-5} to 10^{-4}	5.3	-	Anson	2
1.0 mol·L^{-1} H_2SO_4	10^{-6} to 10^{-5}	3.11	0.42	Gerischer	1
1.0 mol·L^{-1} H_2SO_4	1.0 x 10^{-5}	4.75 to 5.26	0.61	Wijnen and Smit	48
1.0 mol·L^{-1} † H_2SO_4	1.0 x 10^{-5} 1.0 x 10^{-4}	2.5 0.8	- -	Bockris et al.	46
0.91 mol·L^{-1} $NaHSO_4$	1.0 x 10^{-4}	3.94	0.5	Barnartt	4
0.87 mol·L^{-1} $NaHSO_4$	9.6 x 10^{-5}	3.86	0.5	Barnartt	47

* Anodic transfer coefficient. † Ammonium salts.

References

1. H. Gerischer, *Z. Elektrochem.*, 1950, **54**, 362, 366.
2. F.C. Anson, *Anal. Chem.*, 1961, **33**, 7, 939.
3. H.P. Agarwal, *J. Electroanal. Chem.*, 1963, **5**, 236.
4. S. Barnartt, *Can. J. Chem.*, 1969, **47**, 1661.
5. A.J. Bard and L.R. Faulkner, "Electrochemical Methods", J. Wiley, New York, 1980, p 166.
6. Z. Samec and J. Weber, *J. Electroanal. Chem.*, 1977, **77**, 163.
7. Z. Galus and R.N. Adams, *J. Phys. Chem.*, 1963, **67**, 866.
8. D.H. Angell and T. Dickinson, *J. Electroanal. Chem.*, 1972, **35**, 55.
9. J.E.B. Randles, *Can. J. Chem.*, 1959, **37**, 238.
10. F.R. Smith and C.S. Su, *J. Chem. Soc., Chem. Comm.*, 1972, 159.
11. C.S. Su, M.Sc. Thesis, Memorial University of Newfoundland, 1972.
12. J.T. Wadden, M.Sc. Thesis, Memorial University of Newfoundland, 1978.
13. F.R. Smith and J.T. Wadden, Preprints of 6th Canadian Symposium on Catalysis, Ottawa, 1979, pp 263-270.
14. R. Parsons, *Trans. Faraday Soc.*, 1951, **47**, 1332.
15. P. Delahay in ed. P. Delahay, "Advances in Electrochemistry and Electrochemical Engineering", Wiley-Interscience, Vol. 1, 1961, p 240.
16. Reference 5, p 103.
17. P.A. Allen and A. Hickling, *Trans. Faraday Soc.*, 1957, **53**, 1626.
18. V.G. Levich, "Physicochemical Hydrodynamics", Prentice Hall, New Jersey, 1962, pp 60, 72.
19. Reference 5, p 120.

20. Reference 5, p 283.

21. Reference 18, p 68.

22. D.P. Gregory and A.C. Riddiford, *J. Chem. Soc.*, 1956, **10**, 3756.

23. D. Jahn and W. Vielstich, *J. Electrochem. Soc.*, 1962, **109**, 849.

24. J. Newman, *J. Phys. Chem.*, 1966, **70**, 1327.

25. P. Delahay, "Double Layer and Electrode Kinetics", Wiley-Interscience, New York, 1965.

26. A.C. Riddiford and K. Blurton, *J. Electroanal. Chem.*, 1967, **10**, 457.

27. F. Opekar and P. Beran, *J. Electroanal. Chem.*, 1976, **69**, 76.

28. A.C. Riddiford, in ed. P. Delahay, "Advances in Electrochemistry and Electrochemical Engineering", Wiley-Interscience, New York, Vol. 4, 1965, p 47.

29. M.W. Breiter, *Electrochim. Acta*, 1966, **11**, 905.

30. T. Biegler, *J. Electrochem. Soc.*, 1969, **116**, 1131.

31. G.P. Rao and S.K. Rangarajan, *J. Electroanal. Chem.*, 1973, **41**, 473.

32. P.B. Sweetser and C.E. Bricker, *Anal. Chem.*, 1953, **25**, 253.

33. R. Woods in ed. A.J. Bard, "Electroanalytical Chemistry", Marcel Dekker, New York, Vol. 9, 1976, p 1.

34. M.W. Breiter, *Electrochim. Acta*, 1966, **11**, 905.

35. T. Biegler, *J. Electrochem. Soc.*, 1969, **116**, 1131.

36. F.A. Lewis, "The Palladium-Hydrogen System", Academic Press, London,

37. S. Gilman, *J. Phys. Chem.*, 1963, **67**, 78.

38. Reference 5, p 105.

39. S. Gilman in ed. A.J. Bard, "Electroanalytical Chemistry", Marcel Dekker, New York, Vol. 2, 1967, p 111.

40. F.C. Anson and D.M. King, *Anal. Chem.*, 1961, **34**, 362.

41. J.P. Howe, *Electrochim. Acta*, 1964, **9**, 599.

42. T. Biegler, *J. Electrochem. Soc.*, 1967, **114**, 1261.

43. K.J. Vetter, and J.W. Schultze, *J. Electroanal. Chem.*, 1972, **34**, 31.

44. Reference 25, p 278.

45. D.F. Boltz and J.A. Howell, "Colorimetric Determination of Nonmetals", J. Wiley, New York, 2nd Edn., 1978, p 104.

46. J. O'M. Bockris, R.J. Mannan and A. Damjanovic, *J. Chem. Phys.*, 1968, **48**, 1898.

47. S. Barnartt, *Electrochim. Acta*, 1970, **15**, 1313.

48. M.D. Wijnen and W.M. Smit, *Rec. Trav. Chim. Pays-Bas*, 1960, **79**, 289.

49. Z. Samec and J. Weber, *J. Electroanal. Chem.*, 1973, **44**, 229; 1972, **38**, 115.